ISSN 1816-8957

No. 25, June 2019

Scientific Drilling

Reports on Deep Earth Sampling and Monitoring

The open-access ICDP and IODP journal • www.scientific-drilling.net

Editorial preface

Dear Reader,

Recent volcanic eruptions in Italy, Indonesia and Guatemala remind us about the heat and magma pump that drives our restless planet. Scientific drilling is one key method to sample and study volcanoes in situ for the advancement of understanding volcanic processes. This issue (Vol. 25) of Scientific Drilling encompasses six science papers, four of which focus on different aspects of drilling, coring and exploration of volcanoes.

The SUSTAIN drilling campaign on Surtsey Island, Iceland **(p. 35)**, was conducted about 50 years after a first exploratory well penetrated the tip of this volcano in 1979 just a few years after its emergence in 1963–1967. Drilling at Surtsey provided a record of global significance for studying the mechanics of marine basaltic eruptions, the deep structure of young oceanic islands in shallow rift-zone environments, and the processes of tephra lithification causing resistance of volcanic islands to incessant marine erosion. One of the three boreholes drilled in 2017 has been equipped with a novel type of subsurface observatory dedicated to in situ experiments for monitoring water–rock–microbial processes in situ and on artificial rock samples **(p. 57)**.

Combined core, wireline logging and downhole image log studies in the subsurface of Hawai'i **(p. 15)** link borehole facies to surface analogues to shed light on geological processes that form petrophysical variations preserved in the rocks. Such studies allow improved confidence in the interpretation of borehole imaging of volcanic sequences where core is not available.

Volcanic maar lakes can serve as significant archives for paleoclimate and paleoenvironmental studies. A prime example is the Orakei maar lake in the Auckland Volcanic Field, New Zealand **(p. 47)**, due to its low surface-to-volume ratio and limited catchment. The drilling campaign opened its lake sediments as an ideal library of SW Pacific climate signals. The maar lakes also preserve ashes of the neighbouring volcanoes allowing for geochronological control. The sediment coring sequence spans the last glacial cycle from the phreatomagmatic eruption to the crater rim breach due to post-glacial sea-level rise.

Paleoclimate studies are the focus of two other papers of this issue. Further west in the South Pacific, Darwin Crater on Tasmania provides not only a suspected Pleistocene meteorite impact structure but also another climate record of the Southern Hemisphere. A report on the drilling operations and initial science **(p. 1)** shows first results from petrophysical whole core logging, lithological core description and multi-proxy pilot analysis on 160 m of combined sediment cores. The multi-proxy dataset includes spectrophotometry, grain size, natural gamma rays, paleo and rock magnetism, loss on ignition, and pollen analyses. The sediment succession includes a pre-lake silty sand deposit overlain by lacustrine silts.

A workshop in Beijing served to discuss the scientific opportunities for drilling in Lake Nam Co on the Tibetan Plateau **(p. 63)** and to form an international team with more than 40 scientists from 13 countries. Such an attempt would be of peculiar societal relevance as the Tibetan Plateau provides freshwater from the so-called "Water Tower of Asia" to a large portion of the Asian population.

All in all, the enclosed papers show the continued importance of volcanic studies and highlight current frontiers. Scientific drilling is once again demonstrated to be a critical element of our push to better understand volcanoes.

Your editors,
Ulrich Harms, Thomas Wiersberg, Jan Behrmann, Will Sager, and Tomoaki Morishita

Aims & scope

Scientific Drilling (SD) is a multidisciplinary journal focused on bringing the latest science and news from the scientific drilling and related programmes to the geosciences community. Scientific Drilling delivers peer-reviewed science reports from recently completed and ongoing international scientific drilling projects. The journal also includes reports on engineering developments, technical developments, workshops, progress reports, and news and updates from the community.

Editorial board

Additional information

ISSN 1816-8957 | eISSN 1816-3459

Copernicus Publications
The Innovative Open Access Publisher

Copernicus Publications
Bahnhofsallee 1e
37081 Göttingen
Germany
Phone: +49 551 90 03 39 0
Fax: +49 551 90 03 39 70

editorial@copernicus.org
production@copernicus.org

http://publications.copernicus.org

View the online library or learn more about Scientific Drilling on:
www.scientific-drilling.net

Cover figure: View of the 2017 SUSTAIN drilling operation at the base of the Surtur tuff cone. Photograph by Magnús T. Gudmundsson.
Insert 1: Hawai'i drill core cut in sections for additional sampling. Photograph by Dougal A. Jerram et al. 2019.
Insert 2: Open wellhead of the SUSTAIN borehole observatory. Photograph by Steve Cole.

Contents

Science Reports

Progress Reports

Technical Developments

Workshop Reports

News & Views

Sci. Dril., 25, 1–14, 2019
https://doi.org/10.5194/sd-25-1-2019

Scientific Drilling
Open Access

Scientific drilling of sediments at Darwin Crater, Tasmania

Agathe Lisé-Pronovost[1,2], Michael-Shawn Fletcher[3], Tom Mallett[2], Michela Mariani[3,4], Richard Lewis[5], Patricia S. Gadd[6], Andy I. R. Herries[2], Maarten Blaauw[7], Hendrik Heijnis[6], Dominic A. Hodgson[8,9], and Joel B. Pedro[10]

[1]School of Earth Sciences, University of Melbourne, Melbourne, Australia
[2]The Australian Archaeomagnetism Laboratory, Department of Archaeology and History, La Trobe University, Melbourne Campus, Bundoora, 3086, VIC, Australia
[3]School of Geography, University of Melbourne, Melbourne, Australia
[4]School of Geography, University of Nottingham, Nottingham, UK
[5]School of Earth and Environmental Sciences, University of Adelaide, Adelaide, SA, Australia
[6]Australian Nuclear Science and Technology Organisation, Lucas Heights, NSW, Australia
[7]School of Natural and Built Environment, Queen's University Belfast, Belfast, UK
[8]British Antarctic Survey, Cambridge, CB3 0ET, UK
[9]Department of Geography, University of Durham, Durham DH1 3LE, UK
[10]Antarctic Climate and Ecosystems CRC, University of Tasmania, Hobart, 7001, TAS, Australia

Correspondence: Agathe Lisé-Pronovost (agathe.lise@unimelb.edu.au)

Received: 9 October 2018 – Revised: 27 November 2018 – Accepted: 14 December 2018 – Published: 12 June 2019

Abstract. A 70 m long continental sediment record was recovered at Darwin Crater in western Tasmania, Australia. The sediment succession includes a pre-lake silty sand deposit overlain by lacustrine silts that have accumulated in the ∼ 816 ka meteorite impact crater. A total of 160 m of overlapping sediment cores were drilled from three closely spaced holes. Here we report on the drilling operations at Darwin Crater and present the first results from petrophysical whole core logging, lithological core description, and multi-proxy pilot analysis of core end samples. The multi-proxy dataset includes spectrophotometry, grain size, natural gamma rays, paleo- and rock magnetism, loss on ignition, and pollen analyses. The results provide clear signatures of alternating, distinctly different lithologies likely representing glacial and interglacial sediment facies. Initial paleomagnetic analysis indicate normal magnetic polarity in the deepest core at Hole B. If acquired at the time of deposition, this result indicates that the sediment 1 m below commencement of lacustrine deposition post-date the Matuyama–Brunhes geomagnetic reversal ∼ 773 ka.

1 Introduction

Pleistocene glacial and interglacial cycles involved repeated massive reorganisations of the Earth system. Proxies in ocean, ice-core, and continental records capture a range of these changes at global to regional and local scales. Continental records show how terrestrial environments responded to the large-scale shifts between glacial and interglacial states, providing valuable insights into the interactions between the atmosphere, oceans, cryosphere and biosphere, and the long-term context from which to interpret current and future trends. This is particularly important in the mid- to high latitudes of the Southern Hemisphere, where Antarctic climate and circumpolar atmosphere–ocean dynamics exert a dominant influence not only on southern terrestrial climates but also on the global carbon cycle (Saunders et al., 2018; Skinner et al., 2010; Toggweiler, 2009; Toggweiler et al.,

2006). These studies highlight the role of the Southern Hemisphere westerly winds (SWWs) in regulating the Southern Ocean carbon sink and the global carbon cycle. Empirical data from long paleoclimate records are therefore needed to test different theories of how the Earth system operates and if they can be simulated in Earth system models.

Crater lake sediment records often have great scientific value and can provide local to global climate histories (e.g. Wilke et al., 2016). Examples of impact craters with lacustrine sediment records include Bosumtwi in Ghana (6°30′ N; 1 Ma; Scholz et al., 2007), Colônia in Brazil (23°52′ S; 5 Ma; Ledru et al., 2015), El'Gygytgyn in Russia (67°30′ N; 2.8 Ma; Melles et al., 2012), and Pingualuit in Canada (61°16′ N; 1.4 Ma; Guyard et al., 2011). There is, to date, no sediment record from an impact crater in the mid-latitudes of the Southern Hemisphere, however there are volcanic crater sediment records, such as Potrok Aike in south-eastern Patagonia (51°58′ S; 107 m; 51 ka; Zolitschka et al., 2013), Lake Pupuke in New Zealand (37°47′ S; 48 ka; Stephens et al., 2012), and a series of volcanic craters in the Newer Volcanics Province in south-eastern Australia (∼ 38°; Matchan et al., 2017 and references therein). Long Pleistocene lake sediment records are extremely rare in Australia because of the aridity and the general absence of glaciers and recent tectonic activity able to form deep freshwater basins. Many mainland Australian lakes are ephemeral, and very few originate from before the last glacial period (Falster et al., 2018). Exceptions include discontinuous paleo-lakes in mainland Australia, such as Stony Creek basin (37°21′ S; 1.85–1.55 Ma; Sniderman et al., 2007) and mega-lake Bungunnia (∼ 35° S; 2.5–0.8 Ma; McLaren and Wallace, 2010), and glacial lakes extending back to the last glacial in Tasmania (Beck et al., 2017; Colhoun, 2000; Colhoun et al., 1999). Our knowledge of Pleistocene climate in Australia is therefore incomplete.

Here we report on the drilling operations at Darwin Crater, a ∼ 816 ka old meteorite impact crater in western Tasmania, Australia (42°18′ S, 145°39′ E). Drilling at Darwin Crater 40 years ago recovered 60 m of lacustrine sediments overlying 160 m of coarser crater-fill deposits, including polymictic and sandy unconsolidated breccia overlying deformed slates (Howard and Haines, 2007). While low-resolution pollen data were compiled on the upper 20 m of that core, revealing excellent pollen preservation and clear shifts between glacial and interglacial vegetation and climate (Colhoun and van der Geer, 1998), little further analyses were completed or published from this important archive. A note on paleomagnetic polarity of the original core by Barton (1987) in congress proceedings stated that the base of the Darwin lake sediments was of normal polarity, however no paleomagnetic data were published. Here, we present the first results from a new drilling campaign at Darwin Crater in 2018. The aim of this drilling was to recover the lacustrine sediment sequence (the uppermost 60 m of sediments in the crater) to bridge a time gap in the Australian paleoclimate record and provide a long continental record of Pleistocene climate in the mid-latitudes of the Southern Hemisphere. The results include data from non-destructive whole core logging (natural gamma ray, magnetic susceptibility, and resistivity) and multi-proxy pilot analysis of core end samples (spectrophotometry, grain-size, magnetic, loss-on-ignition, and pollen analyses). We interpret this data and outline the ongoing and potential future research directions.

2 Drilling target and geological settings

Darwin Crater is a 1.2 km diameter unconfirmed meteorite impact crater in western Tasmania, Australia (42°18′13″ S, 145°39′36″ E; Fig. 1). Gravity and magnetic surveys and scientific drilling in 1975 and 1983 revealed that the circular depression is filled with 60 m of lake sediments overlying 40 m of mixed muds, sands and rock fragments (unconsolidated breccia) and 120 m of deformed, brecciated, slumped, and fractured slate and quartzite laying over coherent local slate (Richardson, 1984; Howard and Haines, 2007). The stratigraphy is consistent with a small simple impact crater, however it is unconfirmed, because no diagnostic shock indicators have been found (Howard and Haines, 2007). The impactite "Darwin glass" is found within a 400 km^2 strewn field around Darwin Crater, where it most likely originates (Fudali and Ford, 1979; Howard and Haines, 2007; Howard, 2009) and is dated at 816 ± 7 ka by $^{40}Ar/^{39}Ar$ (Lo et al., 2002). Darwin glass is frequently found in archaeological cave sites in the region because this sharp and resistant material was used as a cutting tool by Aboriginal Tasmanians during the Pleistocene (Allen et al., 2016).

Darwin Crater lies 170 m above sea level, and the lake that formerly occupied the crater drained a small catchment area of 2.2 km^2 (Fig. 1d). The regional geology is dominated by sedimentary rocks and Quaternary deposits in the valley around the crater, volcanic and volcaniclastic rocks to the north-west (e.g. Mount Darwin, Mount Sorell), and quartzite to the east (e.g. Frenchman's Cap in the Engineer Range). The modern climate is cool temperate, with mean annual temperatures at nearby Queenstown (20 km distant) ranging from 5.6–16.4 °C and with 2405 mm rain per year (Australian Bureau of Meteorology). The climate is dominated by the SWWs which, together with orography, control precipitation in Tasmania and throughout the mid- to high latitudes of the Southern Hemisphere (Fig. 1b) (Garreaud, 2007). The crater is vegetated with shrubs, sedges, and grasses (including *Melaleuca squamea*, *Leptospermum* spp., *Monotoca glauca*, *Gymnoschoenus sphaerocephalus*, and *Restio australis*) occupying the basin floor, whilst the surrounding slopes are occupied by a cool temperate rainforest assemblage including *Lagarostrobos franklinii*, *Nothofagus cunninghamii*, and *Phyllocladus asplenifolius*.

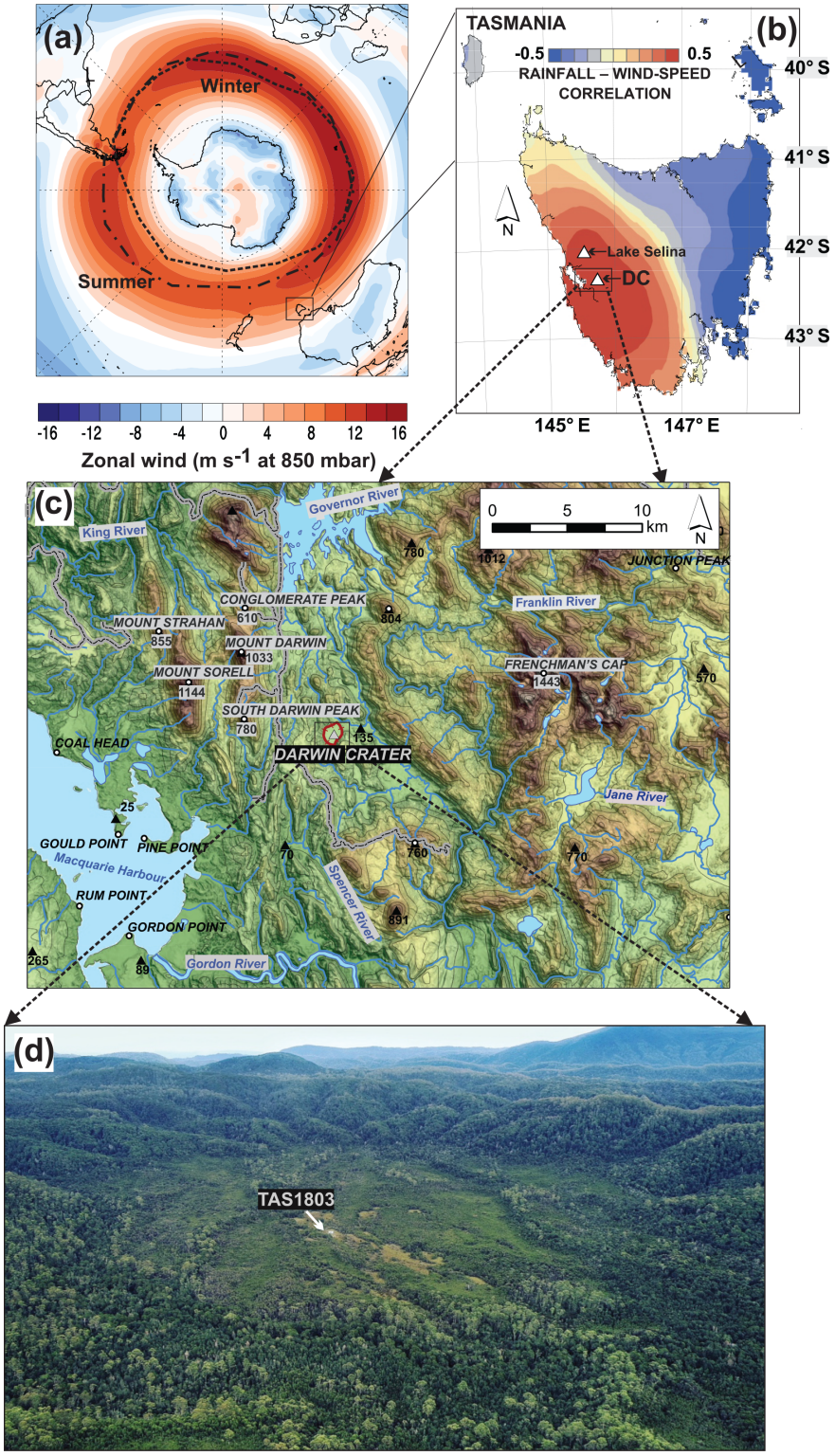

Figure 1. **(a)** Zonal wind speed at 850 mbar in the mid-latitude of the Southern Hemisphere, and average winter and summer core position of the Southern Hemisphere westerly winds (SWWs). **(b)** The SWWs are a dominant climate control in western Tasmania, where rainfall is strongly correlated to wind intensity and orography. **(c)** Regional topographic map showing the location of Darwin Crater, and **(d)** aerial oblique drone image of Darwin Crater during the scientific drilling operations in April 2018. The drill and camp site are visible in white. Wind data from the NCEP and NCAR Reanalysis V1 (Kalnay et al., 1996).

3 Drilling operations

The scientific drilling operations at Darwin Crater took place on 18–25 April 2018. The drill team was composed of six people, including two drillers, two students, and two researchers. Darwin Crater is in the remote Tasmanian Wilderness World Heritage Area. While a road was bulldozed to access the crater for drilling in the 1970s, today the crater is inaccessible by road. Therefore, the team, drill rig, camp, and equipment were transported to the site by helicopter (Fig. 2a–b).

The drill site TAS1803 (Fig. 1d; 42°18′16.46″ S, 145°39′33.09″ E) was selected in the approximate centre of the paleolake and in open sedgeland vegetation to facilitate camp set-up. Three parallel holes were drilled using a Boart Longyear 47 drill rig and HQ pipes (96 mm outside and 63.5 mm inside diameter) with a diamond drill bit (Fig. 3d). The same tools were used for all cores drilled. Core catchers were only required in the first few runs of Hole A because sediment lower down the sequence were sufficiently cohesive to be retained in the tube without loss. The drill rig was pushed 1.1 m eastward from Hole A to Hole B and 1.3 m eastward from Hole B to Hole C. The sediment recovery was initially low in the upper half of Hole A as we worked on establishing the best method for sediment retention. The optimal method proved to involve minimal flushing with water and rotation of the core barrel to allow efficient recovery of the poorly consolidated lake sediments. Once the optimal method was identified, operations went smoothly, and Hole B was successfully drilled the next day with 95.6 % recovery (Table 1). Holes A and B were abandoned when the top of the pre-lake crater infill described by Howard and Haines (2007) was reached, which indicated that the full lake sediment sequence had been successfully recovered. Hole C was drilled to ca. 44 m to obtain full overlap of the uppermost part of the record, which had lower recovery than the lower part of the record (Table 1).

Cores were retrieved in standard 10 ft long (3.048 m) transparent PVC HQ wire-line core liners. Each core was immediately wrapped in black plastic foil to protect from sunlight and allow for future optically stimulated luminescence (OSL) dating analyses (Fig. 2c). The core end sediments that protruded from the core liners or those retained in the core catchers (up to 6.5 cm) were collected in labelled bags (Fig. 2e–g) for preliminary analyses. Each 3 m core was cut into ca. 150 cm sections to facilitate transport and storage (total 93 core sections). We use the nomenclature "-TM" for the top to middle and "-MB" for the middle to base sections (e.g. core TAS1803-B10 is cut into TAS1803-B10-TM and TAS1803-B10-MB). Cores are stored in cold rooms and curated at the University of Melbourne within the School of Geography. All data will be deposited upon publication in the National Oceanic and Atmospheric Association (NOAA), NEOTOMA (https://www.neotomadb.org/, last access: 11 January 2019), and PANGAEA (https://pangaea.de/, last access: 11 January 2019) public data repositories.

Table 1. Summary of holes drilled and core recovery at Darwin Crater site TAS1803.

Hole	Start (m)	End (m)	Drilled (m)	Recovered (m)	Recovery (%)
A	1.66	70.76	69.10	55.39	80.2
B	0.56	69.26	68.70	65.66	95.6
C	0	43.66	43.66	39.58	90.7
Total			181.5	160.6	

4 Core scanning and multi-proxy analyses of core end samples

Whole core scanning of non-destructive petrophysical properties was performed using a Geotek Multi-Sensor Core Logger (MSCL) for all cores from Holes A, B, and C, in the Petrophysics Laboratory at the University of Melbourne. Volumetric magnetic susceptibility in low field (k_{LF}; 0.565 kHz) was measured using a Bartington MS2C loop sensor with a diameter of 8 cm, and the non-contact resistivity was measured using a Geotek sensor at 1 cm intervals. Natural gamma ray (NGR) emission integrated over 20 cm of core was counted for 1 min using Geotek NaI(Tl) at 40 cm intervals on the cores from Hole A.

The cores from Hole B were split lengthwise using a Geotek core splitter. Core splitting was conducted under red light, and one core half was wrapped in black plastic foil and stored at 4 °C for OSL and paleomagnetic sampling. The other half was used for visual lithological core descriptions and sent to Australia's Nuclear Science and Technology Organisation (ANSTO) for micro-XRF (Itrax) core scanning and core photography. The scanned half will be subsampled for multi-proxy analysis (including pollen, charcoal, grain size, magnetic properties, and aDNA). These procedures are repeated for the cores from each hole.

The core end samples from Holes A, B, and C (total 57 samples) were analysed for their magnetic properties, spectrophotometry, grain size, and loss on ignition, while only select core end samples were analysed for pollen.

Room-temperature magnetic measurements were performed at The Australian Archaeomagnetism Laboratory at La Trobe University to characterise the magnetic mineral assemblage and evaluate the potential for changes in the paleomagnetic field to provide a geochronological tool. Standard 8 cm^3 paleomagnetic boxes (unoriented) were used for all the core end samples from Holes A, B, and C. In addition, four box samples (A20, A21, B9, and B10) were taken partially oriented from well-preserved cylinder-shaped core ends (known vertical z axis), and four contiguous cubes were taken oriented (1, 2, 3, and 4) in the deepest core of

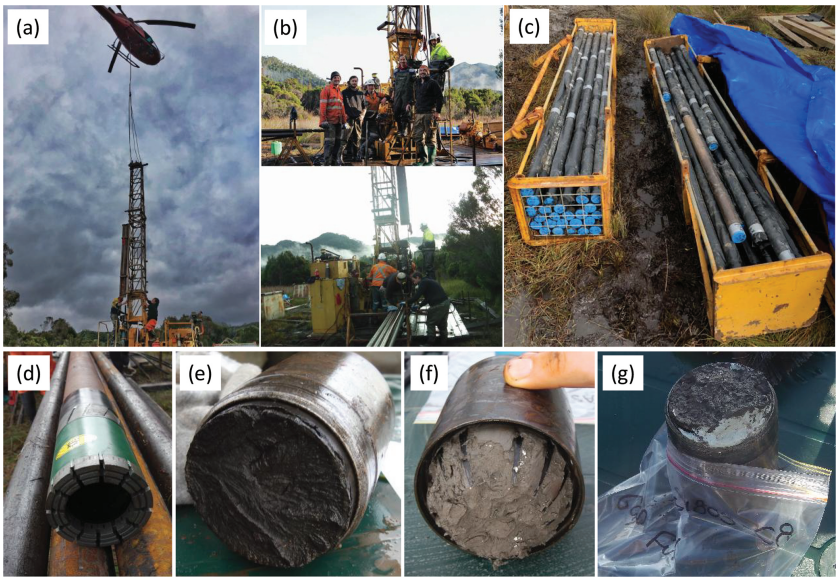

Figure 2. Photos of TAS1803 scientific drilling at Darwin Crater. **(a)** Helicopter-assisted drill rig assembly. **(b)** The drill team and view of the drilling and core handling set-up. **(c)** After recovery, the cores were immediately wrapped in black plastic to protect from light to allow for OSL dating. **(d)** The drill bit, **(e)** core end view from the top, **(f)** core end view from the base, together with the core catcher, and **(g)** core end sample C8 includes a white mineral tentatively identified as vivianite.

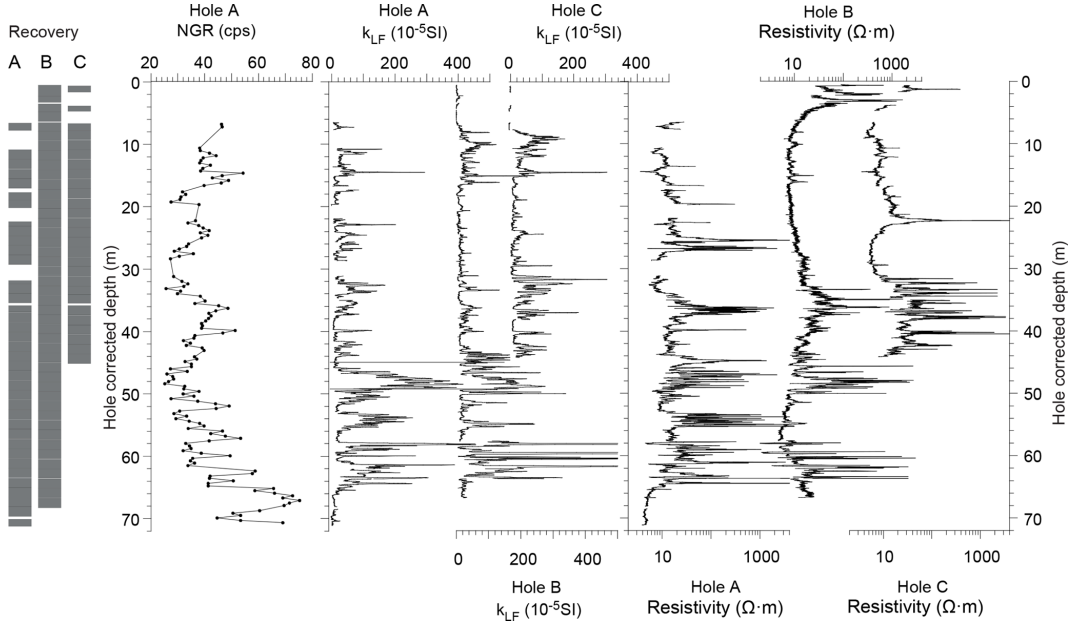

Figure 3. Core recovery log for each core hole and whole core MSCL-scanning data. Grey indicates full recovery, and white indicates no recovery. Natural gamma ray (NGR) was measured at 40 cm intervals, and volumetric magnetic susceptibility (k_{LF}) and resistivity were measured at 1 m intervals.

Hole B (section TAS1803-B-23MB). Magnetic susceptibility was measured using a Bartington MS2B sensor, and the natural and laboratory-induced (anhysteretic in peak alternating field (AF) 0.1 T with 0.05 mT DC biasing field and isothermal in 0.3 T and 2 T DC field) remanent magnetisations (NRM, ARM, and IRM) were acquired using an AGICO AF Demagnetizer LDA5, an AGICO Magnetizer PAM1, a Magnetic Measurements Pulse Magnetizer MMPM10, and an AGICO JR-6 Spinner Magnetometer. Demagnetisation data were analysed using the Demagnetization Analysis in Excel (DAIE) workbook (Sagnotti, 2013). Finally, first-order reversal curves (FORC) were acquired for three samples us-

ing a LakeShore VSM8600 Vibrating Sample Magnetometer to investigate the magnetic domain state. The FORCs were processed in Forcinel 3.0 (Harrisson and Feinberg, 2008) using VARIFORC smoothing (Egli, 2013).

Quantitative sediment colour (L^*, a^*, and b^*) was acquired using a handheld Konica Minolta CM-700d Spectrophotometer applied directly on the sediments of the paleomagnetic box samples.

Grain-size analysis was carried out on all the core end samples from Holes A, B, and C using a Beckman Coulter LP13320 particle sizer at the School of Geography at the University of Melbourne. Samples were pre-treated with hydrogen peroxide (10 %–30 %) for at least 4 weeks until organic-matter digestion was complete. Sediments were then treated with a dispersing agent, sodium pyrophosphate, and sonicated for at least 5 min prior to analysis. The statistical grain-size parameters were calculated with the GRADISTAT software (Blott and Pye, 2001).

Loss-on-ignition (LOI) analysis was performed on all core end samples using standard techniques, which involved sequential temperature treatments of 1 cc sediment to ascertain water content (60 °C overnight), carbonate content (950 °C for 2 h), and organic content in two parts (360 °C for 24 h for labile carbon; 550 °C for 4 h for black carbon; Heiri et al., 2001). The residual sediment after temperature treatments is an inorganic fraction that may include siliciclastic material, diatoms, oxides and sulfides, and it is herein after referred to as the siliciclastic fraction.

Pollen analysis was performed on the 20 core end samples of Hole B following standard techniques (Faegri and Iversen, 1989), with a set volume (0.5 cc) of sediment sieved with a 100 µm sieve, followed by sequential acid and alkali treatments (KOH, HCl, HF, and acetolysis) to isolate the pollen, spores, and other palynomorphs from the sediment matrix. Pollen and spore counts were then tallied to a minimum count of 300 pollen grains of terrestrial origin under 400X and 630X magnification. An exotic marker was added to each sample to allow calculation of pollen, spore, and other palynomorph (e.g. *Botryococcus*, microscopic charcoal, and pyrite spherules) concentrations.

Principal component analysis (PCA) of selected core end data (pollen, LOI, grain size) was performed to identify relationships between these variables. The data were first normalised to the standard deviation to meet the requirements of data normality required by PCA.

5 Initial results

5.1 Core scanning

The drilled depths and recovery information (Table 1) were combined with the MSCL data to derive a common depth scale ("hole corrected depth" used in Figs. 3, 4, and 8). Recovery gaps were generally assumed to occur at the base of core drives, except for the compaction of peat which resulted in sediment gaps at the hole top (Hole A – unknown; Hole B – 56 cm; Hole C – 70 cm). In most cases, the top depth of the MSCL data from each core section sequentially follows the base depth of the previous core section. If the previous core section had sediment gap, the top depth of MSCL core data was set at the measured drilling depth. The Hole corrected depth did not include the core end thickness (sediment in the core end), which ranged from 0 to 6.5 cm per drilled core (3 m). The difference between the drilled depth and the hole-corrected depth and core end thickness can be attributed to sediment expansion. Hole B depth was further corrected to account for sediment gaps seen in core sections during splitting (nine sections had gaps ranging from 2–8 cm) and thus constitutes the most representative depth with respect to the sediments accumulated in the crater.

The whole core MSCL-scanning results are presented in Fig. 3. The NGR displays small amplitude variations, with higher values of naturally occurring gamma radiation reflecting a higher content of mineral phases rich in potassium (K), uranium (U), and thorium (Th), such as clay minerals and K feldspar. The magnetic susceptibility (k_{LF}) values display a series of sharp and large amplitude changes and good reproducibility of depth between smoothed records from the three holes (Fig. 4). k_{LF} varies by more than 2 orders of magnitude, which indicates large changes in the concentrations of ferrimagnetic minerals. Intervals with high k_{LF} values generally correspond to low NGR values, especially in the lower section of the core (ca. 65–45 m). A series of peaks in k_{LF} of up to ca. 1000×10^{-5} SI were measured in the lowermost portion of the core from Hole B (Fig. 3). Such high values are not observed in the parallel core from Hole A and hint at possible differential post-depositional diagenesis, chemical precipitation or differential preservation of iron oxides in the different cores. The resistivity values vary mostly between 5–500 Ωm, which is a small range relative to the full range of variability found in geological samples (0.01–10 000 Ωm; Gueguen and Palciauskas, 1994). The resistivity over that range of values has two main controls: the porosity of the material (clays having lower values than sands), and the water content (Gueguen and Palciauskas, 1994). The intervals with consistent inter-hole resistivity primarily reflect the sediment porosity. The intervals with different resistivity behaviours (Fig. 4) reflect variable water content of the sediment and are useful for identifying potential minor disturbances in individual core sections from drilling operations, transport and handling of the cores.

5.2 Core description

The simplified lithology for Hole B (Fig. 4a) is based on visual observations of split core surfaces. The transition from the pre-lake sediment (unconsolidated sand-dominant breccia) to lake sediment is at ∼ 65 m and is marked by a shift to higher magnetic susceptibility and lower NGR values (Fig. 3). The lake sediment unit is 61 m thick and is capped

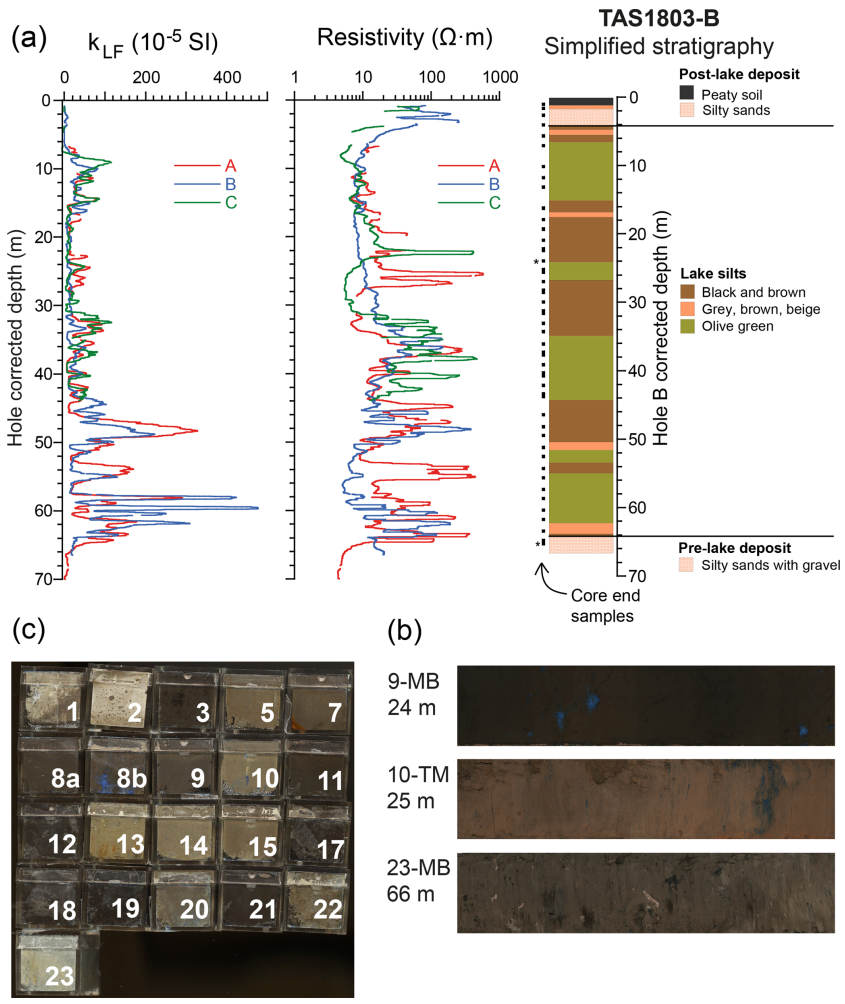

Figure 4. **(a)** Superimposed plots of volumetric magnetic susceptibility (k_{LF}) and resistivity data from Holes A, B, and C (smoothed over 50 data points), and simplified stratigraphy of site TAS1803 Hole B, which was split in half lengthwise, visually described, and photographed. The position of the core end samples and the paleomagnetic samples in Fig. 6 are indicated with square and asterisk (*), respectively. **(b)** Core end cube samples from Hole B, and **(c)** representative lithologies for black-brown silt (section 9-MB), olive-green silt (section 10-TM) and pre-lake deposits (section 23-MB). The blue mineral visible in sections 9-MB and 10-TM, and cubes 8b and 10 is tentatively identified as vivianite.

by a ∼ 3 m thick coarse-grained clastic layer followed by a ∼ 1 m thick peaty soil layer. The lake sediment is primarily composed of alternating black-brown and olive-green muds with gradual colour transitions. There are occasional sharp contacts between these lithologies and grey muds, mottled muds, and sandy layers. The sediment displays occasional vertical structures interpreted as drilling disturbances or deformation from pressure release between sediment layers of different densities.

Deposits of a white mineral, ranging from very small "specks" to structures > 3 cm in size (Figs. 2g and 4b–c), occur throughout the cores, in both black-brown and olive-green lake sediment units. These minerals were observed changing colour from white to blue upon contact with air (oxidation) and to bright yellow upon contact with a solution of ammonium molybdate and nitric acid. This indicates that it is a phosphate mineral that we tentatively identify as authigenic vivianite, which can form in organic and iron-rich lake sediments under reducing conditions (Rothe et al., 2016). Vivianite constitutes a promising target for uranium series dating (Goetz and Hillaire-Marcel, 1992; Nuttin et al., 2013).

5.3 Core end sample analyses

5.3.1 Physical properties (spectrophotometry and grain size)

The lake sediment deposit has distinctively finer grain sizes (48 samples; fine to coarse silts with mean size of 20 µm) than the pre-lake deposit (three samples; silty sands and sandy silts with mean size of 102 µm) and the post-lake de-

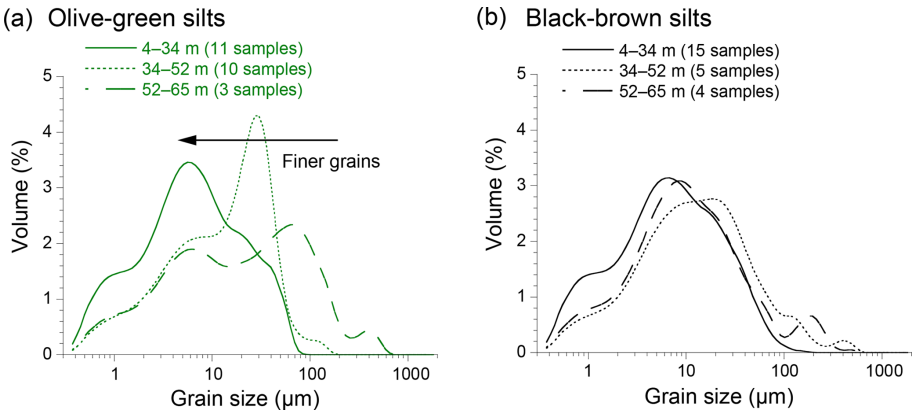

Figure 5. Mean grain-size distribution for the two main types of lake sediments at Darwin Crater. **(a)** Olive-green silts and **(b)** black-brown silts. Shifts to finer grain sizes in olive silts at 52 and 34 m define three depth intervals.

posit (three samples; silty sands and sandy silts with mean size of 167 µm) and has higher L^* values (darker colour). Within the lake sediment unit, L^* (black to white) and b^* (blue to yellow) have distinct values for the two principal lithotypes, with relatively lower L^* and b^* values in the black-brown silts and higher L^* and b^* values in the olive-green silts (Fig. 8d–e). The lake sediment succession above 34 m is more fine grained (fine silts with mean size of 12 µm; 26 samples) than the lowermost part (coarse silts with mean size of 28 µm; 22 samples). Figure 5 illustrates that this shift to finer grains is attributable to the olive-green silts. The mean grain-size distribution of olive-green silts in the uppermost part of the lacustrine sediment succession (4–34 m; solid line in Fig. 5a) is comparable to that of the black-brown silts (Fig. 5b); however, distinctively coarser grain sizes are present in the olive-green silts of the lowermost part (34–65 m; dashed lines in Fig. 5a).

5.3.2 Pollen

A total of 114 different pollen, spore, and palynomorphs were identified in the core end samples from drill Hole B. Overall, the pollen spectra are characterised by either (1) a high proportion of cold climate indicators (Poaceae, Asteraceae, and alpine taxa), including *Tubuliforidites pleistocenicus*, which is now palynologically extinct, and an Asteraceae pollen grain known only from glacial stage pollen flora in south-eastern Australia (Macphail et al., 1993) or (2) a high proportion of warm climate indicators (rainforest plants such as *Lagarostrobos franklinii*, *Nothofagus cunninghamii*, and *Phyllocladus aspleniifolius*; Fletcher and Thomas, 2007). While the coarse resolution of the pollen data currently precludes alignment of the record with glacial-to-interglacial climate shifts, observed variability in pollen abundance clearly reflect shifts between cooler and warmer periods.

5.3.3 Loss on ignition

LOI results reveal high detrital siliciclastic contents in the TAS1803 sediment succession, with values ranging from 38 % to 97 % and an average value of 80 %. The total organic carbon content varies between 1 % and 61 %. Carbonate content is consistently < 4 % for all core end samples.

5.3.4 Magnetic properties

The room-temperature magnetic properties indicate complex magnetic mineral assemblages. The concentration-dependant parameters display large amplitude changes (k_{LF}, χ, NRM, ARM, IRM), with low χ values characteristic of greigite, pyrrhotite, goethite, and hematite as well as high values indicative of magnetite, titanomagnetite, and maghemite (Peters and Dekkers, 2003). The magnetic assemblage is dominated by low-coercivity minerals, as indicated by mostly saturated samples in 0.3 T field (average $IRM_{0.3\,T}$ / $IRM_{2\,T}$ value of 0.96). The magnetic grain-size indicators (SIRM / k_{LF}, kARM / k_{LF}, and ARM / IRM) display different behaviours at times that indicate non-uniform down-core magnetic mineralogy. Stepwise alternating field (AF) demagnetisation of the lake sediment samples (cubes B9t, B10t, A20t, A21t, B23-MB-1, and B23-MB-4; at 2444, 2743, 5896, 6201, 6523, and 6531 cm hole-corrected depth) reveal a stable and well-defined component of NRM (Fig. 6) and the presence of high coercivity minerals (10 %–40 % of NRM remaining after AF 60 mT) and greigite (gyroremanent magnetisation; Fig. 6a; Roberts et al., 2011).

5.3.5 Principal component analysis

The first two PCA axes accounted for 55 % of the variance within the pollen, LOI, and grain-size data. PCA axis 1 (37 % explained variance) separates samples with high siliciclastic content, coarser grain size, and cold climate pollen taxa from samples with high organic content, finer grain size,

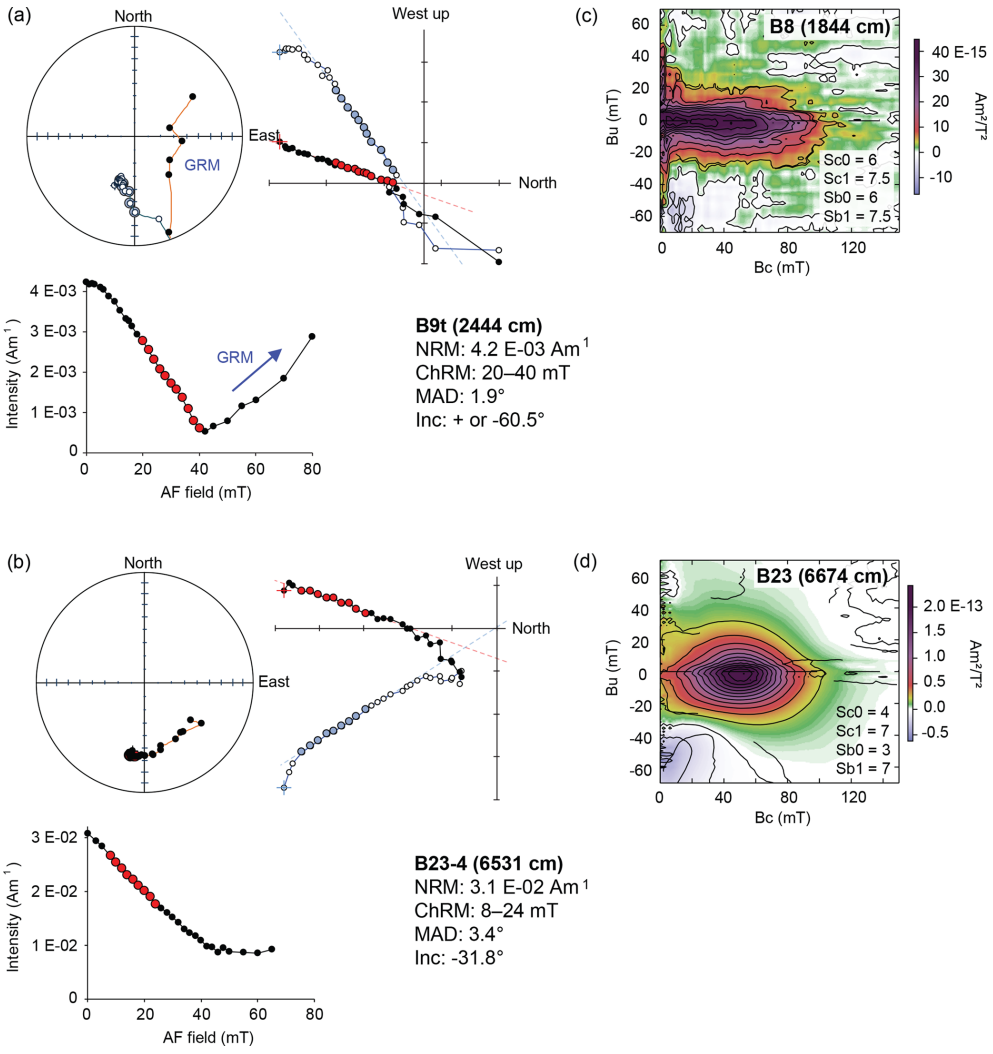

Figure 6. Selected paleo- and rock-magnetic results. Orthogonal projections and alternating field demagnetisation plot for **(a)** lake sediment sample B9t, and **(b)** oriented pre-lake sediment sample B23-4 displaying normal polarity. The down-core position of the samples are indicated by an asterisk in Fig. 5. The acquisition of gyroremanence (GRM) in AF >40 mT is typical of greigite (Roberts et al., 2011). A hard coercivity component is present in sample B23-4, where about one third of the NRM remains after AF 65 mT. First-order reversal curve (FORC) diagrams for samples **(c)** B8 and **(d)** B23. The closed peak distribution indicates single domain (SD) magnetic particles (Roberts et al., 2014), which are stable remanence carriers.

and warm climate pollen taxa (Fig. 7). This suggests that these parameters will help to differentiate between cold and warm climate states. PCA axis 2 (18 % explained variance) separates samples with cool climate rainforest pollen taxa, high aquatic taxa (*Isoetes*, *Botryococcus*, and *Myriophyllum*) medium grain size, and higher carbonate values. This suggests that parameters on this axis will help to differentiate between wetter and drier climates.

6 Discussion

The core logging data and pilot multi-proxy analysis of the TAS1803 cores show a stratigraphy broadly in agreement with the first drillings at Darwin Crater (Howard and Haines, 2007) and provide exciting new insights into the nature and timing of lake sediment deposition. Two main lithotypes alternate throughout the 61 m thick lacustrine sediment succession; dark organic-matter-rich silts and olive-green siliciclastic silts. These lithotypes are interpreted as being deposited under interglacial and glacial climate conditions, based primarily on the NGR, spectrophotometry (L^* and b^*), LOI, and pollen data (Fig. 8). The olive-green silts, with higher NGR counts, relatively high L^* and b^* values, higher siliciclastic content, coarser grain size, and more abundant cold climate pollen taxa correspond to the sediments deposited during glacial periods. The brown-black silts with low NGR counts, relatively low L^* and b^* values, low sili-

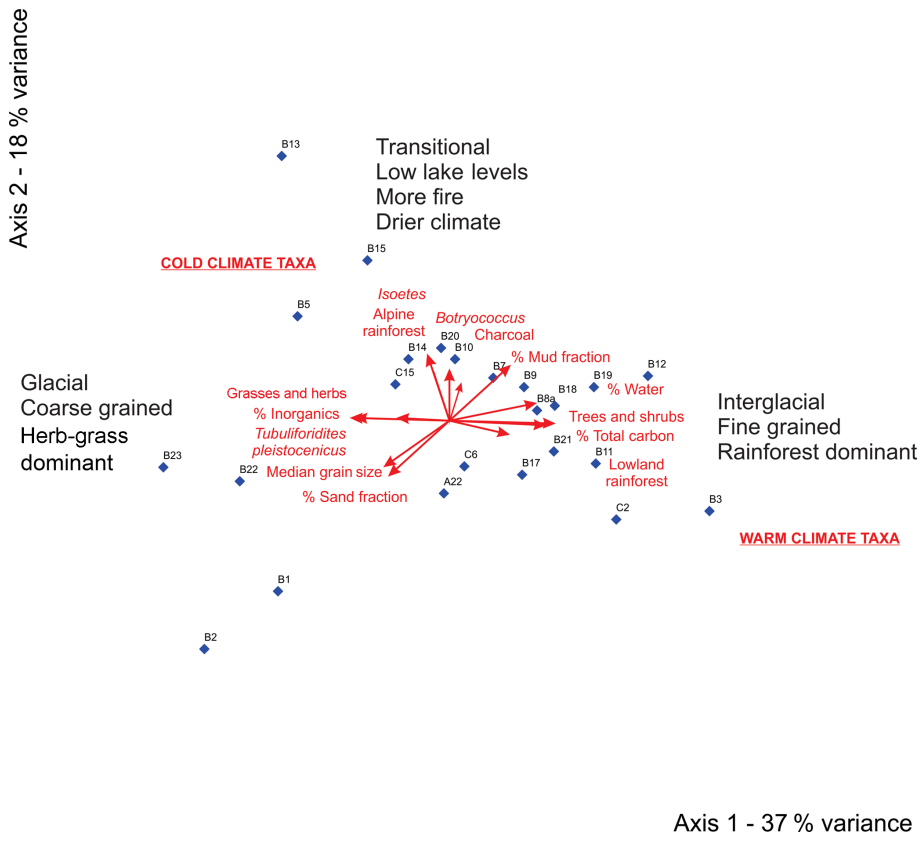

Figure 7. PCA bi-plot of core end data (pollen, LOI, and grain size). Correlations between data and axes $>0.4r^2$ are shown as red arrows (indicating the direction of correlation). A preliminary interpretation of the environmental significance of the axes is included.

ciclastic content, finer grains, and more abundant warm climate pollen taxa possibly correspond to sediments deposited during warm interglacial climate conditions (horizontal grey bars, Fig. 8). This is supported by the PCA of core end pollen and grain-size and LOI data, which indicate a principal gradient that separates samples that have coarse grains, low siliciclastic content, and pollen types indicative of a colder climate from samples that have fine grains, high organic content, and pollen types indicative of warmer climate conditions (Figs. 7 and 8j). These results are consistent with previous pollen studies, which indicate that glacial stages in western Tasmania are characterised by sparse open vegetation and poor organic soil development, which allows deposition of coarse siliciclastic sediment into lake basins (Beck et al., 2017; Colhoun, 2000; Colhoun et al., 1999). In contrast, interglacial periods in western Tasmania are characterised by maximum rainforest development, well-developed organic soils, and deposition of fine-grained and highly organic lake sediment (Beck et al., 2017; Colhoun, 2000; Colhoun et al., 1999).

The preliminary results of the Darwin Crater record suggest that the 61 m-thick lake deposit apparently covers a minimum of the seven full glacial cycles (interglacials tentatively highlighted in grey in Fig. 8). The length of each apparent glacial cycle is variable, which may reflect different sedimentation rates, lake levels, and climate regimes through time. Similarly, the different grain-size distributions in the glacial olive silts (Fig. 5) may reflect changes in lake levels, sediment sources, availability, preservation, and/or climate regimes. High-resolution Itrax surface element scanning, multi-proxy analyses, and dating of the sediment archive (OSL, ^{36}Cl, U series, and magnetostratigraphy) are underway and will be used to precisely define, date, and determine how many climate cycles are present, especially in the lower part of the core where some proxies display high-frequency changes.

The preliminary results provide evidence for reducing conditions in the lake sediments. The visual observation of vivianite throughout the cores and the magnetic evidence for greigite (see GRM in Fig. 6a) imply reducing conditions. Moreover, framboidal pyrite was observed under the microscope in the basal core end samples at >60 m depth (samples B21, A22, B22, and B23) as well as C6 (16.7 m). The magnetic susceptibility values are not null for these samples with pyrite, which suggests that iron oxides were not limiting the pyritisation process and/or that ferrimagnetic minerals formed sometime after pyrite formation. The k_{LF} variability, including intervals with near-zero values, does not seem

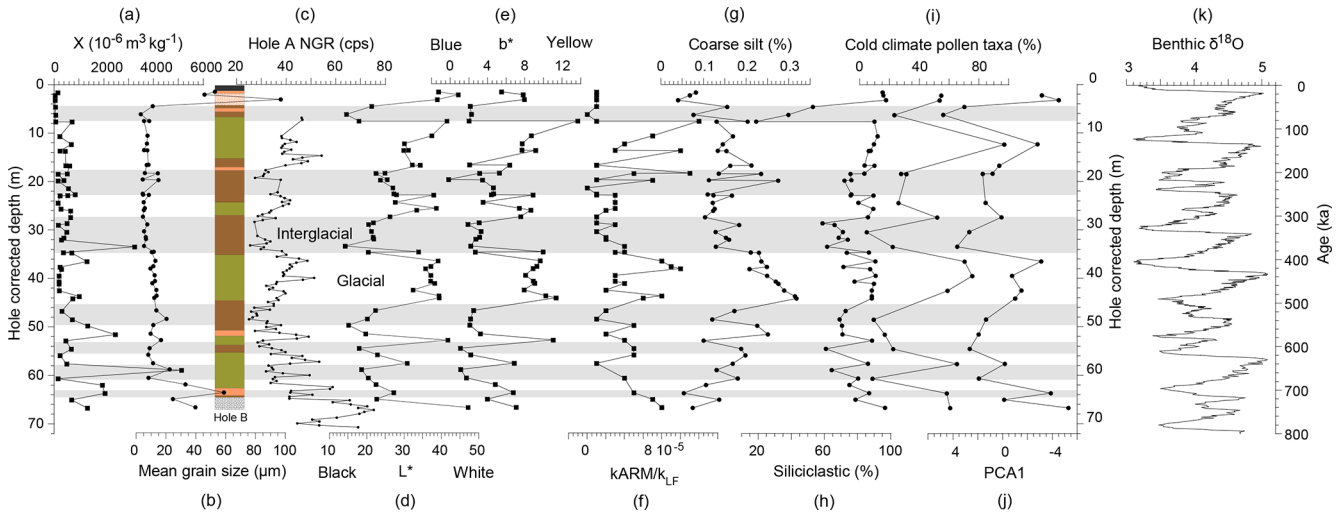

Figure 8. Selected parameters of the pilot multi-proxy analyses. **(a)** Mass-normalised magnetic susceptibility (χ), **(b)** mean grain size, **(c)** Natural gamma ray (NGR), **(d)** Color data L^* and **(e)** b^*, **(f)** Magnetic grain-size indicator kARM / k_{LF}, **(g)** coarse silt, **(h)** siliciclastic content, **(i)** cold climate pollen taxa, and **(j)** PCA axis 1 from left (warm) to right (cold). The starting and ending ages of the Darwin lacustrine sediment succession are unknown and will be identified by ongoing dating work. **(k)** A benthic $\delta^{18}O$ stack (Lisiecki and Raymo, 2005) is shown as a reference for Pleistocene glacial and interglacial climate cycles. A simplified lithology log for Hole B is included. The horizontal grey shaded bars tentatively indicate interglacial periods. Different symbols are used for different sample types: square symbols for measurements performed on the same cube samples, large circles for core end samples, and small circles for whole core MSCL samples.

correlated with the occurrence of pyrite, greigite, and vivianite. This suggests that factors other than the redox conditions may also control the k_{LF}, such as detrital input, biogenic iron oxides, their relative dilution in dia- and paramagnetic material, and/or chemical precipitation of magnetic minerals.

The lake in Darwin Crater formed sometime after 816 ± 7 ka ($^{40}Ar/^{39}Ar$ dating of Darwin glass; Lo et al., 2002) and lake sedimentation terminated during a warm interglacial period which will be identified by ongoing dating work (Sect. 7). Pilot paleomagnetic analysis of the deepest core of Hole B (cube samples TAS1803-B23-MB-1, -2, -3, and -4) indicate normal magnetic polarity 1 m under the lake deposit (Fig. 6b). If this remanence was acquired at the time of deposition, this result constrains the entire lacustrine deposition to an age younger than 773 ka (Matuyama-Brunhes geomagnetic reversal; Ogg, 2012; Singer, 2014), which is consistent with the inferred interpretation of seven glacial cycles discussed above. Ongoing paleo- and environmental magnetic investigations aim to characterise the complex magnetic mineral assemblage, investigate reducing diagenesis, and build a full-vector paleomagnetic field record and paleoclimate proxies.

7 Future plans

The next stages of the project will focus on producing a chronologically constrained paleoclimate record. Core splitting of Holes A and C, Itrax XRF scanning, and subsampling for the planned multi-proxy analyses are underway, and collaborators have been engaged for testing and development of other sediment proxies, such as beryllium isotopes, diatoms, Cladocera, aDNA, and stable isotopes.

7.1 Planned analyses

7.1.1 Dating

Our immediate focus is on building a robust chronostratigraphy including OSL dating of quartz and feldspar grains in the sandy deposits, ^{36}Cl in the pre-lake deposits, uranium–thorium dating of vivianite, and radiocarbon dating of the uppermost sediments. There is potential for a full-vector paleomagnetic record combining remanent magnetisation and cosmogenic nuclide beryllium-10 (^{10}Be) for relative dating, using the global geomagnetic dipole field at the millennial scale (eg., Channell et al., 2009; Ziegler et al., 2011; Simon et al., 2016), and for independent comparison to paleoclimate records, including other continental records, marine sediments, and ice cores (via cosmogenic isotopes). The preliminary pollen data indicate potential targets for a tuning approach to changes in orbital geometry and associated insolation changes and global-scale climate records such as the LR04 benthic oxygen isotope stack (Fig. 8k; Lisiecki and Raymo, 2005).

7.1.2 Paleoclimate

For paleoclimate reconstructions, we are planning to employ a multi-proxy and high-resolution approach combining physical and biogenic indicators, including pollen, charcoal, magnetic properties, grain size, stable isotopes, and elemental composition. The long record of the Darwin Crater will be combined with a long record (2–3 glacial cycles; unpublished data) from neighbouring Lake Selina (location in Fig. 1) to help to establish a long and continuous continental record in Australia and one of the oldest in the Southern Hemisphere. The proxy dataset will then be used to test global climate model simulations to help understand climate dynamics and interactions (e.g. Menviel et al., 2014; Pedro et al., 2018).

7.2 Questions that will be addressed

The multi-proxy dataset will be collectively applied to address the main question motivating this project: what is the role of the SWWs in the Pleistocene climate cycles? In particular, we will investigate the following questions:

- How did the SWWs respond during the transition from glacial to interglacial climates (e.g. terminations), and what were the environmental impacts of these changes in Western Tasmania?
- Are inferred changes in SWW position or intensity related to changes in the concentration of atmospheric CO_2 over glacial cycles, and can these be related to changes in the capacity of the Southern Ocean CO_2 sink?
- Do the SWWs shift equatorward during glacial phases (Toggweiler et al., 2006; Toggweiler, 2009)?
- Do the SWWs display the proposed pattern of poleward contraction and the coupling with North Atlantic climate variability during terminations (Denton et al., 2010)?
- What is the environmental impact of the middle Pleistocene transition (if recorded) on the terrestrial environment in the southern mid-latitudes?

It is anticipated that the new lake sediment paleoclimate record from the mid-latitude Australian region will constitute an empirical test for conceptual models of SWW dynamics and provide essential boundary conditions for predictive climate models.

Data availability. The pilot data presented here form the basis of several more detailed studies which are currently underway. Once these studies are finished and published, sediments from the curated Darwin Crater cores will be available to the scientific community, and the data will be made available in publicly available repositories.

Author contributions. MF, ALP, MB, HH, DH, and JP collaborated on the project design and funding acquisition. ALP, MF, TM, and RL were part of the drilling team. ALP, MF, TM, MM, and PG performed analysis in MF, AH, and HH's research laboratories. ALP wrote the original draft, and all co-authors provided contributions and reviews.

Competing interests. The authors declare that they have no conflict of interest.

Acknowledgements. Thanks to Max Harvey and Adam Debresteli for drilling operations and Bruce Maxwell for helicopter transport. Thanks to Malcolm Wallace and David Belton for fruitful discussions, Brad Dodrill from Lake Shore for performing FORC analysis, Rachael Fletcher for pollen sample preparation, and Chee Hoe Chuan for LOI analysis. This project is funded by the Australian Research Council (ARC) Discovery Indigenous project IN170100062 to Michael S. Fletcher and Agathe Lisé-Pronovost. Agathe Lisé-Pronovost is supported by a McKenzie Fellowship at the University of Melbourne and funding from La Trobe University's Deputy Vice Chancellor Research (DVCR). Tom Mallett is supported by a La Trobe University Postgraduate Research Scholarship. Joel B. Pedro acknowledges support from the European Research Council under the European Union's Seventh Framework Programme (FP7/2007-2013) and ERC grant agreement no. 610055 (the ice2ice project).

Edited by: Thomas Wiersberg
Reviewed by: Marie-Pierre Ledru, James M. Russell, and Hendrik Vogel

References

Allen, J., Cosgrove, R., and Garvey, J.: Optimality models and the food quest in Pleistocene Tasmania, J. Anthropol. Archaeol., 44, 206–215, 2016.

Barton, C.: Paleomagnetism, Age of the Darwin Crater, Bureau of Mineral Resources Yearbook, 36–37, 1987.

Beck, K. K., Fletcher, M.-S., Gadd, P. S., Heijnis, H., and Jacobsen, G. E.: An early onset of ENSO influence in the extra-tropics of the southwest Pacific inferred from a 14 600 year high resolution multi-proxy record from Paddy's Lake, northwest Tasmania, Quaternary Sci. Rev., 157, 164–175, 2017.

Blott, S. J. and Pye, K.: GRADISTAT: a grain size distribution and statistics package for the analysis of unconsolidated sediments, Earth Surf. Proc. Land., 26, 1237–1248, 2001.

Channell, J. E. T., Xuan, C., and Hodell, D. A.: Stacking paleointensity and oxygen isotope data for the last 1.5 Myr (PISO-1500), Earth Planet. Sci. Lett., 283, 14–23, 2009.

Colhoun, E. A.: Vegetation and climate during the last interglacial–glacial cycle in western Tasmania, Australia, Palaeogeogr. Palaeocl., 155, 195–209, 2000.

Colhoun, E. A. and van der Geer, G.: Pollen analysis of 0–20 m at Darwin Crater, western Tasmania, Australia, International Project of Paleolimnology and Late Cenozoic Climate, 11, 68–89, 1998.

Colhoun, E. A., Pola, J. S., Barton, C. E., and Heijnis, H.: Late Pleistocene vegetation and climate history of Lake Selina, western Tasmania, Quatern. Int., 57–58, 5–23, 1999.

Denton, G. H., Anderson, R. F., Toggweiler, J. R., Edwards, R. L., Schaefer, J. M., and Putnam, A. E.: The last glacial termination, Science, 328, 5986, https://doi.org/10.1126/science.1184119, 2010.

Egli, R.: VARIFORC: An optimized protocol for the calculation of non-regular first-order reversal curve (FORC) diagrams, Global Planet. Change, 110, 302–320, 2013.

Falster, G., Tyler, J., Grant, K., Tibby, J., Turney, C., Löhr, S., Jacobsen, G., and Kershaw, P. A.: Millenial-scale variability insouth-east Australian hydroclimate between 30 000 and 10 000 years ago, Quaternary Sci. Rev., 192, 106–122, 2018.

Faegri, K. and Iversen, J. (Eds.): Textbook of pollen analysis, Wiley, New York, 1989.

Fletcher, M.-S. and Thomas, I.: Modern pollen–vegetation relationships in western Tasmania, Australia, Rev. Palaeobot. Palyno., 146, 146–168, 2007.

Fudali, R. F. and Ford, R. J.: Darwin glass and Darwin Crater: A progress review, Meteoritics, 14, 283–296, 1979.

Garreaud, R. D.: Precipitation and circulation covariability in the extratropics, J. Climate, 20, 4789–4797, 2007.

Goetz, C. and Hillaire-Marcel, C.: U-series disequilibria in early diagenetic minerls from Lake Magali sediments, Kenya: Dating potential, Geochim. Cosmochim. Ac., 56, 1331–1341, 1992.

Gueguen, Y. and Palciauskas, V. (Eds.): Introduction to The Physics of Rocks, Princeton Universiy Press, UK, 1994.

Guyard, H., St-Onge, G., Pienitz, R., Francus, P., Zolitschka, B., Clarke, G. K. C., Hausmann, S., Salonen, V.-P., Lajeunesse, P., Ledoux, G., and Lamothe, M.: New insights into Late Pleistocene glacial and postglacial history of northernmost Ungava (Canada) from Pingualuit Crater Lake sediments, Quaternary Sci. Rev., 30, 3892–3907, 2011.

Harrison, R. J. and Feinberg, J. M.: FORCinel: An improved algorithm for calculating first-order reversal curve distributions using locally weighted regression smoothing, Geochem. Geophy. Geosy., 9, Q05016, https://doi.org/10.1029/2008GC001987, 2008.

Heiri, O., Lotter, A. F., and Lemcke, G.: Loss on ignition as a method for estimating organic and carbonate content in sediments: reproducibility and comparability of results, J. Paleolimnol., 25, 101–110, 2001.

Howard, K. T.: Physical trends in Darwin glass, Meteorit. Planet. Sci., 44, 115–129, 2009.

Howard, K. T. and Haines, P. W.: The geology of Darwin Crater, western Tasmania, Australia, Earth Planet. Sc. Lett., 260, 328–339, 2007.

Kalnay, E., Kanamitsu, M., Kistler, R., Collins, W., Deaven, D., Gandin, L., Iredell, M., Saha, S., White, G., Woollen, J., Zhu, Y., Chelliah, M., Ebisuzaki, W., Higgins, W., Janowiak, J., Mo, K. C., Ropelewski, C., Wang, J., Leetmaa, A., Reynolds, R., Jenne, R., and Joseph, D.: The NCEP/NCAR 40-year reanalysis project, B. Am. Meteorol. Soc., 77, 437–470, 1996.

Ledru, M.-P., Reimold, W. U., Ariztegui, D., Bard, E., Crósta, A. P., Riccomini, C., and Sawakuchi, A. O.: Why deep drilling in the Colônia Basin (Brazil)?, Sci. Dril., 20, 33–39, https://doi.org/10.5194/sd-20-33-2015, 2015.

Lisiecki, L. E. and Raymo, M. E.: A Pliocene-Pleistocene stack of 57 globally distributed benthic δ^{18}O records, Paleoceanography, 20, PA1003, https://doi.org/10.1029/2004PA001071, 2005.

Lo, C.-H., Howard, K. T., Chung, S.-L., and Meffre, S.: Laser fusion argon-40/argon39 ages of Darwin impact glass, Meteorit. Planet. Sci., 37, 1555–1562, 2002.

Macphail, M. K., Jordan, G. J., and Hill, R. S.: Key Periods in the Evolution of the Flora and Vegetation in Western Tasmania I. the Early-Middle Pleistocene, Aust. J. Bot., 4, 673–707, 1993.

Matchan, E. L., Philips, D., Traine, E., and Zhu, D.: 40Ar/39Ar ages of alkali feldspar xenocrysts constrain the timing of intraplate basaltic volcanism, Quat. Geochronol., 47, 14–28, 2017.

McLaren, S. and Wallace, M.: Plio-Pleistocene climate change and the onset of aridity in southeastern Australia, Global Planet. Change, 71, 55–72, 2010.

Melles, M., Brigham-Grette, J., Minyuk, P. S., Nowaczyk, N. R., Wennrich, V., DeConto, R. M., Anderson, P., Andreev, A. A., Coletti, A., Cook, T. L., Haltia-Hovi, E., Kukkonen, M., Lozhkin, A. V., Rosen, P., Tarasov, P., Vogel, H., and Wagner, B.: 2.8 Million years of Arctic climate change from Lake El"gygytgyn, NE Russia, Science, 337, 6092, https://doi.org/10.1126/science.1222135, 2012.

Menviel, L., Timmermann, A., Elison Timm, O., and Mouchet, A.: Deconstructing the Last Glacial termination: the role of millennial and orbital-scale forcings, Quaternary Sci. Rev., 30, 1155–1172, 2011.

Nuttin, L., Francus, P., Preda, M., Ghaleb, B., and Hillaire-Marcel, C.: Authigenic, detrital and diagenetic minerals in the Lagnua Potrok Aike sediment sequence, Quaternary Sci. Rev., 71, 109–118, 2013.

Ogg, J. G.: Geomagnetic Polarity Time Scale, Chapter 5, in: The Geologic Time Scale 2012, edited by: Gradstein, F. M., Ogg, J. G., Schmitz, M., and Ogg, G., Elsevier, 1176 pp., https://doi.org/10.1016/B978-0-444-59425-9.00005-6, 2012.

Pedro, J., Jochum, M., Cuisert, C., He, F., Barke, S., and Rasmussen, S. O.: Beyond the pipolar seesaw: Toward a process understanding of interhemispheric coupling, Quaternary Sci. Rev., 192, 27–46, 2018.

Peters, C. and Dekkers, M. J.: Selected room temperature magnetic parameters as a function of mineralogy, concentration and grain size, Phys. Chem. Earth, 28, 659–667, 2003.

Richardson, R. G.: Geophysical surveys of the Darwin Crater, Report UR1984_06, Mineral Resources of Tasmania, 1984.

Roberts, A. P, Heslop, D., Zhao, X., and Pike, C. R.: Understanding fine magnetic particle systems through use of first-order reversal curve diagrams, Rev. Geophys., 52, 557–602, https://doi.org/10.1002/2014RG000462, 2014.

Roberts, A. P., Chang, L., Rowan, C. J., Horng, C.-S., and Florindo, F.: Magnetic properties of sedimentary greigite (FeS4): an update, Rev. Geophys., 49, RG1002, https://doi.org/10.1029/2010RG000336, 2011.

Rothe, M., Kleeberg, A., and Hupfer, M.: The occurrence, identification and environmental relevance of vivianite in waterlogged soils and aquatic sediments, Earth-Sci. Rev., 158, 51–64, 2016.

Sagnotti, L.: Demagnetization Analysis in Excel (DAIE). An open source workbook in Excel for viewing and analyzing demagnetization data from paleomagnetic discrete samples and u-channels, Ann. Geophys.-Italy 56, 1–9, 2013.

Saunders, K. M., Roberts, S. J., Perren, B., Butz, C., Sime, L., Davies, S., Van Nieuwenhuyze, W., Grosjean, M., and Hodgson, D. A.: Holocene dynamics of the Southern Hemisphere westerly winds and possible links to CO_2 outgassing, Nat. Geosci., 11, 650–655, 2018.

Scholz, C. A., Karp, T., and Lyons, R. P.: Structure and morphology of the Bosumtwi impact structure from seismic reflection data, Meteorit. Planet. Sci., 42, 549–560, 2007.

Simon, Q., Thouveny, N., Bourlès, D. L., Valet, J. P., Bassinot, F., Ménabréaz, L., Guillou, V., Choy, S., and Beaufort, L.: Authigenic $^{10}Be/^{9}Be$ ratio signatures of the cosmogenic nuclide production linked to geomagnetic dipole moment variation since the Brunhes/Matuyama boundary, J. Geophys. Res.-Sol. Ea., 121, 7716–7741, 2016.

Singer, B. S.: A Quaternary geomagnetic instability time scale, Quat. Geochronol., 21, 29–52, 2014.

Skinner, L. C., Fallon, S., Waelbroeck, C., Michel, E., and Barker, S.: Ventilation of the Deep Southern Ocean and Deglacial CO_2 Rise, Science, 328, 1147–1151, 2010.

Sniderman, K. J. M., Pillans, B., O'Sullivan, P. B., and Kershaw, A. P.: Climate and vegetation in southeastern Australia respond to Southern Hemisphere insolation forcing in the late Pliocene-early Pleistocene, Geology, 35, 41–44, 2007.

Stephens, T., Atkin, D., Augustinus, P., Shane, P., Lorrey, A., Street-Perrott, A., Nilsson, A., and Snowball, I.: A late glacial Antarctic climate teleconnection and variable Holocene seasonality at Lake Pupuke, Auckland, New Zealand, J. Paleolimnol., 48, 785–800, 2012.

Toggweiler, J. R.: Shifting Westerlies, Science, 323, 1434–1435, 2009.

Toggweiler, J. R., Russell, J. L., and Carson, S. R.: Midlatitude westerlies, atmospheric CO_2, and climate change during the ice ages, Paleoceanography, 21, PA2005, https://doi.org/10.1029/2005PA001154, 2006.

Wilke, T., Wagner, B., Bocxlaer, B. V., Albrecht, C., Ariztegui, D., Delicado, D., Francke, A., Harzhauser, M., Hauffe, T., Holtvoeth, J., Just, J., Leng, M. J., Levkov, Z., Penkman, K., Sadori, L., Skinner, A., Stelbrink, B., Vogel, H., Wesselingh, F., and Wonik, T.: Scientific drilling projects in ancient lakes: Integrating geological and biological histories, Global Planet. Change, 143, 118–151, 2016.

Ziegler, L. B., Constable, C. G., Johnson, C. L., and Tauxe, L.: PADM2M: a penalized maximum likelihood model of the 0–2 Ma palaeomagnetic axial dipole moment, Geophys. J. Int., 184, 1069–1089, 2011.

Zolitschka, B., Anselmetti, F., Ariztegui, D., Corbella, H., Francus, P., Lücke, A., Maidana, N. I., Ohlendorf, C., Schäbitz, F., and Wastegård, S.: Environment and climate of the last 51000 years new insights from the Potrok Aike maar lake Sediment Archive Drilling prOject (PASADO), Quaternary Sci. Rev., 71, 1–12, 2013.

Sci. Dril., 25, 15–33, 2019
https://doi.org/10.5194/sd-25-15-2019

Scientific Drilling
Open Access

Understanding volcanic facies in the subsurface: a combined core, wireline logging and image log data set from the PTA2 and KMA1 boreholes, Big Island, Hawai‘i

Dougal A. Jerram[1,2,a], John M. Millett[3,4], Jochem Kück[5], Donald Thomas[6,7], Sverre Planke[1,3], Eric Haskins[6,7], Nicole Lautze[7], and Simona Pierdominici[5]

[1]CEED, University of Oslo, Oslo, Norway
[2]DougalEARTH, Solihull, UK
[3]VBPR – Volcanic Basin Petroleum Research, Oslo, Norway
[4]Department of Geology and Petroleum Geology, University of Aberdeen, Aberdeen, UK
[5]Helmholtz-Zentrum Potsdam, Deutsches GeoForschungsZentrum, Potsdam, Germany
[6]University of Hawai‘i at Hilo, 200 W. Kāwili St., Hilo, HI 96720-4091, USA
[7]Hawaii Groundwater and Geothermal Resources Center, University of Hawai‘i at Manoa, 1680 East West Road, Honolulu, HI 96822, USA
[a]visiting research fellow at: Earth, Environmental and Biological Sciences, Queensland University of Technology, Brisbane, Queensland, Australia

Correspondence: Dougal A. Jerram (dougal@dougalearth.com)

Received: 18 August 2018 – Revised: 20 December 2018 – Accepted: 2 January 2019 – Published: 12 June 2019

Abstract. To help understand volcanic facies in the subsurface, data sets that enable detailed comparisons between down-hole geophysical data and cored volcanic intervals are critical. However, in many cases, the collection of extended core intervals within volcanic sequences is rare and often incomplete due to challenging coring conditions. In this contribution we outline and provide initial results from borehole logging operations within two fully cored lava-dominated borehole sequences, PTA2 and KMA1, on the Big Island of Hawai‘i. Data for spectral gamma, magnetic susceptibility, dipmeter resistivity, sonic, total magnetic field, temperature and televiewer wireline logs were successfully acquired for the open hole interval ca. 889 m to 1567 m within the PTA2 borehole. Spectral gamma was also collected from inside the casing of both wells, extending the coverage for PTA2 to the surface and covering the interval from ca. 300 to 1200 m for KMA1. High-quality core material was available for both boreholes with almost complete recovery which enabled high-resolution core-to-log integration. Gamma data are generally low commonly in the range ca. 7–20 gAPI but are shown to increase up to API of ca. 60 with some intrusions and with increases in hawaiite compositions in the upper part of PTA2. Velocity data are more variable due to alteration within porous volcanic facies than with burial depth, with a general degrease down-hole. The high-resolution televiewer data have been compared directly to the core, enabling a comprehensive analysis of the variations in the televiewer responses. This has enabled the identification of key features including individual vesicles, vesicle segregations, strained vesicles, chilled margins, rubble zones, intrusive contacts and pāhoehoe lobe morphologies, which can be confidently matched between the televiewer data and the full diameter core. The data set and results of this study include findings which should enable improved borehole facies analysis through volcanic sequences in the future, especially where down-borehole data and images but no core are available.

Published by Copernicus Publications on behalf of the IODP and the ICDP.

1 Introduction

Volcanic rocks (including intrusive and extrusive) occur in a variety of facies which reflect their composition, mode of emplacement and interaction with their host environment. The resultant volcanic units in turn comprise highly variable rock properties. When we examine the subsurface by remote geophysical tools we see an expression of these associated physical properties rather than the facies themselves, and where volcanic facies exist we can often be faced with a number of challenges in interpreting what we see, or in some cases cannot see. To this extent we can ask the following question: what are the key volcanic facies, what are their physical properties and how are these properties spatially distributed? Good onshore analogues provide an integral method of investigating these rock properties and heterogeneities in a way to help inform us as to their likely properties in the subsurface. Subsurface examples where fully cored sections through volcanic units combined with a comprehensive set of down-borehole remote data do exist, most notably from scientific drilling; however, examples where near-complete recovery exists are more limited (Ildefonse et al., 2007). This is in main part due to the highly variable physical properties of volcanic rocks and the consequence of these properties on drilling operations (Teagle et al., 2012; Millett et al., 2016), resulting commonly in challenging drilling conditions and incomplete core recovery. This is also compounded by many such drilling operations being conducted offshore, where ocean conditions make core recovery more challenging still. In consequence, our general understanding of volcanic facies in the subsurface is fairly comprehensive, but numerous gaps remain at the detailed level which require new data to better constrain the relationships between geophysical observations and formation characteristics.

Some significant studies do exist that have looked at the nature of volcanic rocks in the subsurface from borehole data (e.g., Planke, 1994; Helm-Clark et al., 2004; Bartetzko et al., 2005; Nelson et al., 2009). Perhaps some of the most significant developments in the interpretation of volcanic rocks from borehole data have come from the combined Ocean Drilling Program (ODP) and Integrated Ocean Drilling Program (IODP) literature which records the scientific findings of extensive offshore coring programs targeting both the oceanic crust and many of the world's volcanic rifted margins (e.g., Goldberg, 1997; Brewer et al., 1998; Teagle et al., 2012). In more recent years, offshore exploration for hydrocarbons in many of the world's rifted margins has also increased the number of data and studies relating to downhole measurements through volcanic successions (e.g., Nelson et al., 2009, 2015; Andersen et al., 2009; Watton et al., 2014a; Millett et al., 2015; Fornero et al., 2018). In more direct relevance to this study, findings associated with drilling operations on Hawai'i including the over 3 km deep HSDP2 borehole have also led to significant advances in the identification and interpretation of volcanic rocks in the subsurface (e.g., Katz and Cashman, 2003; Garcia et al., 2007). Despite the many advances in volcanic borehole analysis, many challenges still remain. These include the delineation of volcanic intra-facies from remote-sensing data where a full core is not available along with an associated relative lack of high-quality petrophysical data for relevant volcanic intra-facies from variable depths and degrees of alteration. In most instances, the lack of fully cored intervals within the volcanic units hinders a full assessment of the volcanic facies present, especially in scenarios where large overlaps in petrophysical property ranges exist (e.g., Bartetzko et al., 2005; Nelson et al., 2009).

This contribution presents results from wireline logging operations undertaken in two fully cored boreholes within the Humu'ula Saddle region between the Mauna Kea and Mauna Loa volcanoes on the Big Island of Hawai'i (Fig. 1). The primary aim of this project was to attain high-quality wireline log data from the boreholes in order to undertake detailed core–log integrations for the penetrated volcanic facies. The two boreholes, PTA2 and KMA1, penetrated 1764 and 1528 m of subaerial lava-dominated sequences with subordinate minor intrusives and sediments respectively, with the entire sections fully cored. Lava facies include pāhoehoe, 'a'ā and transitional types on a range of scales. The volcanic sequences comprise basaltic to picritic shield stage lavas of Mauna Kea capped by a thinner sequence of post-shield basalt-dominated (Hamakua Volcanics) to hawaiite-dominated (Laupahoehoe Volcanics) lavas (Frey et al., 1990). A wireline logging data set including spectral gamma, magnetic susceptibility, dipmeter resistivity, sonic, total magnetic field, temperature and televiewer images was acquired within the open hole interval ca. 889 to 1567 m of the PTA2 borehole. Additionally spectral gamma was collected from inside the casing of both wells, extending the coverage for PTA2 up to 0 m depth and covering the interval from ca. 300 to 1200 m for KMA1. The availability of a good-quality, near-continuous core for each well, along with the range and types of encountered volcanic facies, enabled a unique opportunity to improve our understanding of borehole characterization in volcanic sequences by comparison of remote data directly with cored intervals. This database, and in particular the comparison of image log data with core, highlights the potential for subsurface volcanic facies analysis where core data are not available.

2 Background and data acquisition

The boreholes investigated within this paper were drilled as part of the Humu'ula Groundwater Research Project (HGRP), which commenced in 2013, affiliated with the Hawai'i Groundwater and Geothermal Resources Center (University of Hawai'i). One borehole (PTA2) was drilled on the Island of Hawai'i at the Pohakuloa Training Area (PTA) in 2013 and a second (KMA1) was drilled in 2015 ca. 11 km

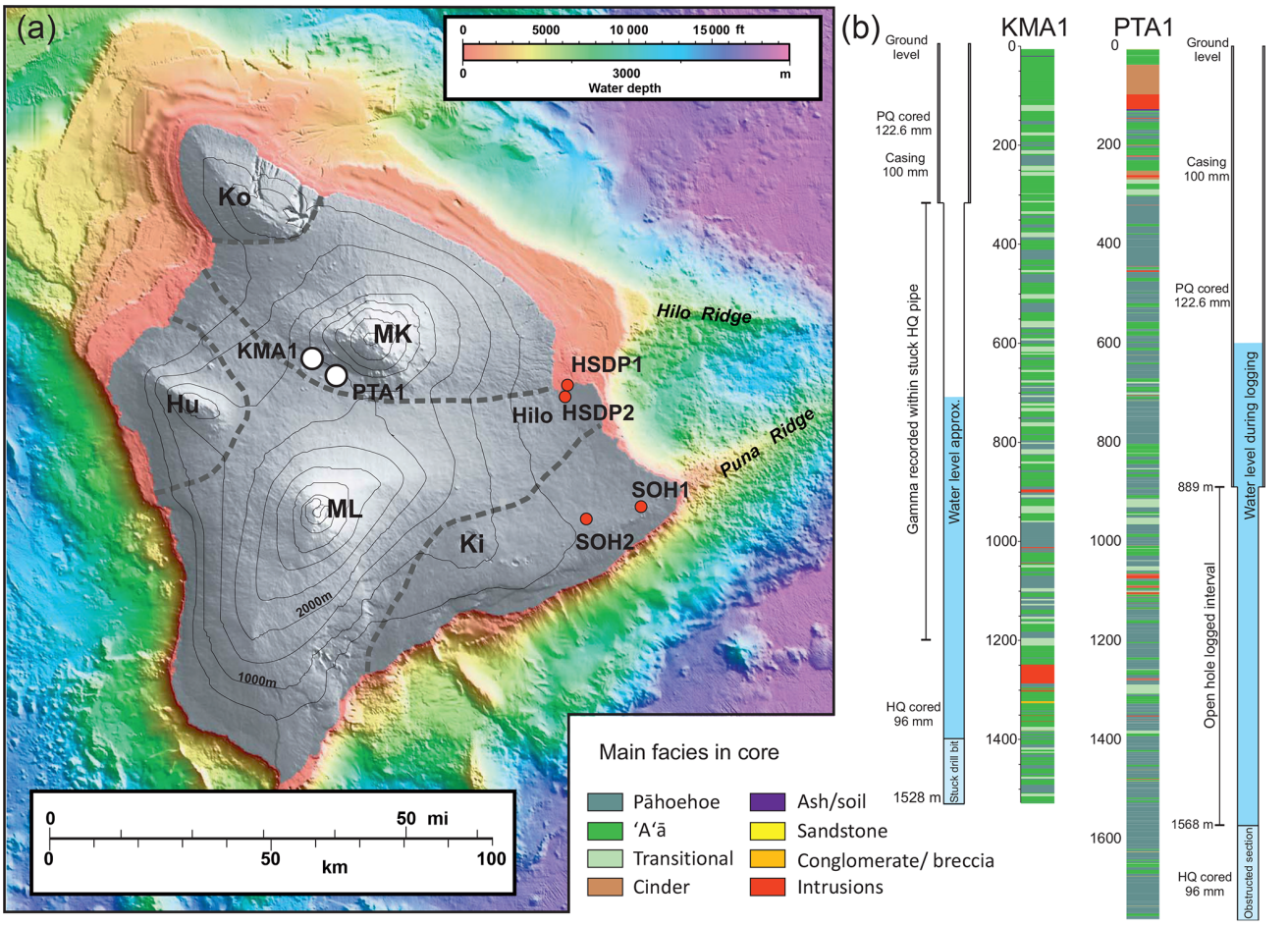

Figure 1. **(a)** Location map of the PTA2 and KMA1 boreholes on a topographic and bathymetric map of Hawai'i (bathymetric map from USGS, Eakins et al., 2003). Locations of a selection of additional cored boreholes drilled on Hawai'i are also indicated (red dots) (SOH4 1989, 2.0 km; SOH1 1991, 1.7 km; HSDP1 1993, 1.1 km; HSDP2 1999, 3.1 km) (see also Garcia et al., 2007) (MK – Mauna Kea, ML – Mauna Loa, KI – Kilauea, HU – Hualālai, Ko – Kohala). **(b)** The cored sections of PTA2 and KMA1 are indicated with their generalized volcanic facies and well information.

to the NW (Fig. 1). HGRP's primary scientific objective was to research and characterize the groundwater resources in Hawai'i Island's saddle region, which comprises a sequence of entirely subaerial lava flow with additional minor intrusions and sediments. The US Army, through the Army Corps of Engineers' Cooperative Ecosystem Studies Unit (CESU), provided funding for the drilling and core collection, whereas the US National Science Foundation provided funding for the initial characterization and logging of the core. The initial part of this project did not plan for any geophysical logging data acquisition.

Discussions with Donald Thomas and Nicole Lautze (the principle project leaders) and Eric Haskins (core archive manager), from the University of Hawai'i, were initially sparked from scientific exchanges at the American Geophysical Union (AGU) 2013 meeting in San Francisco, USA. These exchanges identified the cored data set as a potentially valuable resource for further analysis. The idea of generating a complete core-to-remote-sensing suite for these wells was then further explored by Dougal Jerram (DougalEARTH Ltd. and University of Oslo), Sverre Planke (VBPR and University of Oslo) and John Millett (VBPR and University of Aberdeen) along with Donald Thomas. Funding for geophysical logging of the two boreholes was proposed and provided by the VMAPP (Volcanic Margin Petroleum Prospectivity) project (VBPR, DougalEARTH, and TGS) as part of the research module program. The aim was to generate one of the most complete data sets of fully cored volcanics with associated borehole measurements, to aid in our understanding of volcanic facies in the subsurface. The Operational Support Group (OSG) of ICDP (International Continental Scientific Drilling Program) at the GFZ German Research Centre for Geosciences in Potsdam (Germany) was then approached to undertake the logging. The logging project reported here was formed from a collaboration between VMAPP, the University of Hawai'i and OSG. Through this collaboration, the

Table 1. Summary data of lithologies (facies) intersected in hole PTA2.

PTA2 unit summary (total cored section thickness: 1759.1 m)							
Unit type	No. of units	No. of flows or subunits	Occurrence	Thickness (m)			Percent of section
				total	avg. unit	avg. flow or subunit	
Pāhoehoe	228	1933	57.1 %	1087.8	4.8	0.6	61.8 %
Transitional	18	123	4.5 %	99.7	5.5	0.8	5.7 %
ʻAʻā	113	211	28.3 %	400.1	3.5	1.9	22.7 %
Intrusives	21	37	5.3 %	66.1	3.1	1.8	3.8 %
Ash	2	2	0.5 %	0.2	0.1	0.1	0.01 %
Cinder/scoria	3	46	0.8 %	100.3	33.4	2.2	5.7 %
Soil	1	1	0.3 %	3.1	3.1	3.1	0.18 %
Sandstone	1	1	0.3 %	0.15	0.15	0.15	0.01 %
Conglomerate	10	10	2.5 %	1.37	0.14	0.14	0.08 %
Breccia	2	2	0.5 %	0.37	0.19	0.19	0.02 %
Grand total	399	2366	100.0 %	1759.1	–	–	100.0 %
Total flow	359	2267	90.0 %	1587.6	–	–	90.25 %
Total nonflow	40	99	10.0 %	171.5	–	–	9.75 %

(1) There is one extremely thick laccolith or lopolith at the base of the Laupahoehoe section that is 29.7 m thick, nearly doubling the overall thickness of intrusives in the section.
(2) Cinder/scoria intervals are thought to represent cones or flanks of cones built from this material during the post-shield stages of Mauna Kea's growth (alternating with pāhoehoe of constant lithology in the deeper cases; see stratigraphic column).
(3) Potential ash and soil intervals are currently being interpreted by Dr. Nicole Lautze; the number of these units may increase based on these interpretations.
(4) While most of the conglomerate units are interpreted as fluvial or colluvial, the uppermost (recovered in the first run of drilling) is thought to be glacial in origin.

project gained full access to the core material enabling the unique opportunity of undertaking detailed core–log integration from a thick sequence of heterogeneous lava facies in order to improve our understanding of the geophysical response of these facies under differing subsurface regimes.

2.1 Borehole coring operations

The overall purpose of the project was an effort to better define hydrologic conditions in the central region of Hawaii Island. The prevailing hydrologic model for Hawaii is one of a relatively thin basal freshwater lens underlain by saltwater-saturated rocks below (e.g. Thomas et al., 1996). The findings of the Hawai'i Scientific Drilling Project (HSDP) for freshwater-saturated rocks at depths of ~ 3 km below sea level near the Hawaii Island shoreline suggested that much more substantial freshwater resources were present within the interior of the island (Stolper et al., 2009). Surface resistivity surveys (Pierce and Thomas, 2009) identified subsurface conductive features that were consistent with high-elevation groundwater and two sites were selected for deep test holes. In light of the near absence of detailed stratigraphic data for the interior of Hawai'i Island, diamond wireline core drilling was selected as a means of both defining the elevation of the water table and recovering information on the stratigraphic features associated with high-elevation groundwater in the area.

The drilling approach was to install shallow, large-diameter conductor casing, core to a depth of ~ 65 m with PQ (122 mm diameter) coring tolls, open the hole with rotary tools and set surface (177 mm) casing to that depth, continue drilling with PQ to stable formations at one-third to one-half of the target depth, set (114 mm) casing to that depth, and continue to total depth (TD) with HQ (96 mm) coring tools. The PTA2 borehole was cored to a depth of 889 m (top of casing at 1943 m) with PQ tools and to at total depth of 1764 m with HQ tools. The KMA1 test hole was drilled to a depth of 298 m with PQ tools and to TD of 1531 m with HQ. Core recovery for the PTA2 hole averaged for the entire depth was about 97 %; core recovery for the KMA1 hole over the entire depth was about 91 %. A summary of the lithology of the cores from the PTA2 and KMA1 holes is presented in tabular form (see Tables 1 and 2).

More information about the project along with a complete photographic archive of the two borehole cores is available at the HGRP website (https://www.higp.hawaii.edu/hggrc/projects/humuula-groundwater-research-project/, last access: 2 February 2019). No geophysical logging data acquisition was planned as part of the HGRP project.

2.2 Logging operations

The initial logging project outline involved a single logging operation planned for December 2015 during which time logging of the open hole sections of both PTA2 and KMA1 was scheduled. Sonic, resistivity, spectral gamma, dipmeter, magnetic susceptibility, temperature, total magnetic field and televiewer tool logging were planned for both wells in order

Table 2. Summary data of lithologies (facies) intersected in hole KMA1.

KMA1 unit summary (total cored section thickness: 1522.2 m)							
Unit type	No. of units	No. of flows or subunits	Occurrence	Thickness (m)			Percent of section
				total	avg. unit	avg. flow or subunit	
Pāhoehoe	98	418	30.2 %	409.5	4.2	1.0	26.90 %
Transitional	49	120	15.1 %	239.8	4.9	2.0	15.75 %
ʻAʻā	168	236	51.9 %	819.7	4.9	3.5	53.85 %
Intrusives	7	16	2.2 %	48.5	6.9	3.0	3.19 %
Ash/soil/sand	1	1	0.3 %	1.0	1.0	1.0	0.07 %
Breccia	1	1	0.3 %	3.7	3.7	3.7	0.24 %
Grand total	324	792	100.0 %	1522.2	–	–	100.0 %
Total flow	315	774	97.2 %	1469.0	–	–	96.5 %
Total nonflow	9	18	2.8 %	53.2	–	–	3.5 %

Table 3. Summary of all logging runs from the project.

Sonde run	Date	Logging speed (m min^{-1})	Logged interval (m)	Borehole	Logging trip
TS1-SGR	15/02/2016	2 to 3	313–1204	KMA1	1
TS1-SGR	17/02/2016	2 to 4	0–808	PTA2	1
TS1-SGR-MS	15/06/2016	2	742–1567	PTA2	2
TS1-BS	16/06/2016	6 to 7	885–1567	PTA2	2
TS1-DIP	16/06/2016	6 to 7	908–1567	PTA2	2
ABI43	17/06/2016	1.6	886–1567	PTA2	2

to allow detailed volcanic facies assessment and to test correlations between the two boreholes. Neutron and density tools have also been demonstrated to give important insights into volcanic facies (e.g., Planke, 1994; Shervais et al., 2013); however, due to the active radioactive sources in both tools, it was not possible to include these logs in the logging suite on Hawaii due to operational restrictions. In the end two logging trips were undertaken, the first in February 2016 and the second in June 2016, and only the open hole section of PTA2 was logged due to major complications associated with the final stages of drilling within KMA1 and subsequent efforts to resolve the resulting stuck pipe problem. In Fig. 2 selected photographs of the site and operations are presented.

The slim hole wireline logging tools deployed during the logging operations were made by Antares, Germany, except for the acoustic televiewer ABI43, made by ALT, Luxembourg. All tool combinations included a natural total gamma ray (GR) measurement for depth correlation except for the ABI43. Logging was undertaken using a Comprobe electric winch with a Rochester 3/16″, four-conductor cable provided by HGRP. The depth reference for all logging runs was ground level at ca. 1943 m above sea level (based on GPS elevation determination). Details of all the combined logging runs, logging speeds and measured intervals are given in Table 3.

2.3 Wireline log and televiewer processing

All borehole data were screened and processed by GFZ prior to interpretation. Depth corrections were applied to all logs primarily by gamma peak matching other than for the ABI43 which does not contain a gamma sensor. For depth correlation of the ABI43 logs the caliper data from the DIP meter proved useful in comparison with the televiewer travel time and amplitudes which are also highly sensitive to borehole size. The accuracy of this caliper match is even better than that of the GR match. Due to the very low total gamma response of the open hole section, the individual spectral gamma results for K, Th and U have been deemed below quantitative spectrum values and therefore only the total gamma is presented for this interval.

The raw sonic waveform data were processed using a combination of first arrival trace picking for P and S waves along with additional semblance analysis. In general, the P-wave picking was straight forward for most of the borehole; however, a strong direct wave interferes with the P-wave first arrival at lower velocities in the near receiver (Fig. 4), making accurate picking challenging. The S-wave arrival also becomes highly unclear in the upper part of the well above ca. 1100 m. Velocity data for the open hole section of PTA2 are therefore of mixed quality with generally improved confidence levels towards the base of the well.

Figure 2. **(a)** Drill truck at the KMA1 site. **(b)** Spectral gamma logging within casing at PTA2. **(c)** Jochem Kück and Marco Groh (GFZ) with the sonic sonde at PTA2. **(d)** Borehole televiewer sonde being lowered into the borehole at PTA2. **(e)** Eric Haskins cuts sections of core for additional sampling.

The televiewer data from PTA2 were acquired at the highest resolution and optimized logging speed to ensure the highest possible data quality. For both travel time and amplitude, static and dynamic (10 cm vertical window) normalizations were applied to improve imaging (Fig. 5). Each channel (raw, static, dynamic) for travel time and amplitude in particular displays minor to major differences in the resulting images depending on the scale and variations between different intervals and features. All output logs are displayed with a logarithmic scale with the ranges optimized for clarity (Fig. 5). Breakouts are very common in some intervals of the wellbore (e.g., ca. 1223.5 and ca. 1352 m). Examples of both key seat and breakouts are present. The correlation between sonic Vp and the televiewer amplitude data is variable, with some intervals showing clear associations (e.g., Fig. 5c) while in other examples the expected relationships are not apparent.

Figure 3. Example of the exceptional core recovery from the wells (further examples can be seen in Figs. 9 and 10).

In summary, the logging data derived from the PTA2 borehole includes very high-quality data for the majority of the open hole logged sequence, and the separate log traces have been confidently depth matched. Accurate comparison between the borehole core and the inter-relationships of the geophysical properties can therefore be undertaken with similar confidence.

3 Wireline logging results

Within this section, results from the borehole logging are presented. The log data for the main open hole logged section are summarized in Fig. 6 along with a summary of the volcanic facies based on the core logging (Thomas and Haskins, 2013). Data from each sonde are described individually in relation to the volcanic stratigraphy in the following section. Unless otherwise stated, the presented logs display data with a 3 m running average applied to reduce data noise.

3.1 Caliper

The four-arm caliper sonde gives information on borehole diameter and shape. The caliper results from the open hole section of PTA2 display a generally good hole condition with a uniform diameter of ca. 98 mm (HQ core bit outer diameter ca. 96 mm) for the majority of the logged section (Fig. 6). Semi-continuous breakouts occur through large intervals of the borehole associated with the in situ stress field (breakouts parallel to minimum horizontal stress). These breakouts are often best developed within the most coherent and stiff facies, e.g., ʻaʻā interiors and intrusions, and are being investigated in ongoing research relating to the in situ stress regime of the Mauna Kea volcano.

The borehole diameter only exceeds 20 mm off-gauge in eight separate intervals, and, in a number of these cases, only one of the two caliper arm pairs exceed this deviation from the baseline indicative of an irregular borehole shape (e.g., key seat). Wider diameters occur over the full range of major facies within the borehole (Fig. 6); however, correlation between these and facies within some intervals is also observed. Most notably, in the upper ca. 300 m of the logged interval, the largest washouts occur dominantly either within ʻaʻā and transitional facies or at the transitions between these and pāhoehoe-dominated sequences. Washouts are also closely associated with minor intrusions leading up to ca. 1100 m. These observations appear consistent with the generally rubbly loose nature of ʻaʻā and, to a lesser degree, transitional

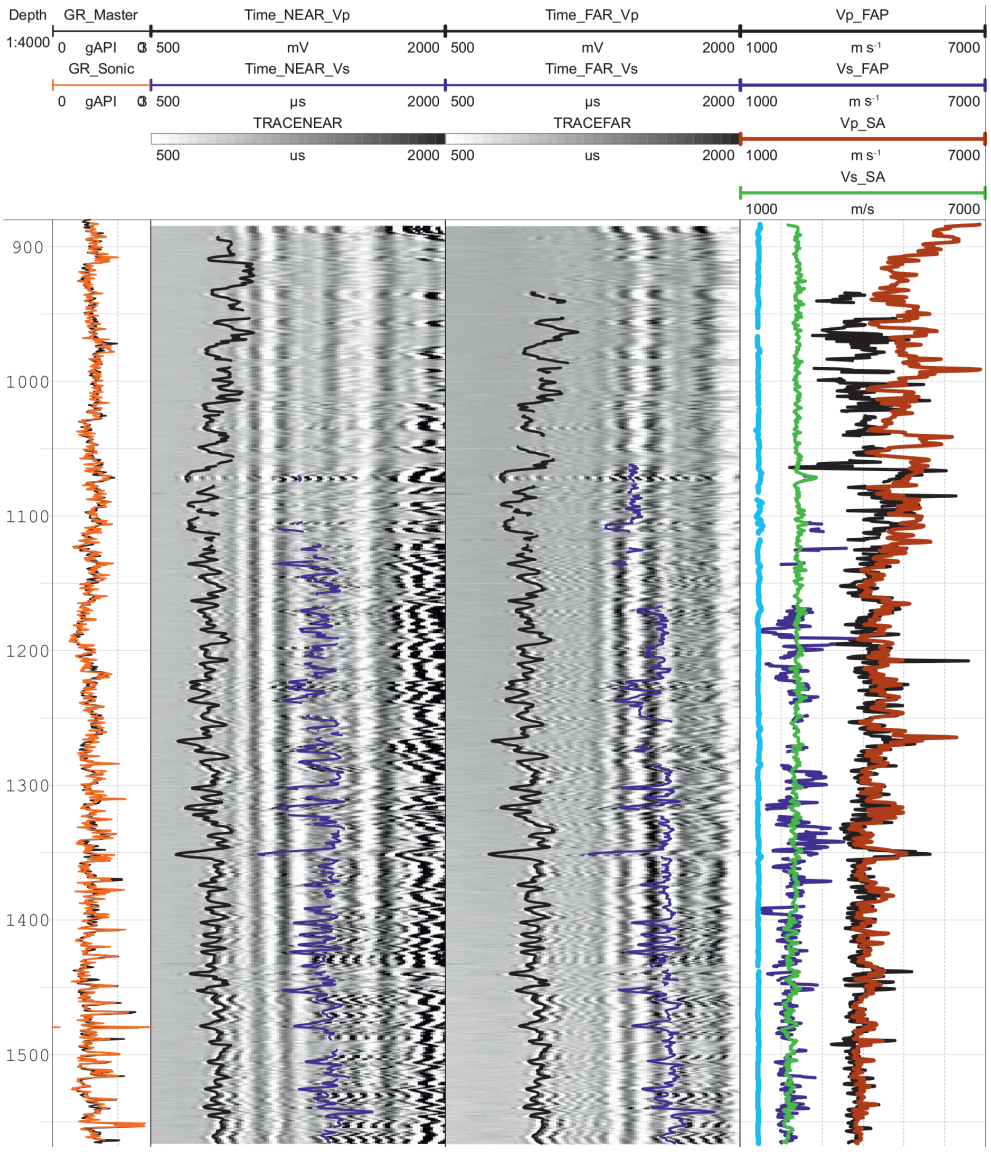

Figure 4. Example of raw borehole sonic waveform data analysis from PTA2. Near- and far-receiver traces (50 cm spacing) with first arrival picking (FAP) results. The derived velocities are shown on the right side together with results from a separate semblance analysis (SA). The light-blue curve is the measured water wave velocity, and total GR is shown for depth correlation.

lava flow margins which would be expected to cave most easily (Millett et al., 2016).

Fractures associated with intrusions along with the baking effect that they have on host rocks are also commonly associated with borehole breakouts in volcanic boreholes and therefore the caliper response in the upper part of the well is largely as expected. The largest washouts in the borehole occur in the lower part of the well, e.g., at ca. 1350, 1450 and 1520 m. These examples are less facies constrained, with two occurring largely within pāhoehoe sequences and, therefore, fracturing and/or alteration, known to be more pervasive within the lower borehole intervals, may have contributed to borehole instability in these cases.

3.2 Gamma

Gamma log responses are related to the abundance of the radioactive large ion lithophile elements K, U and Th in the measured rock volume. In volcanic rocks, the abundance of these elements is related to the primary magma composition that produced the resulting volcanic facies. In general, basaltic igneous rocks have very low abundances of the K, U and Th, especially in tholeiitic low K melts. Due to the general incompatibility of these elements during early fractional crystallization of basaltic melts, their abundance and therefore related API gamma responses increase with fractional crystallization and differentiation. Gamma ray responses can therefore be a good proxy for the degree of differentiation

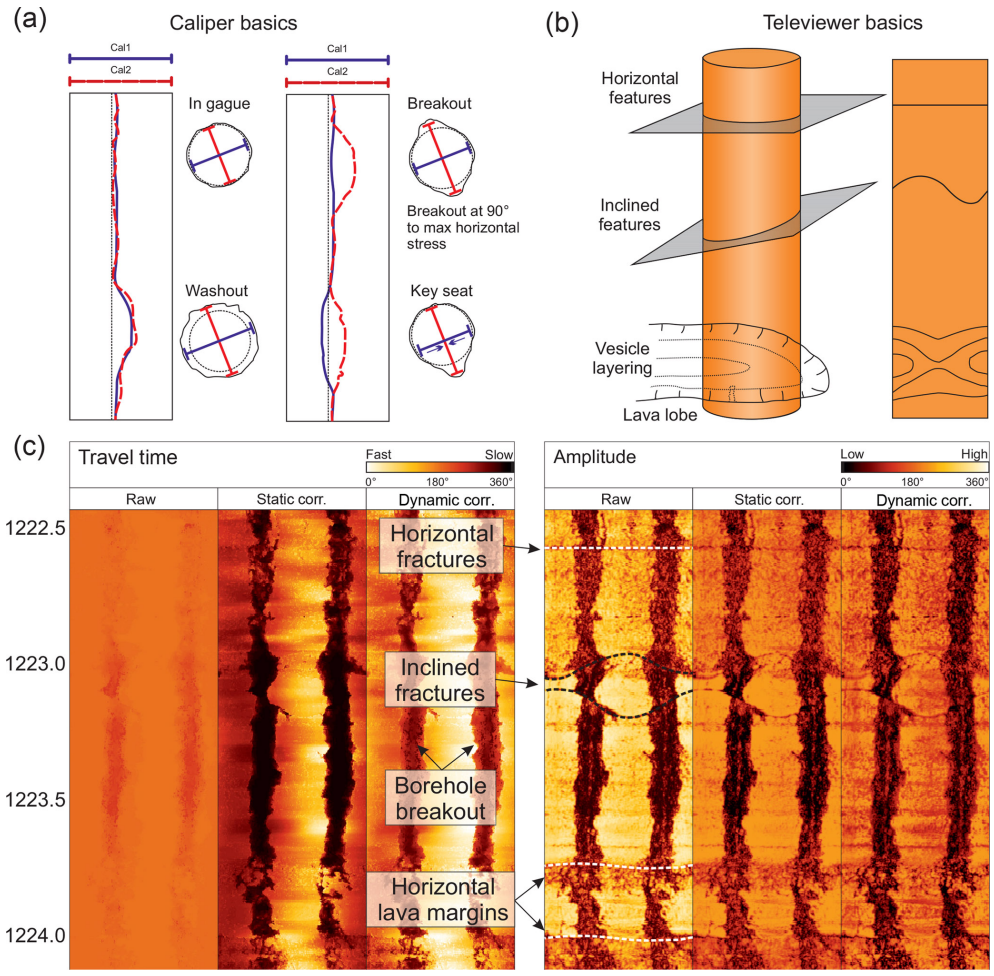

Figure 5. **(a)** Simplified schematic displaying the four-arm caliper response to common borehole conditions (following Reinecker et al., 2003). **(b)** Basics of televiewer imaging of borehole features. **(c)** Example of some of these features from the PTA2 borehole televiewer data.

in volcanic rock suites (Stefansson et al., 2000; Delpino and Bermúdez, 2009), with higher gamma responses indicating more evolved compositions. Alteration and weathering processes are also known to affect gamma responses in basaltic rocks largely due to the water solubility and therefore mobility of K during alteration (e.g., Planke, 1994). In basaltic rocks, weathering at flow tops generally causes an increase in the gamma response above background levels within flow interiors (e.g., Planke, 1994).

The gamma response for the PTA2 borehole is generally very low with the majority of the well, displaying relatively uniform API counts of <20. Intervals with high API counts do occur in the upper part of the borehole but are restricted to depths shallower than ca. 700 m (Fig. 7) and increase in frequency and extent upwards over this depth interval. Interestingly, the highest gamma intervals, which reach up to API of ca. 60, are almost exclusively associated with intrusions identified from the core logging. A number of lava flows within the upper section of the well also show elevated API when compared to similar lava facies at greater depth. It is noted from the core descriptions of PTA2 that hawaiite compositions become more common towards the top of the sequence, associated with the post-shield pāhoehoe lavas, in addition to the multiple fine-grained minor intrusions identified within these sections (e.g., Fig. 7). Hawaiite comprises a more evolved melt than basalt and therefore is expected to contain larger percentages of incompatible elements such as K, U and Th, resulting in increased gamma response.

Within the lower part of the well, gamma variations are far more restricted with values generally within the range ca. 7–20 API. In Fig. 7c, an expanded example from the interval ca. 1450–1550 m is presented. It is clear that systematic variations in gamma response are also exhibited within this lava-dominated sequence. Flow margins are highlighted for clarity and it is seen that inflections in the gamma peaks and troughs are readily associated with flow margins. Flow margins are not, however, always associated with increases in gamma response and therefore a combination of resolution, alteration and subtle base-level compositional differences be-

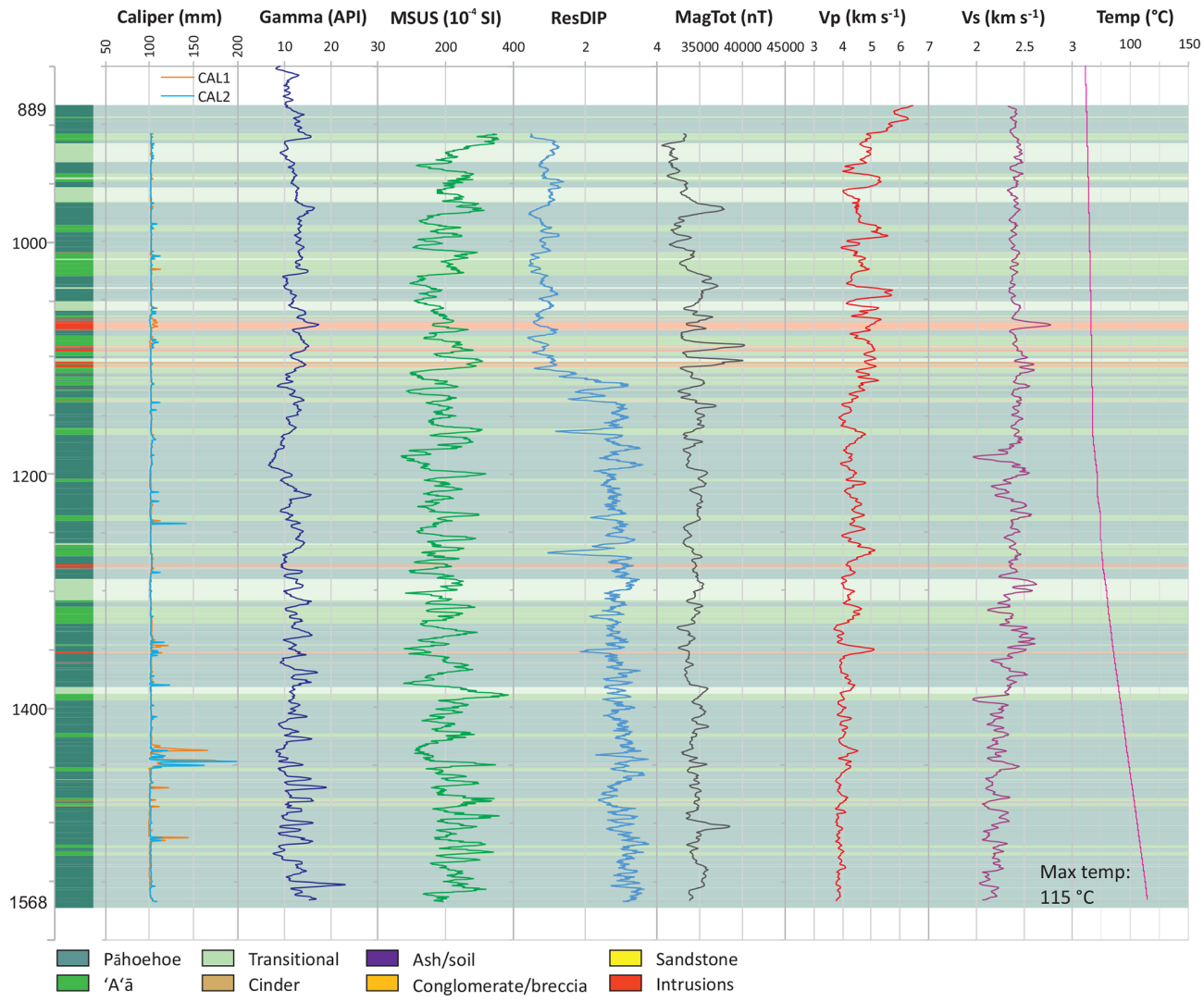

Figure 6. Summary of the full borehole logging results for PTA2.

tween the flows of the lower sequence are the cause of the gamma variations.

The results for KMA1, collected from within the HQ drill string during the time it was stuck, are also presented in Fig. 7d alongside the detailed core-based stratigraphy. Very little variation is observed within the gamma response for the logged interval of KMA1. The high gamma peaks observed in the upper parts of PTA2 are not observed within the sampled interval; however, the data do not cover the upper 300 m in KMA1. It could therefore be that higher gamma compositions are also present within this upper sequence of KMA1; however, the lack of any intrusions in this sequence (which hosted the majority of the higher gamma intervals in PTA2) may suggest that they are not present at KMA1.

3.3 Magnetic susceptibility (MSUS) and total magnetic field (MagTot)

Basaltic rocks have the potential to record strong magnetic signatures due to the common presence of accessory iron and iron–titanium oxide minerals such as magnetite, spinel and ilmenite. The remnant magnetic response of basaltic rocks is determined by a combination of the presence, type and abundance of these Fe–Ti oxides in addition to crystal size and alteration (e.g., Planke et al., 1999). Magnetic susceptibility measures the ability of a rock formation to become magnetized in response to an applied magnetic field and in its simplest application gives inference to the abundance of ferromagnetic magnetic minerals within the tested rock volume. Magnetic susceptibility in basaltic rocks is therefore affected by much the same parameters as the total magnetic field.

Magnetic susceptibility within the open hole section of PTA2 is dominantly within the range of ca. 100–350 10^{-4}

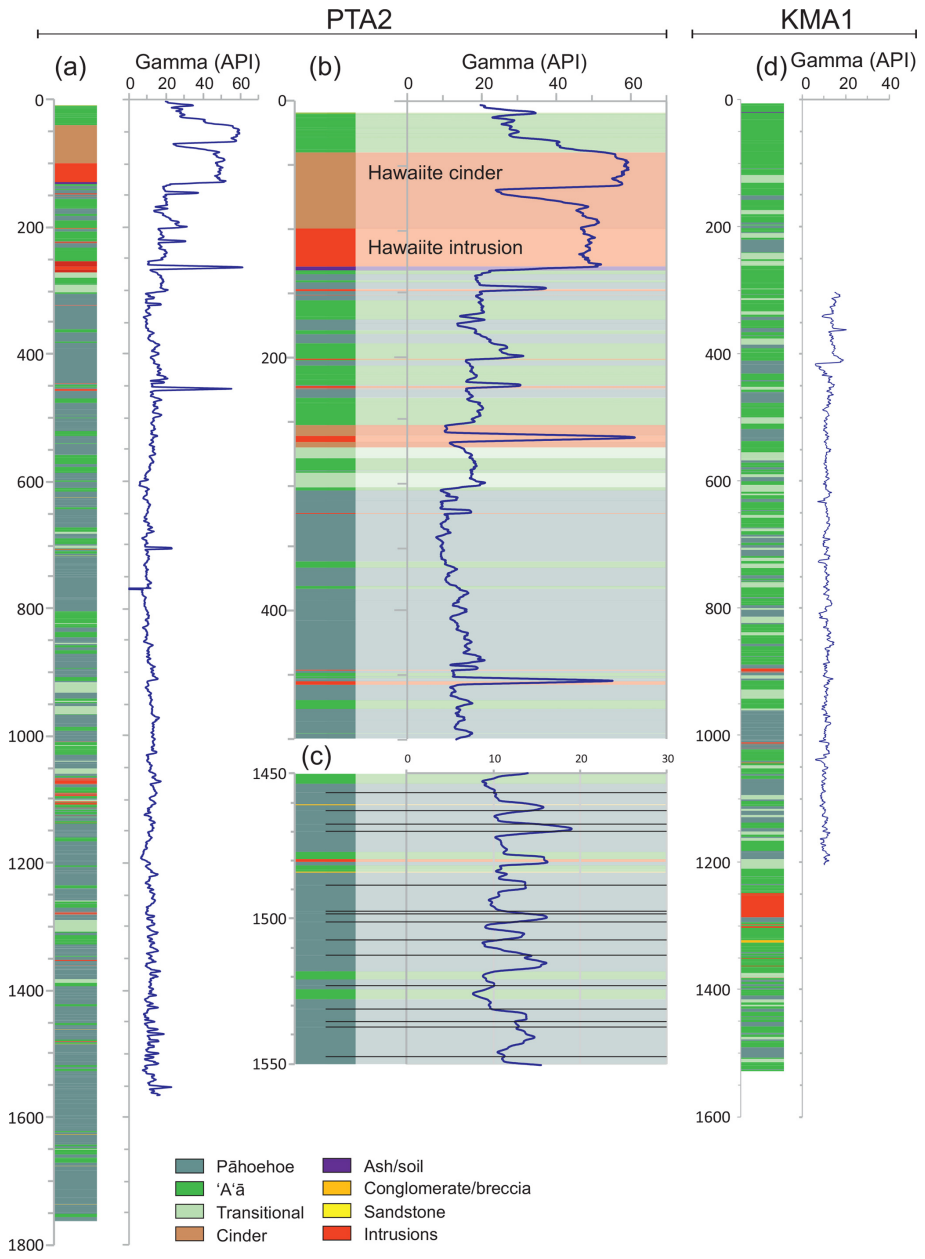

Figure 7. Gamma ray log results compared to volcanic facies in the PTA2 and KMA1 boreholes **(a, d)**. Two panels in the center display key intervals from PTA2 at a larger scale **(b, c)**. Black lines display flow boundaries within pāhoehoe packages in the bottom middle panel.

SI units while the total magnetic field displays values dominantly around the ca. 35 000 nT mark with a small number of excursions reaching higher values of maximum ca. 40 000 nT and some lower values down to ca. 32 100 nT in the upper part of the logged interval. The two highest peaks in total magnetic field are broadly associated with intrusions at ca. 1100 m, both of which also display elevated susceptibilities (Fig. 6). In some other cases intrusions display clearly elevated values; however, in others, no observable increase from background is seen. No clear and general relationship is observed between MSUS and MagTot; in some cases they appear linked, in others they appear independent. Magnetic susceptibility shows a significant level of systematic variations associated with lava facies flow packages and boundaries. The response is not uniform in nature but, in many instances, a sharp reduction or increase in susceptibility can be seen at or in other cases immediately prior to the facies boundaries (e.g., Fig. 6). Planke et al. (1999) demonstrated that flow top alteration can cause a kick in susceptibility values at the transition from lava interiors up into the crust and at least in some instances; this feature appears to be replicated in the PTA2 lavas.

3.4 DIP meter

The DIP meter records resistivity data but is uncalibrated and therefore it may be used to qualitatively assess relative resistivity of the formation. With the lack of laterolog resistivity data this comprises the best available inference for the PTA2 borehole. Figure 6 displays the DIP meter resistivity for the PTA2 borehole plotted against the other wireline data. The most striking feature of the resistivity data is a large step shift to higher average values at ca. 1130 m. Above and below this transition the variations are quite scattered with an irregular serrated character but importantly there is almost no overlap in the absolute ranges within these two sections.

Geologically there is not a sufficient change in the penetrated facies which could account for this change in the resistivity range. Alteration is known to increase within the lower interval which could potentially explain some of the increased resistivity where pores are filled with secondary minerals, but cannot explain the sharp transition. Interestingly, the jump in resistivity corresponds to a depth at which very slow drilling conditions were encountered that were associated with a particular type of secondary mineral products (zeolites). The secondary minerals formed a thick film on the bit face that the diamond chips on the standard bit were not able to penetrate through; after a change in the bit to larger diamonds this issue was overcome. This is still problematic to explain the base-level shift as the lava cores within each section should show broadly similar values. Another more likely possibility is that it is associated with the borehole fluids. A range of mud additives were added to the drilling fluid during clearing of the borehole ca. 2 months prior to the logging operations and, therefore, it could be that density stratification may have occurred and that the heavier muds in the lower section have a higher resistivity than fresh formation water above.

A number of aquifer feed points are known from within the upper part of the well (Thomas and Haskins, 2013) and therefore circulation of aquifer waters into the borehole may have added to this effect. An inflection to a higher temperature gradient ca. 100 m deeper than the step in resistivity also points to different fluid regimes within the borehole and could support some sort of fluid stratification. More work is required to constrain this further.

Although there is some correlation between the volcanic stratigraphy and the resistivity (Fig. 6), the relationship is not consistently related to the primary volcanic facies. Resistivity usually decreases at lava flow boundaries due to increases in vesicles, alteration and fracturing (Planke, 1994; Nelson et al., 2009). This is observed at some flow margins but not at others. Dense intrusion interiors and non-vesicular lava flow interiors are expected to display high resistivity, which is observed in some cases, e.g., the intrusions at ca. 1050–1110, but not in other cases, e.g., ca. 1480 m. Extensive fracturing may explain some of these deviations; however, some concerns regarding the consistency and accuracy of the data remain due these poor correlation examples along with the poorly understood jump in values described above.

3.5 Sonic

Velocity data from the sonic log has historically proven to provide some of the most instructive information for the interpretation of volcanic rocks in the subsurface (Planke, 1994). This is because different volcanic facies show a very wide range of velocity but also display distinctive distributions of velocity (e.g., Nelson et al., 2009), which can be tied back to volcanic facies at a variety of scales. P-wave (Vp) and S-wave (Vs) results from the picked and processed sonic log data are presented in Fig. 8. P-wave velocity data for the borehole give robust data, whereas picking for S waves was significantly more challenging and therefore gave lower confidence results in the upper part of the sequence. The average Vp for the logged interval is ca. 4.4 km s^{-1} while the average Vs is ca. 2.35 km s^{-1}. There is a generally good correlation between dense crystalline core material associated with sheet intrusions and ‘a‘ā lava cores and high Vp signatures in some cases exceeding 6 km s^{-1}. Exceptions do occur where high Vp is associated with pāhoehoe lavas with no obvious evidence for denser-than-normal cores and in these cases (e.g., at ca. 1045 m) the higher densities may be related to a combination of denser (high Vp) phenocrysts phases (e.g., olivine) and significantly denser (Mg rich) basic magmas (Watton et al., 2014b).

The largest variations observed within the sequence occur within the zone ca. 950–1150 m in which the greatest diversity of volcanic facies exists. Low peak velocities down to ca. 4 km s^{-1}, within the lower part of the well, are associated with dominantly compound-braided pāhoehoe facies (e.g., Jerram, 2002; Nelson et al., 2009). The low velocity is associated with the facies which display generally high levels of vesicularity and porosity along with increased levels of alteration with burial. It is also clear that background velocity values appear to be more affected by alteration than they are by the increase in burial compaction stresses. This is explicable by the fact that fresh basalt at ambient pressure can commonly exceed velocities of 5 km s^{-1} due to its hard interlocking crystal structure, and, due the strength within this structure, even moderately vesicular basalts show little reduction in porosity (and hence velocity) with burial effects alone (Millett et al., 2016). At the same time, alteration (where pervasive) can reduce the velocity of basalt by up to 2 km s^{-1}. Therefore, at relatively shallow burial depths, average velocity can clearly reduce with depth in association with facies that are susceptible to alteration as is the case for the porous pāhoehoe-dominated lava sequence. Clear correspondence between Vp and Vs is visible for some intervals of the well (e.g., Fig. 8); however, in other intervals, no or limited correspondence exists. The Vp / Vs ratio for the entire well is ca. 1.88, whereas for the interval at the bottom of the well where good correspondence exists it is slightly lower

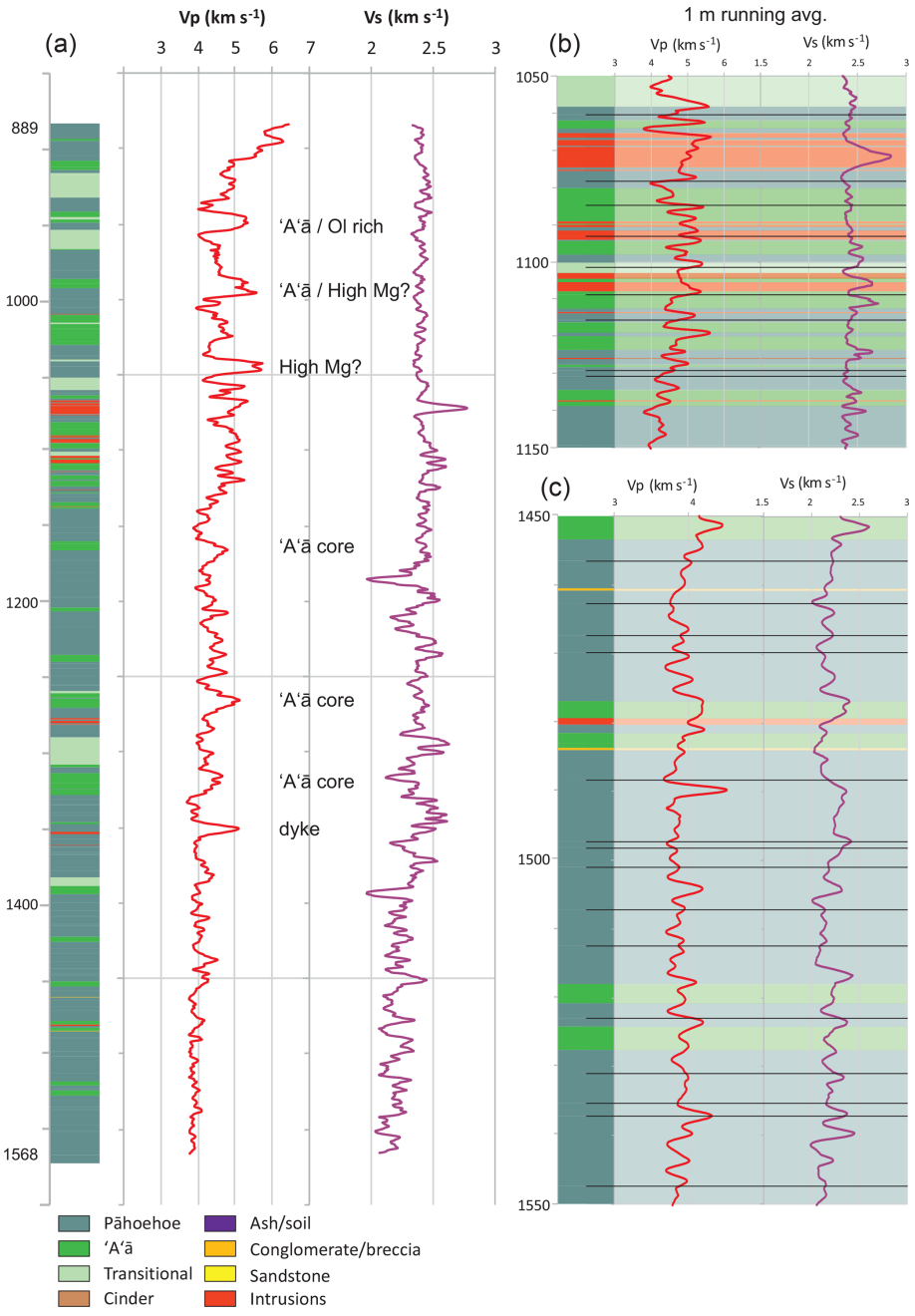

Figure 8. **(a)** Vp and Vs data from the PTA2 sonic log plotted against the volcanic lithofacies. **(b, c)** Zoomed-in logs which both display data with a 1 m running average applied; black lines indicating flow and contact boundaries between similar facies. Ol rich stands for olivine rich.

at ca. 1.79. Both values are within the same range as for older lava sequences, e.g., from eastern Greenland (Planke and Cambray, 1998); however, they are slightly higher than the average of 1.69 recorded from laboratory measurements on Hawaiian compositions (e.g., Manghnani and Woollard, 1968). As discussed in the processing section, the confidence in the S-wave picking in the upper part of the borehole is reduced. It is interesting to note that the S-wave data become challenging to pick at a very similar depth to that which the resistivity data displays a large jump in base level. It could therefore be that something relating to the fluid properties within the upper part of the open hole section also affected the sonic log data, although this also requires additional investigation beyond the scope of this report.

3.6 Televiewer

The televiewer tool collects high-resolution velocity data (amplitude and travel time) for the full circumference of the borehole which is processed to give a continuous acoustic image of the borehole surface (Zemaneck et al., 1969). The televiewer is most commonly utilized for structural and stress field analysis (e.g., Zoback et al., 1985; Ziegler et al., 2016; Millett et al., 2018); however, the images may also give potentially important information about volcanic facies and intra-facies. The ability for image logs to characterize volcanic facies elements has been highlighted for the FMS and FMI logs (resistivity imaging, Brewer et al., 1998; Tominaga, 2013; Watton et al., 2014a; Fornero et al., 2018); however, similar dedicated studies for the interpretation of volcanic facies from the televiewer appear somewhat limited and of lower apparent image quality to date (e.g., Massiot et al., 2015). Acquisition of high-quality televiewer data formed one of the primary objectives of the Hawai'i borehole operations.

In general, the image quality from the PTA2 borehole is very good, with many intervals displaying exceptional feature clarity while in a few intervals image quality is reduced and acquisition artefacts obscure the images. The key objective for collecting high-resolution image data was to test the ability of the televiewer to capture detailed volcanic intra-facies remotely, which is made possible by the availability of continuous core data. A full core is rarely available for volcanic wells, even for scientific drilling (e.g., Brewer et al., 1998), whereas for petroleum exploration wells, only very small core sections are commonly taken but these rarely intersect volcanic intervals. Throughout the logged interval, there is a depth discrepancy whereby the televiewer depths are generally ca. 1.6 m deeper than the core depth values. Additional to this correction, in many cases the resulting boxed core material from individual core pipe runs (ca. 10 ft) may exceed or not equate exactly to the known penetration. This is simply due to the fact that the core is sometimes broken and fragmented and therefore does not fit perfectly back together, resulting in longer recorded lengths compared to the known penetration. The depth is reset at the start of each core run and therefore only minor errors (generally < 30 cm) may be encountered at the bottom of some runs.

To highlight the potential of televiewer images for volcanic facies delineation, in Fig. 9, type examples of pāhoehoe and 'a'ā lava facies are presented and compared to observations from core. In Fig. 9a, an individual simple pāhoehoe lava lobe is characterized by clear vesicle size and abundance variations with dense small vesicles at the lower and upper vesicle zones (LVZ and UVZ following Katz and Cashman, 2003), transitioning into fewer larger vesicles within the central portion of the flow interior. Large vesicles within the central portion of the flow lobe can be clearly seen within the televiewer amplitude data along with subparallel vesicle coalescence bands within the UVZ to flow top transition. As is typical of pāhoehoe lavas, the altered flow top crust is thicker than the flow base and has also been baked by the overlying flow increasing the degree of alteration. This is also observed on the televiewer data, with a broader band of lower amplitudes at the top of the flow. Flow top fractures which terminate within the flow core are also clearly observed from the televiewer amplitude data, which importantly suggests that the corresponding fractures in the core are primary and not drilling induced. Along compound pāhoehoe lava sections within the data, multiple thin lava lobes and pāhoehoe "toes" in addition to internal boundaries delineated by vesicle bands and chilled margins can be seen which would have formed during emplacement. Chilled margins are generally highly altered to clay or palagonite and dominantly display clear low-amplitude boundaries. Spherical-to-sub-spherical features are identified from the televiewer where these chilled margins or internal densely vesicular bands intersect the borehole at a toe termination or margin. Spongy pāhoehoe flow cores or lobe and toe cores display very low amplitudes due to a very low proportion of lava (vesicle walls) compared to open space where porosities commonly exceed 50 % (e.g., Walker, 1989).

'A'ā lavas comprise the other major lava flow type found on Hawai'i and in basaltic lava provinces in general. They are characterized by rubbly and brecciated upper and lower margins due to auto-brecciation of the lava flow crust during emplacement. In Fig. 9b an example of an 'a'ā rubbly flow margin is presented. The flow margin breccia belongs to the underlying flow interior and has been baked and oxidized by the overlying lava flow. The breccia displays a very clear and characteristic fabric comprising high-amplitude clasts within a low-amplitude finer-grained matrix. In other examples clear straining of regions showing different vesicle densities is observed within the flow core, a common feature of 'a'ā lavas where the lava continues to move during cooling and vesiculation causing deformation of the developing vesicular fabric (Cas and Wright, 1988). These sharp boundaries between the zones of different vesicle densities are clearly represented on the televiewer amplitude data along with examples of larger deformed vesicles near flow bases. Vesicle segregations and entrained clinker are also potentially visible as patches of low amplitude which match the core well in a number of examples. Recovery can commonly be poor within 'a'ā lavas due to heavy fracturing and the presence of loose rubble and, therefore, identifying flow features remotely (e.g., televiewer) may prove invaluable in understanding the volcanic sequence where such core gaps occur.

Many other detailed facies and intra-facies features including transitional lavas, sedimentary units, ash layers and intricate intrusive units have been investigated in detail from the Hawai'i boreholes and will form the basis of a standalone study presented elsewhere.

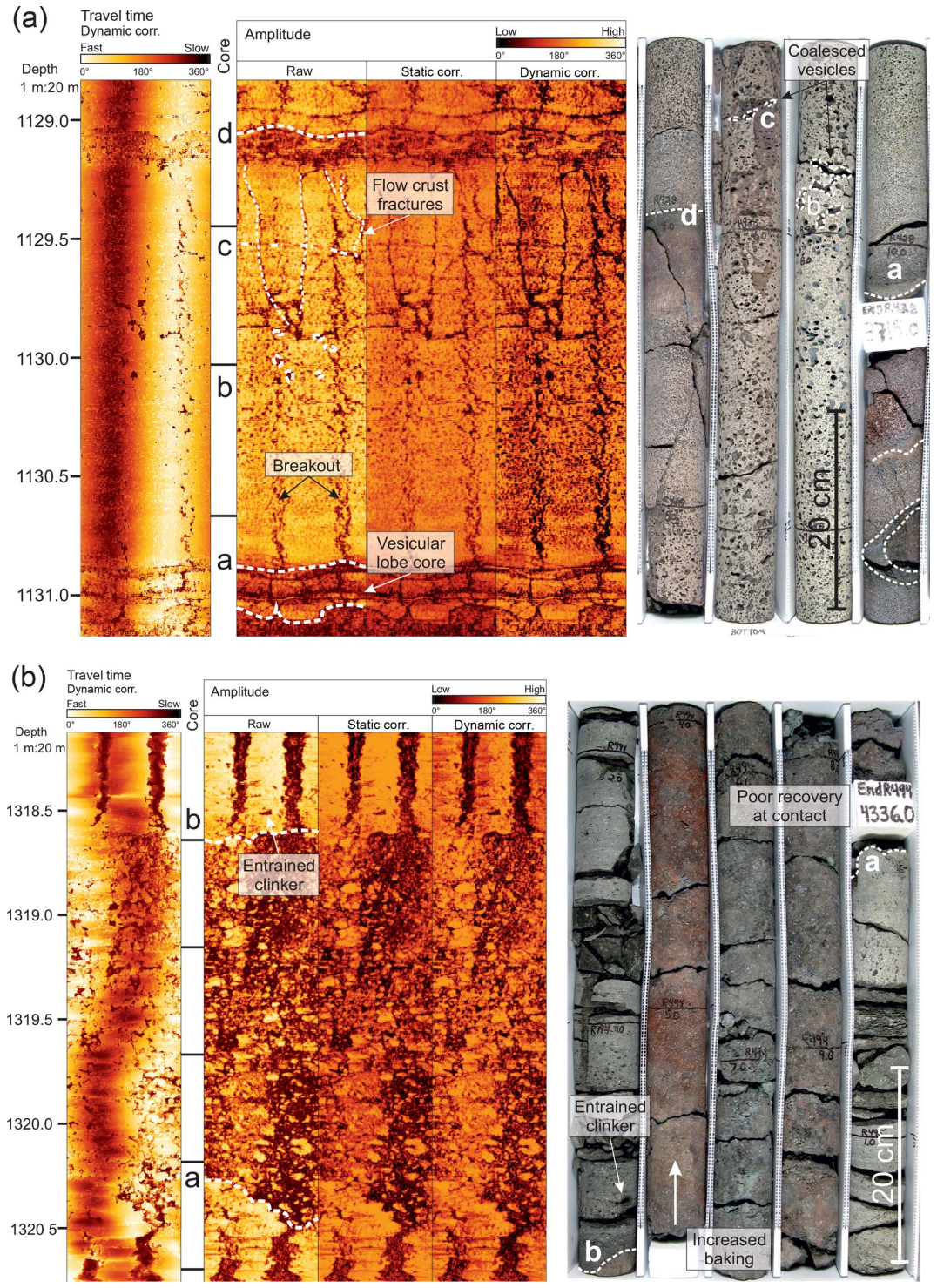

Figure 9. **(a)** Example of a simple pāhoehoe lobe from PTA2 displaying characteristic vesicle size distribution clearly imaged from the televiewer amplitude data along with flow top fractures. **(b)** Detail of a baked ‘a‘ā flow margin breccia from PTA2. Note the detail at the flow margins is clearer from the televiewer data due to the crumbly nature of the contact rubble. In each image, letters (a, b, etc.) highlight linked features on both the core and the image log.

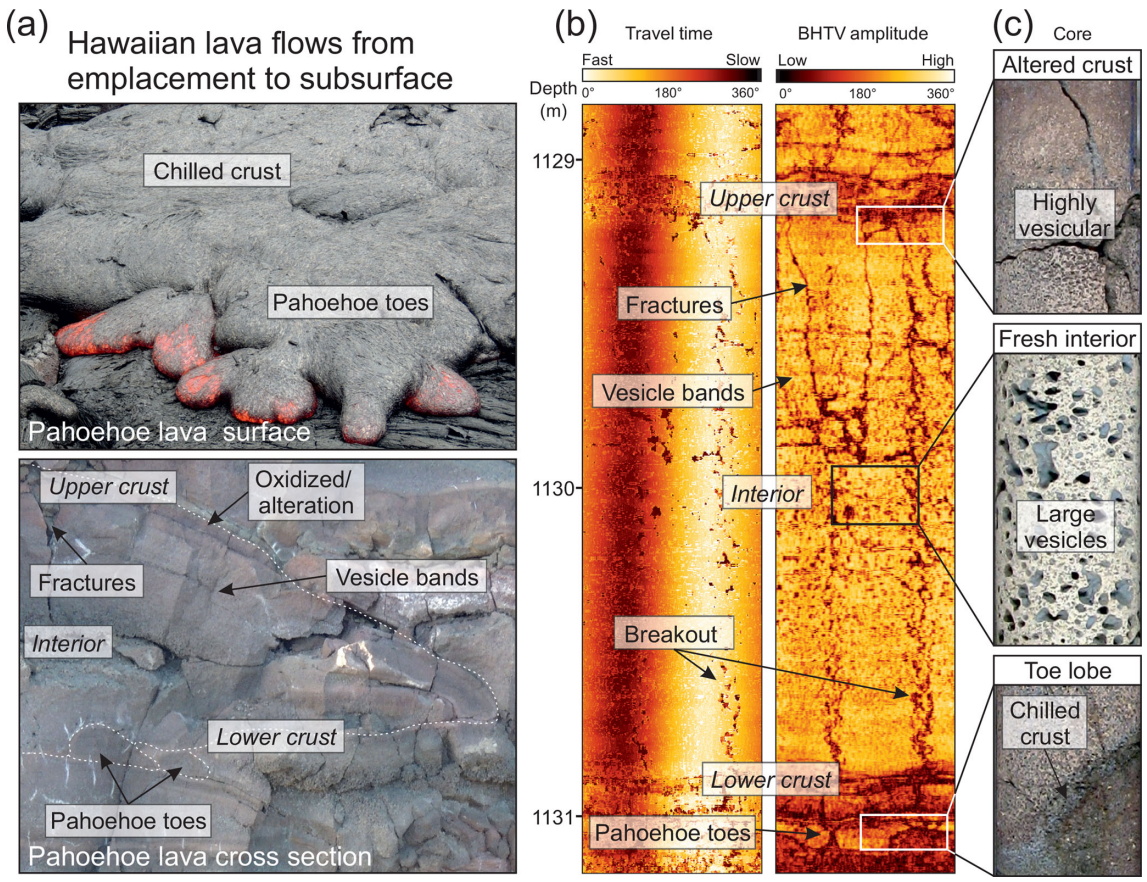

Figure 10. Examples of pāhoehoe and ʻaʻā facies: **(a)** from eruption and outcrop, **(b)** as imaged in televiewer, and **(c)** examples from the cored section.

4 Closing remarks and future outlook

This paper presents results from new borehole wireline logging and image logging of two fully cored boreholes on the Big Island of Hawaiʻi. Through this project an important database of down-borehole petrophysical variations has been collected, which can be interpreted in full due to the exceptional core data available over a large interval of the PTA2 borehole. Such data are often hard to realize in many offshore areas that drill through volcanic successions due to the costs alongside the volcanic intervals often not forming reservoir targets. Additionally the data set provides a valuable resource to look at average flow thickness, number of flow units and flows, and volcanic facies structure.

Gamma data are typically low as expected for basalts with variations occurring where intrusions come in and with an increase due to more evolved hawaiite compositions. Within the magnetic data, the two highest peaks in total magnetic field are broadly associated with intrusions at ca. 1100 m, yet other intrusions and the relation of the magnetic data to the varying volcanic facies show mixed results. Alteration at flow tops can show kicks in the susceptibility, which has been demonstrated to be the case in other lava successions (e.g., Planke et al., 1999). Resistivity data from DIP meter records show some correlation to volcanic facies in some areas but not in others, which could be due to a number of factors (e.g., variations in fracturing, lack of calibration of DIP meter readings). Such data could be improved with better constrained laterolog resistivity data. Variations within the velocity with depth are clearly influenced by alteration of the porous lavas and associated facies, with a noted degrease in velocity in the lower part of the well. The caliper results highlight semi-continuous breakouts occurring down the wells, best developed in the most coherent facies (e.g., ʻaʻā interiors and intrusions), which are associated with the in situ stress field (breakouts occur parallel to minimum horizontal stress). The directions of these breakouts can be of use in unraveling the in situ stress regime of the Mauna Kea volcano and as such are forming the basis of ongoing research.

The televiewer borehole imaging sonde, as an example, can produce highly informative data for delineating small-scale volcanic features and intra-facies when optimized settings are used. Features including individual vesicles, vesicle segregations, strained vesicles, chilled margins, rubble zones, intrusive contacts and pāhoehoe lobe morphologies can be confidently matched between the televiewer data and the full

diameter core. One of our main goals in undertaking such a study is the potential ability to link facies with analogue examples and ultimately get back to the geological processes that have formed the petrophysical variations preserved in the rocks. Figure 10 acts as a summary of this concept by linking back our down-borehole observations to the key volcanic facies that formed them. Going forward, data sets like the one presented here allow improved confidence in the interpretation of borehole imaging through volcanic sequences where core is not available. Ongoing and future work will focus on the detail within the data set to fully explore the key volcanological, structural and geophysical inferences that can be gained from this case example.

Data availability. A digital archive of core photos and detailed core run depth log information is available at https://www.higp.hawaii.edu/hggrc/projects/humuula-groundwater-research-project/ (HGGRS, 2019). The down-hole data are published with a digital object identifier via GFZ Data Services (Kück, 2019).

Author contributions. The manuscript was prepared by DAJ and JMM, with additional contributions and edits by all members of the author list. The project started with initial discussions between DougalEARTH (DAJ) and Hawaii (NL, DT), at the fall AGU meeting in San Francisco in 2013. A program of acquisition was agreed to by VBPR/DougalEARTH (DAJ, SP), GFZ Potsdam (JK) and Hawaii (DT). DAJ and SP visited the site and the core data set with Haskins and Thomas in December 2015 for project planning. Data acquisition was undertaken on site in February and June 2016 (JMM, JK, EH and DT). Once acquired, Pierdominici carried out additional work on the televiewer data.

Competing interests. The authors declare that they have no conflict of interest.

Acknowledgements. This project was made possible by the collaborative outlook of the main partners (VBPR and DougalEARTH, GFZ, and the University of Hawai'i) and the extensive background work undertaken by the researchers at the Hawai'i Groundwater and Geothermal Resources Center (University of Hawai'i) and from the HGRP project. Jehanne Paris is thanked for helping organize the logging operations and helping in the field. Martin Töpfer and Marco Groh (Operational Support Group, OSG, of ICDP, GFZ) are thanked for ensuring the smooth running of the logging operations. Dougal Jerram and Sverre Planke are also supported by the Research Council of Norway, through its Centres of Excellence funding scheme, project 223272 at CEED, University of Oslo. We would like to thank Breno Waichel and John Shervais for constructive reviews and the editorial team at Scientific Drilling for their prompt handling and meticulous guidance through the various stages from submission to publication.

Edited by: Tomoaki Morishita
Reviewed by: Breno Waichel and John Shervais

References

Andersen, M. S., Boldreel, L. O., and Seifaba Group: Log responses in basalt successions in 8 wells from the Faroe-Shetland Channel – a classification scheme for interpretation of geophysical logs and case studies. Faroe Islands Exploration Conference: Proceedings of the 2nd Conference, Annales Societatis Scientiarum Færoensis, Supplementum, 50, 364–391, 2009.

Bartetzko, A., Delius, H., and Pechnig, R.: Effect of compositional and structural variations on log responses of igneous and metamorphic rocks. I: mafic rocks, Geological Society, London, Special Publications, 240, 255–278, https://doi.org/10.1144/GSL.SP.2005.240.01.19, 2005.

Brewer, T. S., Harvey, P. K., Lovell, M. A., Haggas, S., Williamson, G., and Pezard, P.: Ocean floor volcanism: constraints from the integration of core and downhole logging measurements, Geological Society, London, Special Publications, 136, 341–362, https://doi.org/10.1144/GSL.SP.1998.136.01.28, 1998.

Cas, R. A. F. and Wright, J. V.: Lava flows. In Volcanic Successions Modern and Ancient, 58–91, Springer Netherlands, 1988.

Delpino, D. H. and Bermúdez, A. M.: Petroleum systems including unconventional reservoirs in intrusive igneous rocks (sills and laccoliths), The Leading Edge, 28, 804–811, https://doi.org/10.1190/1.3167782, 2009.

Eakins, B. W., Robinson, J. E., Kanamatsu, T., Naka, J., Smith, J. R., Takahashi, E., and Clague, D. A.: Hawaii's volcanoes revealed: U.S. Geological Survey Geologic Investigations Series Map I-2809, 1 plate, https://pubs.usgs.gov/imap/2809/ (last access: 2 February 2019), 2003.

Fornero, S. A., Marins, G. M., Lobo, J. T., Freire, A. F. M., and de Lima, E. F.: Characterization of subaerial volcanic facies using acoustic image logs: Lithofacies and logfacies of a lava-flow deposit in the Brazilian pre-salt, deepwater of Santos Basin, Mar. Petrol. Geol., 99, 156–174, https://doi.org/10.1016/j.marpetgeo.2018.09.029, 2018.

Frey, F. A., Wise, W. S., Garcia, M. O., West, H., Kwon, S. T., and Kennedy, A.: Evolution of Mauna Kea Volcano, Hawaii: Petrologic and geochemical constraints on postshield volcanism, J. Geophys. Res.-Sol. Ea., 95, 1271–1300, https://doi.org/10.1029/JB095iB02p01271, 1990.

Garcia, M. O., Haskins, E. H., Stolper, E. M., and Baker, M.: Stratigraphy of the Hawai'i Scientific Drilling Project core (HSDP2): Anatomy of a Hawaiian shield volcano, Geochem. Geophy. Geosy., 8, https://doi.org/10.1029/2006GC001379, 2007.

Goldberg, D.: The Role of Downhole Measurements in Marine Geology and Geophysics, Rev. Geophys., 35, 315–342, https://doi.org/10.1029/97RG00221, 1997.

Helm-Clark, C. M., Rodgers, D. W., and Smith, R. P.: Borehole geophysical techniques to define stratigraphy, alteration and aquifers in basalt, J. Appl. Geophys., 55, 3–38, https://doi.org/10.1016/j.jappgeo.2003.06.003, 2004.

Hawai'i Groundwater & Geothermal Resources Center (HGGRC): Humu'ula Groundwater Research Project, available at: https://www.higp.hawaii.edu/hggrc/projects/humuula-groundwater-research-project/, last access: February 2019.

Ildefonse, B., Rona, P. A., and Blackman, D.: Drilling the Crust at Mid-Ocean Ridges: An "In Depth" Perspective, Oceanography, 20, 66–77, https://doi.org/10.5670/oceanog.2007.81, 2007.

Jerram, D. A.: Volcanology and facies architecture of flood basalts, Volcanic Rifted Margins, 362, 119, https://doi.org/10.1130/0-8137-2362-0.119, 2002.

Katz, M. G. and Cashman, K. V.: Hawaiian lava flows in the third dimension: Identification and interpretation of pahoehoe and 'a'a distribution in the KP-1 and SOH-4 cores, Geochem. Geophy. Geosy., 4, 8705, https://doi.org/10.1029/2001GC000209, 2003.

Kück, J.: Composite OSG Logging Data from the PTA-2 borehole, Big Island, Hawai'i, GFZ Data Services, https://doi.org/10.5880/GFZ.4.8.2019.011, 2019.

Manghnani, M. H. and Woollard, G. P.: Elastic wave velocities in Hawaiian rocks at pressures to ten kilobars. The Crust and Upper Mantle of the Pacific Area, American Geophysical Union Geophysical Monograph Series, 12, 501–516, https://doi.org/10.1029/GM012p0501, 1968.

Massiot, C., McNamara, D. D., and Lewis, B.: Processing and analysis of high temperature geothermal acoustic borehole image logs in the Taupo Volcanic Zone, New Zealand, Geothermics, 53, 190–201, https://doi.org/10.1016/j.geothermics.2014.05.010, 2015.

Millett, J. M., Hole, M. J., Jolley, D. W., Schofield, N., and Campbell, E.: Frontier exploration and the North Atlantic Igneous Province: new insights from a 2.6 km offshore volcanic sequence in the NE Faroe–Shetland Basin, J. Geol. Soc., 173, 320–336, https://doi.org/10.1144/jgs2015-069, 2015.

Millett, J. M., Wilkins, A. D., Campbell, E., Hole, M. J., Taylor, R. A., Healy, D., Jerram, D. A., Jolley, D. W., Planke, S., Archer, S. G., and Blischke, A.: The geology of offshore drilling through basalt sequences: Understanding operational complications to improve efficiency, Mar. Petrol. Geol., 77, 1177-1192, https://doi.org/10.1016/j.marpetgeo.2016.08.010, 2016.

Millett, J. M., Planke, S., Kästner, F., Blischke, A., Hersir, G. P., Halldórsdóttir, S., Flóvenz, Ó. G., Árnadóttir, S., Helgadóttir, H. M., Vakulenko, S., and Buryak, S.: Sub-surface geology and velocity structure of the Krafla high temperature geothermal field, Iceland: Integrated ditch cuttings, wireline and zero offset vertical seismic profile analysis, J. Volcanol. Geoth. Res., https://doi.org/10.1016/j.jvolgeores.2018.03.024, 2018.

Nelson, C. E., Jerram, D. A., and Hobbs, R. W.: Flood basalt facies from borehole data: implications for prospectivity and volcanology in volcanic rifted margins, Petrol. Geosci., 15, 313–324, https://doi.org/10.1144/1354-079309-842, 2009.

Nelson, C. E., Jerram, D. A., Clayburn, J. A. P., Halton, A. M., and Roberge, J.: Eocene volcanism in 1598 offshore southern Baffin Bay, Mar. Petrol. Geol., 67, 678–691, https://doi.org/10.1016/j.marpetgeo.2015.06.002, 2015.

Pierce, H. A. and Thomas, D. M.: Magnetotelluric and audiomagnetotelluric groundwater survey along the Humu'ula portion of Saddle Road near and around the Pohakuloa Training Area, Hawaii: U.S. Geological Survey Open-File Report 2009–1135, 160 p., on one CD, also available at: https://pubs.usgs.gov/of/2009/1135 (last access: February 2019), 2009.

Planke, S.: Geophysical response of flood basalts from analysis of wire line logs: Ocean Drilling Program Site 642, Vøring volcanic margin, J. Geophys. Res.-Sol. Ea., 99, 9279–9296, https://doi.org/10.1029/94JB00496, 1994.

Planke, S. and Cambray, H.: Seismic properties of flood basalts on rifted volcanic margins based on Ocean Drilling Program (ODP) Hole 917A downhole data, Proc. Ocean Drill. Program Sci. Results, 152, 453–462, https://doi.org/10.2973/odp.proc.sr.152.247.1998, 1998.

Planke, S., Cerney, B., Bücker, C. J., and Nilsen, O.: Alteration effects on petrophysical properties of subaerial flood basalts: Site 990, Southeast Greenland margin, Proc. Ocean Drill. Program Sci. Results, 163, 17–28, https://doi.org/10.2973/odp.proc.sr.163.105.1999, 1999.

Reinecker, J., Tingay, M., and Müller, B.: Borehole Breakout Analysis from Four-arm Caliper Logs, World Stress Map Project, WSM, available at: http://dc-app3-14.gfz-potsdam.de/pub/guidelines/WSM_analysis_guideline_breakout_caliper.pdf (last access: February 2019), 2003.

Shervais, J. W., Schmitt, D. R., Nielson, D., Evans, J. P., Christiansen, E. H., Morgan, L., Pat Shanks, W. C., Prokopenko, A. A., Lachmar, T., Liberty, L. M., Blackwell, D. D., Glen, J. M., Champion, L. D., Potter, K. E., and Kessler, J. A.: First Results from HOTSPOT: The Snake River Plain Scientific Drilling Project, Idaho, U.S.A., Sci. Dril., 15, 36–45, https://doi.org/10.2204/iodp.sd.15.06.2013, 2013.

Stefansson, V., Gudlaugsson, S. T., and Gudmundsson, A.: Silica content and gamma ray logs in volcanic rocks, Proceedings of the World Geothermal Congress, Kyushu–Tohoku, Japan, 28, 2893–2897, 2000.

Stolper, E. M., DePaolo, D. J., and Thomas, D. M.: Deep Drilling into a Mantle Plume Volcano: The Hawaii Scientific Drilling Project, Sci. Dril., 7, 4–14, https://doi.org/10.2204/iodp.sd.7.02.2009, 2009.

Teagle, D. A. H., Ildefonse, B., Blum, P., and the Expedition 335 Scientists: Proc. IODP, 335: Tokyo (Integrated Ocean Drilling Program Management International, Inc.), https://doi.org/10.2204/iodp.proc.335.101.2012, 2012.

Thomas, D. and Haskins, E.: Analysis of the hydrologic structures within an ocean island volcano using diamond wireline core drilling, American Geophysical Union conference, San Fransisco, 2013.

Thomas, D. M., Paillet, F. L., and Conrad, M. E.: Hydrogeology of the Hawaii Scientific Drilling Project borehole KP-1: 2. Groundwater geochemistry and regional flow patterns, J. Geophys. Res., 101, 11–683, https://doi.org/10.1029/95JB03845, 1996.

Tominaga, M.: "Imaging" the cross section of oceanic lithosphere: The development and future of electrical microresistivity logging through scientific ocean drilling, Tectonophysics, 608, 84–96, https://doi.org/10.1016/j.tecto.2013.06.018, 2013

Walker, G. P.: Spongy pahoehoe in Hawaii: a study of vesicle-distribution patterns in basalt and their significance, B. Volcanol., 51, 199–209, https://doi.org/10.1007/BF01067956, 1989.

Watton, T. J., Cannon, S., Brown, R. J., Jerram, D. A., and Waichel, B. L.: Using formation micro-imaging, wireline logs and onshore analogues to distinguish volcanic lithofacies in boreholes: examples from Palaeogene successions in the Faroe–Shetland Basin, NE Atlantic, Geological Society, London, Special Publications, 397, 173–192, https://doi.org/10.1144/SP397.7, 2014a.

Watton, T. J., Wright, K. A., Jerram, D. A., and Brown, R. J.: The petrophysical and petrographical properties of hyaloclastite deposits: Implications for petroleum exploration, AAPG Bulletin, 98, 449–463, https://doi.org/10.1306/08141313029, 2014b.

Zemaneck, J., Caldwell, R. L., Glenn, E. E., Holcomb, S. V., Norton, L. J., and Strauss, A. J. D.: The borehole televiewer – a new logging concept for fracture location and other type of borehole inspection, J. Petrol. Technol., 21, 762–774, https://doi.org/10.2118/2402-PA, 1969.

Ziegler, M., Heidbach, O., Rajabi, M., Hersir, G. P., Ágústsson, K., Árnadóttir, S., and Zang, A.: The stress pattern of Iceland, Tectonophysics, 674, 101–113, https://doi.org/10.1016/j.tecto.2016.02.008, 2016.

Zoback, M. D., Moos, D., Mastin, L., and Anderson, R. N.: Well bore breakouts and in situ stress, J. Geophys. Res.-Sol. Ea., 90, 5523–5530, https://doi.org/10.1029/JB090iB07p05523, 1985.

Sci. Dril., 25, 35–46, 2019
https://doi.org/10.5194/sd-25-35-2019

Scientific Drilling
Open Access

SUSTAIN drilling at Surtsey volcano, Iceland, tracks hydrothermal and microbiological interactions in basalt 50 years after eruption

Marie D. Jackson[1], Magnús T. Gudmundsson[2], Tobias B. Weisenberger[3], J. Michael Rhodes[4], Andri Stefánsson[2], Barbara I. Kleine[2], Peter C. Lippert[1], Joshua M. Marquardt[1], Hannah I. Reynolds[2], Jochem Kück[5], Viggó T. Marteinsson[6,7], Pauline Vannier[6], Wolfgang Bach[8], Amel Barich[3,9], Pauline Bergsten[6,10], Julia G. Bryce[11], Piergiulio Cappelletti[12], Samantha Couper[1], M. Florencia Fahnestock[11], Carolyn F. Gorny[2], Carla Grimaldi[12], Marco Groh[5], Ágúst Gudmundsson[13], Ágúst T. Gunnlaugsson[2], Cédric Hamlin[14], Thórdís Högnadóttir[2], Kristján Jónasson[15], Sigurdur S. Jónsson[3], Steffen L. Jørgensen[14], Alexandra M. Klonowski[7], Beau Marshall[16], Erica Massey[2], Jocelyn McPhie[17], James G. Moore[18], Einar S. Ólafsson[2], Solveig L. Onstad[14], Velveth Perez[2,15], Simon Prause[3], Snorri P. Snorrason[19], Andreas Türke[6], James D. L. White[20], and Bernd Zimanowski[21]

[1]Department of Geology and Geophysics, University of Utah, Salt Lake City, Utah, USA
[2]Nordvulk, Institute of Earth Sciences, University of Iceland, Reykjavík, Iceland
[3]ÍSOR, Iceland GeoSurvey, Reykjavík, Iceland
[4]Department of Geosciences, University of Massachusetts, Amherst, Massachusetts, USA
[5]Helmholtz Centre Potsdam, GFZ German Research Centre for Geosciences, Potsdam, Germany
[6]Matís, Exploration & Utilization of Genetic Resources, Reykjavík, Iceland
[7]Faculty of Food Science and Nutrition, University of Iceland, Reykjavík, Iceland
[8]Department of Geosciences and MARUM, University of Bremen, Bremen, Germany
[9]Geothermal Research Cluster (GEORG), Reykjavik, Iceland
[10]Faculty of Life and Environmental Sciences, University of Iceland, Reykjavík, Iceland
[11]University of New Hampshire, Durham, New Hampshire, USA
[12]Dipartimento di Scienze della Terra, dell'Ambiente e delle Risorse (DiSTAR), University FEDERICO II, Naples, Italy
[13]Jarðtaeknistofan, (GEOICE Geological Services Ltd), Hafnarfjörður, Iceland
[14]K.G. Jebsen Centre for Deep Sea Research, Department of Earth Science, University of Bergen, Bergen, Norway
[15]Collections and Systematics Department, Icelandic Institute of Natural History, Gardabaer, Iceland
[16]DOSECC Exploration Services, Salt Lake City, Utah, USA
[17]School of Natural Sciences, University of Tasmania, Hobart, Australia
[18]U.S. Geological Survey, Menlo Park, California, USA
[19]Verkís Consulting Engineers, Reykjavík, Iceland
[20]Geology Department, University of Otago, Dunedin, New Zealand
[21]Institut für Geographie und Geologie, Universität Würzburg, Würzburg, Germany

Correspondence: Marie D. Jackson (m.d.jackson@utah.edu)

Received: 22 October 2018 – Revised: 3 March 2019 – Accepted: 14 March 2019 – Published: 12 June 2019

Abstract. The 2017 Surtsey Underwater volcanic System for Thermophiles, Alteration processes and INnovative concretes (SUSTAIN) drilling project at Surtsey volcano, sponsored in part by the International Continental Scientific Drilling Program (ICDP), provides precise observations of the hydrothermal, geochemical, geomagnetic, and microbiological changes that have occurred in basaltic tephra and minor intrusions since explosive and

effusive eruptions produced the oceanic island in 1963–1967. Two vertically cored boreholes, to 152 and 192 m below the surface, were drilled using filtered, UV-sterilized seawater circulating fluid to minimize microbial contamination. These cores parallel a 181 m core drilled in 1979. Introductory investigations indicate changes in material properties and whole-rock compositions over the past 38 years. A Surtsey subsurface observatory installed to 181 m in one vertical borehole holds incubation experiments that monitor in situ mineralogical and microbial alteration processes at 25–124 °C. A third cored borehole, inclined 55° in a 264° azimuthal direction to 354 m measured depth, provides further insights into eruption processes, including the presence of a diatreme that extends at least 100 m into the seafloor beneath the Surtur crater. The SUSTAIN project provides the first time-lapse drilling record into a very young oceanic basaltic volcano over a range of temperatures, 25–141 °C from 1979 to 2017, and subaerial and submarine hydrothermal fluid compositions. Rigorous procedures undertaken during the drilling operation protected the sensitive environment of the Surtsey Natural Preserve.

1 Introduction

In late summer 2017, International Continental Scientific Drilling Program (ICDP) expedition 5059, the Surtsey Underwater volcanic System for Thermophiles, Alteration processes and INnovative Concretes (SUSTAIN) project (http://surtsey.icdp-online.org, last access: 30 March 2019), drilled three cored boreholes through the basaltic tuff, tephra, and minor intrusions of Surtsey volcano, an oceanic island on the insular shelf 32 km from the south coast of Iceland. Surtsey was created by explosive and effusive eruptions from 1963 to 1967 in the Vestmannaeyjar archipelago, a young volcanic system that marks the offshore, southward-propagating tip of Iceland's SE rift zone (Einarsson, 2008; Jakobsson et al., 2009) (Fig. 1). The island emerged from a seafloor depth of about 130 m below sea level (b.s.l.) (Thórarinsson et al., 1964; Thors and Jakobsson, 1982; Jakobsson et al., 2009) (Fig. 1) and eventually attained a height of 150 m above sea level (a.s.l.). Explosive eruptions followed by lava flows produced approximately 1 km^3 of eruptive products at the termination of activity in June 1967 (Thórarinsson et al., 1964; Thórarinsson, 1967, 1969). Progressive geochemical changes in the eruptive units over the 3.5 years of activity suggest magmatic mixing of depleted ridge basalt with ponded, enriched alkali basalt at the propagating ridge axis (Schipper et al., 2015, 2016).

A 181 m deep, cored borehole first explored subsurface processes at Surtsey in 1979, through the rim of Surtur, the eastern tephra cone. In early papers this was Surtur I and the western cone was Surtur II. Surtur II was subsequently given the name Surtungur (e.g., Baldursson and Ingadóttir, 2007). The top of the core is approximately 58 m a.s.l. (Fig. 1). Investigations of the core described volcanic structures above and below sea level, the thermal system, and the composition and alteration of basaltic tephra. The lithified volcanic tephra, mostly lapilli tuff, is composed of glass, crystals, and authigenic mineral cements (Jakobsson and Moore, 1982, 1986). Temperatures and fluid compositions in the 1979 borehole have been monitored since 1980 (Jakobsson et al., 2000; Marteinsson et al., 2015). These reveal differential cooling rates in the basaltic deposits (Fig. 2).

Surtsey forms a natural reserve and World Heritage Site of the United Nations Educational, Scientific and Cultural Organization (UNESCO) (https://whc.unesco.org/en/list/1267, last access: 30 March 2019), which "has been protected since its birth, providing the world with a pristine natural laboratory" (Baldursson and Ingadóttir, 2007). Studies of primary biological succession on land provide a unique scientific record of colonization of basaltic lava and tephra by plants, animals, and marine organisms. Furthermore, initial results of 16S rDNA tag sequencing analysis of fluids extracted in 2009 from the submarine zone of the 1979 borehole contain unique sequences of bacteria, archaea, and viruses with icosahedral symmetry below a 140 °C (1980) temperature maxima at 100 m depth below the ground surface (Marteinsson et al., 2015). These indicate methanomicrobia-related sequences at 172 m (54 °C in 2009) and archaeoglobus-like sequences at 145 m (80 °C in 2009) (Fig. 2). The microbial life may be derived from the seafloor and, therefore, potentially indigenous to the submarine volcanic biosphere. Microbial habitats in the submarine Surtsey deposits could potentially represent a subsurface equivalent of the terrestrial colonization of Surtsey basalt, which has been systematically recorded over the past 50 years (Magnússon et al., 2014).

The goal of creating a time-lapse drill core record of basaltic deposits at Surtsey 50 years after eruption was first conceived in 2013 (Jackson et al., 2015; Witke, 2017). Four years of advance planning and preparation resulted in the acquisition of nearly 650 m of core from three boreholes that traverse the still-hot volcano by the SUSTAIN project, sponsored by the ICDP and other international partners. The proposed drilling targets were to (1) create a vertical cored borehole adjacent to the 1979 borehole to investigate the progress of geochemical, mineralogical, and hydrothermal processes in the basalt over the past 38 years (Figs. 2–4); (2) explore potential microbial interactions within the basalt that were not considered during 1979 drilling; (3) create an in situ laboratory, the Surtsey subsurface observatory, within the vertical borehole, dedicated to experiments within the diverse

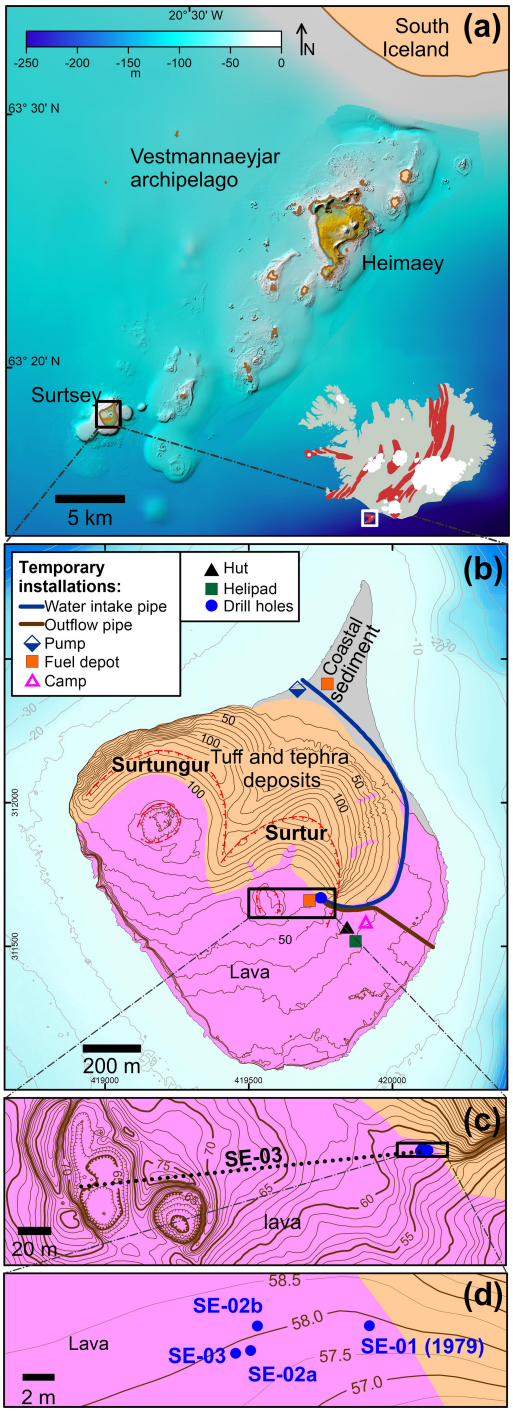

Figure 1. Maps showing drilling at Surtsey volcano, Iceland. **(a)** The Vestmannaeyjar volcanic archipelago at the southern offshore extension of the eastern Iceland rift zone (bathymetry: Icelandic Coast Guard, Hydrographic Department). The red elongated patches on the Iceland map show individual volcanic systems. **(b)** A simplified geological map of Surtsey (following Jakobsson, 2000) and temporary installations of the 2017 SUSTAIN drilling operation. The red dashed tick lines indicate crater rims. **(c)** Horizontal projection of the SE-03 (5059-1-D) cored borehole. **(d)** Wellhead locations: SE-01 (1979) and SE-02b, SE-02b, and SE-03 (or 5059-1-B, 5059-1-C, and 5059-1-D) (2017).

zones of the hydrothermal system (Türke et al., 2019); and (4) further investigate the deep structure of the volcano with a cored borehole inclined below Surtur, the eastern crater, which could potentially intersect the pre-eruption seafloor (Fig. 5).

2 Scientific objectives and societal benefits

SUSTAIN investigations address three central questions. (1) How do explosive eruptions of oceanic volcanoes develop and produce potentially hazardous tephra clouds? (2) How do incipient oceanic volcanic islands develop hydrothermal systems, lithify, and stabilize themselves over time to resist incessant marine erosion? (3) How does life in its many forms inhabit and produce material changes in very young subsurface basaltic deposits? The interdisciplinary, collaborative studies of the drill cores, associated hydrothermal fluids, and incubation experiments in the subsurface observatory are

i. investigating geothermal processes and alteration rates as analogs for rapid changes in the material behavior of the young oceanic crust;

ii. describing how authigenic alteration of glass, olivine and plagioclase, palagonitization processes, and microbial influences record hydrothermal–microbial–basalt interactions over a range of temperatures and fluid compositions;

iii. exploring how processes of chemosynthetic life evolve in extreme temperature conditions;

iv. recording the macroscopic rock-physics properties of lithified lapilli tuffs as geological analogs for ancient Roman and modern seawater concretes; and

v. performing in situ experimental research in the Surtsey subsurface observatory to describe the short-term evolution of microbiological–seawater–rock interactions.

The scientific and societal benefits of the SUSTAIN project will result from

i. investigating explosive Surtseyan eruptive processes as a means to refine the predictions of hazards associated with the subaerial phases and rapid edifice growth of island-forming seafloor volcanoes;

ii. describing chemical, magnetic, and material changes in the Surtsey deposits produced by hydrothermal–microbial–rock interactions, as a means to refine geophysical monitoring of thermal and chemical stimulation in hydrothermal reservoirs and the potential for fluid waste disposal and storage sites in pyroclastic rocks; and

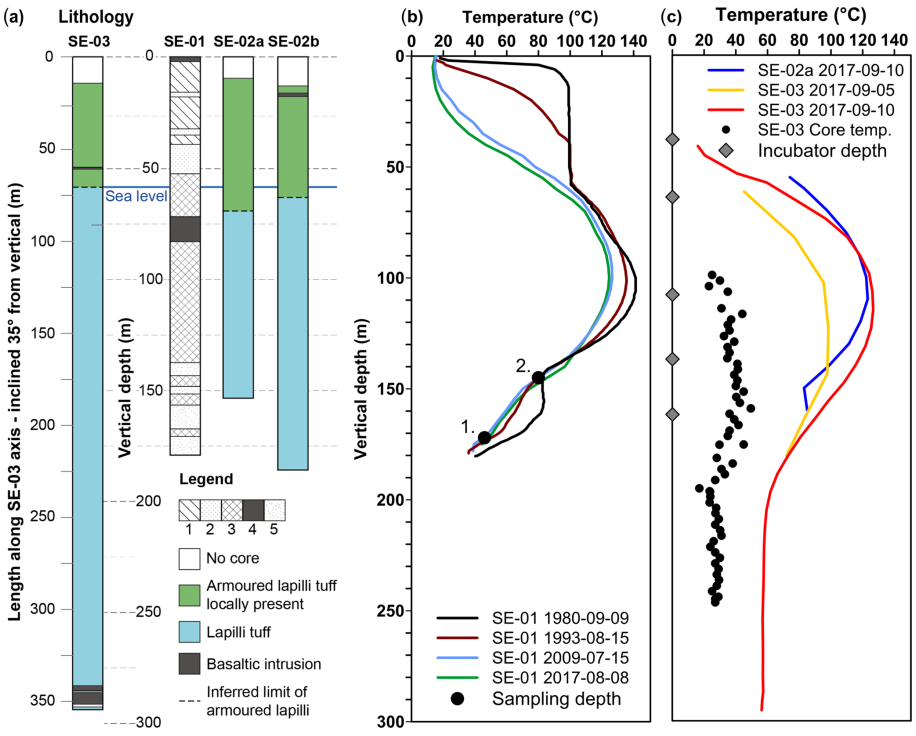

Figure 2. Comparisons of the 1979 and 2017 cored Surtsey boreholes. (**a**) Lithological logs. The 1979 core: SE-01 (following Jakobsson and Moore, 1982). (1) Weakly altered hyaloclastite, brown-black; (2) coarse and poorly graded hyaloclastite, black; (3) sound hyaloclastite, greyish-green; (4) basaltic intrusions and lava (at top), black; and (5) incoherent tephra. The 2017 simplified core logs: SE-02a, SE-02b, and SE-03 (following Weisenberger et al., 2019). (**b**) Borehole temperatures: SE-01 with 1980, 1993, 2009, and 2017 measurements, as well as 2009 microbiological samples (1, 2) (Jakobsson and Moore, 1982; Jakobsson et al., 2000; Marteinsson et al., 2015). (**c**) Borehole temperatures measured shortly after termination of drilling in SE-02b and SE-03 as well as depths of incubation experiments in SE-02b.

iii. determining the role of geochemical and biochemical processes in the development of zeolite and Al-tobermorite mineral cements in basaltic tuff and transferring this information to reproductions of these cementitious fabrics in innovative pyroclastic rock concretes, cementitious barriers, and waste forms using reactive glass aggregates.

3 Permitting and zero-impact drilling strategies

Preparations for the zero-impact drilling operation on Surtsey required 2 years of logistical planning and permitting after ICDP funding was approved in 2015 (Jackson et al., 2015). Every effort was made to fully preserve the sensitive surface and subsurface environments of the Surtsey Nature Reserve and to follow all guidelines set by the Iceland Environment Agency and Surtsey Research Society to avoid any risk to the vegetation, birds, and sea life that inhabit the island and the marine preserve that surrounds it. This special protection has been in place since 1965, with amendments made in 2006 and 2011, to ensure that the island and its geological formations, flora, and fauna evolve without human intervention.

Four permits were required to carry out the drilling operation (Weisenberger et al., 2019). A Planning Agency (Skipulagsstofnun) decision allowed drilling to proceed without an environmental impact assessment. The Environment Agency (Umhverfisstofnun) issued a permit outlining requirements, as well as a license for drilling and construction of temporary facilities. Travel permits for individuals were issued separately. All equipment was cleaned before transport to Surtsey, ensuring that no seeds or organisms were brought to the island. Fuel barrels were stored on four layers of reinforced plastic sheeting and treated with utmost care. All waste, including human waste and cinders at the drill site and all-terrain vehicle parking sites, were transported off-island. All traces of the operation were removed, except the wellheads. Entering bird nesting areas was prohibited before 15 August, and entering the peninsula was prohibited after 1 September. The South Iceland Health Inspectorate (Heilbrigðiseftirlit Suðurlands) issued a permit for running a camp, provisioning of food, and fulfilling hygiene requirements. The Vestmannaeyjar municipality also issued a permit to carry out the operation.

Some of the most challenging aspects of drilling on Surtsey involved the logistical difficulties of establishing and maintaining a camp and drilling operation on a remote is-

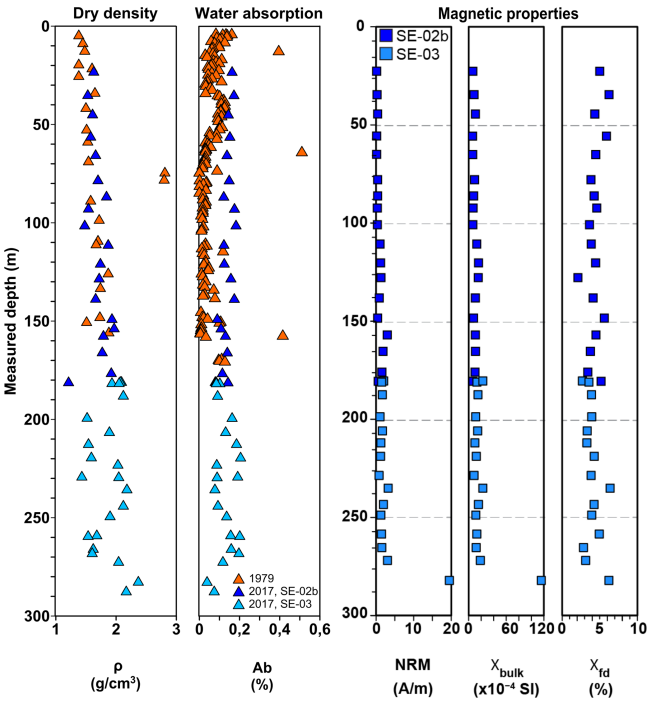

Figure 3. Material and magnetic measurements of Surtsey drill core samples. Dry density and water absorption (ASTM C97/C97M-18), 1979 SE-01 (Jakobsson and Moore, 1982; Oddsson, 1982), and 2017 samples and reference samples, SE-02b and SE-03 (Table S1). Magnetic properties, natural remanent magnetization (NRM), bulk magnetic susceptibility (χ_{bulk}, recorded as χ_{LF}), and frequency-dependent magnetic susceptibility (χ_{fd}) of 2017 reference samples, SE-02b and SE-03 (Table S2).

land that required strict environmental protection and relied almost solely on helicopter support. Logistical planning for drilling strategies, equipment organization, and packing required 3 months of dedicated effort at DOSECC Exploration Services, Salt Lake City, Utah, USA. Logistical planning to secure a functional camp while fulfilling safety and environmental requirements took place in Iceland. Drilling equipment was shipped from Portland, Oregon, USA, to Reykjavík; trucked to Þorlákshöfn on the southern coast of Iceland; and transported to the eastern coast of Surtsey by the Iceland Coast Guard vessel, Þór. The Coast Guard Super Puma helicopter, TF LÍF, then flew about 63 t of material, including the Atlas Copco CS-1000 drill rig disassembled into eight transportable components, and diesel, gas, and fresh water in 107 lifts to the drill, camp, and seawater pumping sites on 28–30 July (Weisenberger et al., 2019). Drilling took place from 7 August to 4 September. Demobilization with the Coast Guard vessel and TF LÍF took place from 10 to 12 September. At the termination of SUSTAIN activities the restoration of the island environment was approved as correctly implemented after inspection by the Environment Agency on 10 September. The 1979 Surtsey drill core and the 2017 SUSTAIN drill cores are archived at the Iceland Institute of Natural History.

The SUSTAIN drilling project has added several milestones to the record of drilling into oceanic basalt. Two vertical, cored boreholes (5059-1-B and 5059-1-C, also known as SE-02a and SE-02b) parallel the 1979 borehole (SE-01). These provide the first time-lapse record of drilling into very young basalt – with minimal live microbial contamination from seawater circulating fluids. A Surtsey subsurface observatory in borehole SE-02b offers the unprecedented opportunity to monitor "zero age" basalt without the expense and risk of a deep ocean operation. Five in situ incubation experiments were hung in perforated sections of an anodized aluminium casing installed from 38 to 161 m measured depth at 36–124 °C at the end of activities in 2017 (Türke et al., 2019; Weisenberger et al., 2019). A third, inclined core borehole, SE-03, is the first to probe the deep submarine structure of a young Surtseyan volcano (Moore, 1985; White and Ross, 2011). The project thus provides a wealth of new information about the structure of the eruptive conduit and explosive eruption mechanics of Surtsey, the evolution of its hydrothermal system, the rates of cementing processes in basaltic glass systems, and the active record of basalt–microbial–seawater interactions that are thought to influence the abundance and diversity of life in the oceanic crust (Santelli et al., 2008).

4 Drilling the 1979 cored borehole

The 1979 borehole was cored in NQ (47.6 mm core diameter) through the eastern crater of the volcano, until the bit became stuck at 176.5 m below the ground surface (Fig. 2) (Jakobsson and Moore, 1982, 1986). It was then completed in BQ (36.5 mm core diameter) to the total depth. Core recovery was very good (97.9 %) to 138 m. Poor recovery and slow drilling progress occurred at 140.0–143.8, 148.5–150.6, 157.4–168.7, and 170.5–180.1 m, mainly in zones of poorly consolidated tephra (Fig. 6). Recurring disturbances of the offshore seawater intake about 0.5 km east of the drill site also caused drilling delays. Seawater was the circulating medium; no drilling mud was employed. Return fluids were flushed back to the ocean. The steel drill casing remains in the hole.

The stratigraphic zones of the volcano include lapilli tuff and basaltic intrusions from 14 to 58 m below the ground surface at steam temperatures (100° C in 1980); a zone of tidal flux centered at 58 m (sea level); an 80 m section of highly altered lapilli tuff that includes the temperature maximum, 141 °C (1980), of the hydrothermal system at 100–106 m; and zones of weakly lithified tuff and unconsolidated tephra at 140–181 m at 40–89 °C in 1980 (Jakobsson and Moore, 1982) (Fig. 2). Hydrothermal mineral assemblages and alteration rates of basaltic glass and olivine varied through these zones (Jakobsson and Moore, 1986).

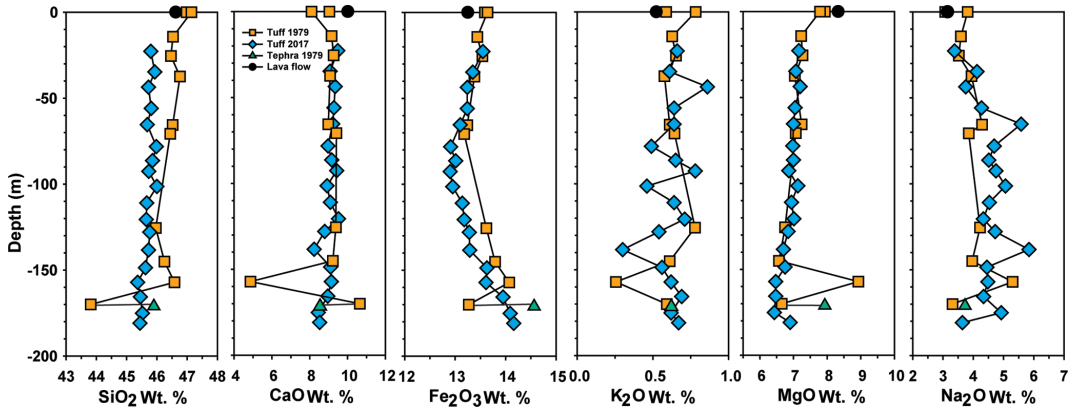

Figure 4. Whole-rock geochemical compositions, 1979 core archive, and 2017 SE-02b reference samples (Table S3) following the methods of Rhodes and Vollinger (2004).

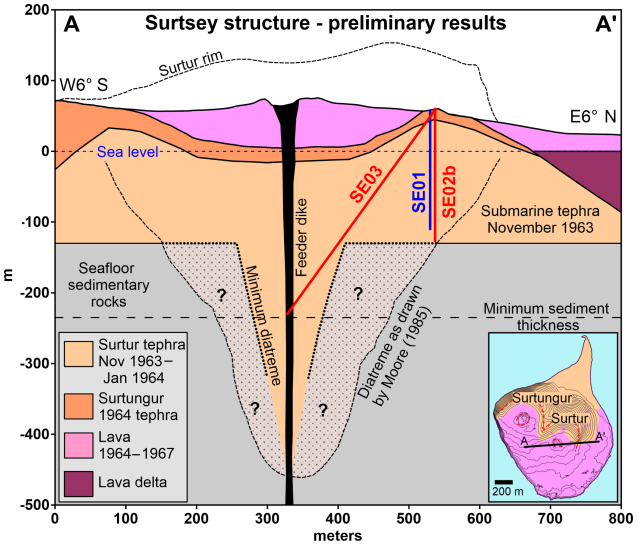

Figure 5. Structural sketch of Surtsey showing the minimum subsurface diatreme required to fit to the drilling results and the Moore (1985) hypothesis. The minimum thickness of marine sedimentary rock below the pre-eruption seafloor is 100 m, based on seismic reflection results from Thors and Jakobsson (1982). The advance of basaltic lava flows in 1964–1967 produced the lava delta.

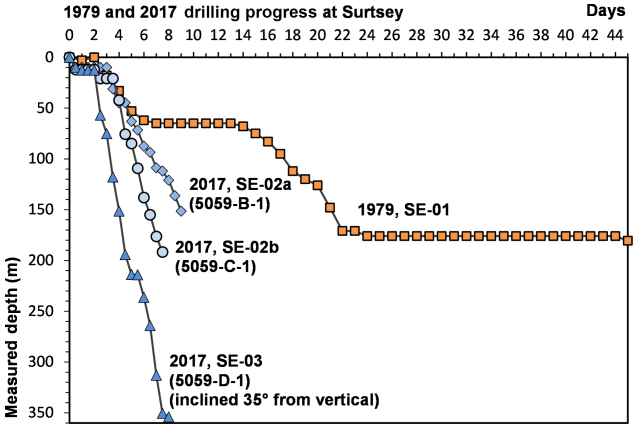

Figure 6. Rates of drilling progress in 1979 and 2017 (following Weisenberger et al., 2019).

During the 1963–1964 explosive activity, intermittent tephra-finger jets and continuous uprush jets 100–250 m in diameter and 500–2000 m in height formed eruption columns up to 9 km high (Thórarinsson, 1967). Measurements of primary bedding, planar slump surfaces, and shear planes core, as well as fragments of indurated marine sediments and rounded exotic pebbles suggested a diatreme-like volcanic conduit produced by explosions that quarried and ejected pyroclastic debris and fragments of host rock from a depth of several hundred meters (Moore, 1985). This contrasts with an assumption of a shallow crater model for the volcano by earlier workers (Thórarinsson, 1967; Kokelaar, 1983), in which any diatreme that formed was narrow and left the pre-eruption seafloor mainly intact underneath the volcanic edifice (Fig. 5).

5 Drilling the 2017 cored boreholes

The opportunity to precisely quantify rates of change at Surtsey strongly influenced the decision to locate the 2017 SUSTAIN boreholes next to the 1979 borehole. The four wellheads, SE-01 (1979) and SE-02a, SE-02b, and SE-3 (2017), lie within a 10 m wide area on the ground surface of unconsolidated tephra on the southern flank of the Surtur tuff cone (Figs. 1c, d, 5). A detailed record of the drilling operation is given in Weisenberger et al. (2019).

Preparation of the drill site, installation of the offshore pumping system and water line, construction of the camp, Coast Guard boat and helicopter mobilization, helicopter-assisted assembly of the drill rig, and rigging up took place 24 July–6 August 2017. Seawater circulating fluid was

pumped 1.4 km from a submerged offshore pump anchored off the western coast of the northern peninsula (Fig. 1b). Drilling the first vertical borehole, SE-02a, began on 7 August using an Atlas-Copco CS-1000 rig (Adkins, 2018). The rig was mounted on a spinner base and anchored by HQ rods drilled into the basaltic lava substrate beneath about 1–2 m of tephra. Seawater was passed through a Pentek Big Blue 30 µm cartridge filter and two AQUA4ALT WEDECO ultraviolet sterilization devices at the drill site to ensure minimal sediment and live microbial contamination of the recovered core; no mud products were employed. SE-02a was vertically pre-drilled with a 6 1/8 in. (15.56 cm) tricone rotary bit to a measured depth of 9.55 m. A 4 1/2 in. (11.43 cm) HWT conductor casing (inner diameter 101.6 mm) was installed to a casing shoe depth of 9.54 m. Coring with an HQ3 bit (63.5 mm core diameter) extended to 151.57 m measured depth below the ground surface (or 93 m b.s.l.). Core recovery was about 97 % overall. Continued problems with seawater supply to the drill site greatly slowed drilling progress (Fig. 6), and hole collapse occurred on 16 August below 46 m measured depth. The 43 HQ drill rods and the bottom-hole assembly (4.14 m) could not be extracted from the borehole, thereby preventing installation of the subsurface observatory. An extension to the casing and a flange were installed to 0.44 m above the ground surface.

A second vertical core, SE-02b, was then drilled from 19 to 26 August to create the borehole for the Surtsey subsurface observatory. After rotating the drill rig (and shack) on the spinner base, pre-drilling with a 6 1/8 in. (15.56 cm) tricone bit proceeded to approximately 13 m measured depth below the ground surface. A 4 1/2 in. (11.43 cm) HWT conductor casing was installed to a casing shoe depth of 12.74 m, but subsequent problems required interventions that eventually resulted in a 14.40 m casing shoe depth. Drilling progress improved substantially relative to borehole SE-2a (Fig. 6), through installation of a 16 000 L storage reservoir constructed of linked plastic totes on the northern peninsula. External pumps in tide pools on the western shoreline of the peninsula were managed continuously to transport seawater to this storage reservoir. The submersible pump was installed in one tote; it pumped the stored seawater 1.3 km to the drill site. Coring with an HQ3 bit reached a total depth of 191.64 m measured depth. A Florigel attapulgite product was employed to ensure stability in the top of the borehole, where fracture and collapse of the borehole walls occurred in SE-02a, and in poorly consolidated deposits below 140 m measured depth. Core recovery was 97 % overall. This is the only hole surveyed with a geophysical downhole log (Fig. 7).

The 6061-T6 anodized aluminum alloy NQ casing (2 3/4 in. (69 mm) outer diameter, 2 1/4 in. (57 mm) inner diameter) of the Surtsey subsurface observatory was run into the borehole to a measured landing depth of 181.25 m. The aluminum casing hangs freely inside the HWT conductor casing from the wellhead, and PVC centralizer tubes minimize contact between the aluminum casing and steel conductor casing (Türke et al., 2019; Weisenberger et al., 2019). A flange was installed to 0.21 m above reference ground height. Five perforated sections allow free fluid flow through the casing at specific depth intervals, which contain temperature loggers and perforated PEEK (polyetherketone) incubators attached to a Vectran rope hung from the wellhead. These were installed at 37.01–38.63 m (36 °C), 62.74–63.96 m (91 °C), 106.11–107.33 m (124 °C), 135.03–136.25 m (102 °C), and 160.48–161.70 m (61 °C) measured depth (Türke et al., 2019; Weisenberger et al., 2019) (Fig. 2c); the temperatures were measured in the SE-01 borehole on 8 August 2017. A 2-year in situ incubation experiment designed to record rock–microbe–water interactions in basaltic glass granules melted from Surtsey lava and in olivine (Fo_{90}) was installed 6 September 2017.

The SE-03 borehole, inclined 35° from vertical in a 264° azimuthal direction (Fig. 1c), was drilled from 28 August to 4 September with untreated seawater and occasional attapulgite mud. After rotating the drill rig on the spinner base, pre-drilling with a 6 1/8 in. (15.56 cm) tricone rotary bit extended to a measured depth of 12.6 m. A 4 1/2 in. (11.43 cm) HWT conductor casing with a casing shoe depth of 11.91 m was cemented in place. Coring with an HQ3 bit continued to 213.9 m, when the supply of HQ drill rods ran out. Coring continued with an NQ3 bit (43 mm core diameter) to a final inclined length of 354.05 m (Figs. 2, 5, 6). Core recovery was nearly 100 % through the lapilli tuff but variable, 40–90 %, in basaltic intrusions within the zone below the crater. The NQ coring string was left in the hole as permanent casing, including the NQ3 bottom-hole assembly. An extension to the casing and a flange were installed to 0.48 m above the ground surface (measured length 0.59 cm).

The SE-03 core traverses the deep Surtur vent structure and intrusions to a total vertical depth of 290 m and a horizontal distance approximately 203 m west of the wellhead (Fig. 1c). Dike intrusions occur in the lowermost 15 m of the core; the overlying deposits are entirely lapilli tuff (Fig. 2a). The SE-03 core thus traverses a diatreme that was excavated into seafloor sedimentary rock during the explosive phase of the Surtsey eruptions (Fig. 5). Lithic fragments ejected from the pre-eruptive seafloor occur in the lapilli tuff; there are also large blocks of seafloor sedimentary rock exposed on the subaerial tuff cone. The stratified sequence of volcaniclastic sedimentary rock is at least 100 m thick and the pre-eruption seafloor at about 130 m b.s.l. is draped by Surtsey pyroclasts close to the island (Jakobsson, 1982; Thors and Jakobsson, 1982; Jakobsson et al., 2009). However, no in situ deposits of the pre-eruption seafloor sedimentary rock were acquired by the either the 1979 or 2017 drilling projects. Preliminary analyses of the lapilli tuff from all three boreholes are examining volcanic fabrics, layering characteristics, the structural features of slump and shear planes (Moore, 1985), and the compositions and volumetric concentrations of xenoliths from seafloor sedimentary rock and ice-rafted glacial debris (Alexandersson, 1972; Reynisson and Jakobs-

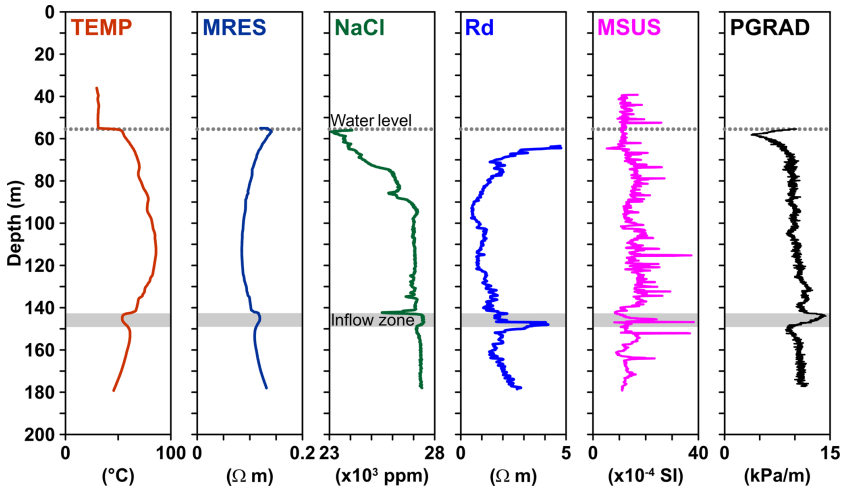

Figure 7. Selected results of geophysical downhole logging, borehole SE-02b, showing temperature (TEMP), fluid resistivity (MRES), fluid salinity as derived from resistivity measurements (NaCl), rock resistivity (Rd), magnetic susceptibility (MSUS), and the fluid pressure vertical gradient (PGRAD) as derived from the measured fluid pressure (not shown) (following Weisenberger et al., 2019).

son, 2009). The results will describe the deep volcanic edifice and pre-eruptive seafloor, the onset of explosive fragmentation at depth, and the possible explosive recycling of tephra (Schipper and White, 2016) in subaerial and submarine environments.

6 Downhole temperature monitoring and fluid sampling

The maximum temperature in borehole SE-01 in 2017 before the initiation of SUSTAIN drilling, 124 °C, occurred at 100–105 m measured depth (Fig. 3b), the same depth as the hydrothermal maximum in 1980, 141 °C (Jakobsson and Moore, 1982). Although the submarine temperature distribution has not substantially changed shape over the intervening 38 years, the temperatures in the subaerial tuff cone show marked decreases (Figs. 1c, 2b).

Borehole measurements undertaken 6 days after completion of SE-03 drilling indicated temperatures of 56–61 °C at 230–354 m measured depth below the ground surface (or 130–232 m b.s.l.) (Fig. 2c) (Weisenberger et al., 2019). Measurements made in summer 2018 gave similar results. This suggests that borehole fluids rapidly approached pre-drilling temperatures in September 2017. These temperatures are higher than the 20–30 °C measured in 1964 in marine sedimentary rocks at 200–300 m depth in a borehole on Heimaey, the largest of the islands forming the archipelago (Tómasson, 1967; Hafstað et al., 2002) (Fig. 1). The lithified tephra of the Surtsey diatreme has not apparently reached thermal equilibrium with the surrounding seafloor sedimentary rocks 50 years after volcanic activity terminated.

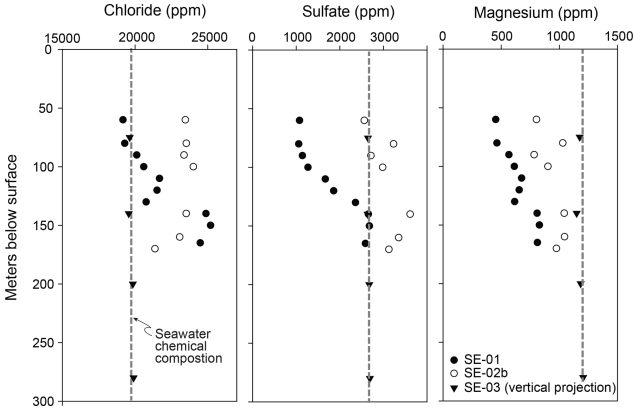

Figure 8. Compositions of fluids sampled from the SE-01, SE-02b, and SE-03 boreholes in September 2017.

Fluid sampling for geochemical and microbiological analyses used a slick line to mechanically open and close a 1 L fluid bailer at the sampling depth. Fluids sampled 1–3 weeks after the termination of drilling in September 2017 indicate that hydrothermal waters in the SE-01 borehole represent modified seawater typical of that involved in hydrothermal alteration of oceanic crust by leaching of basaltic rock and glass (Staudigel, 2004), followed by formation of secondary minerals, for example, anhydrite and Mg-containing phases (Fig. 8). The SE-02b and SE-03 borehole fluids, however, record the influences of the seawater drilling fluid.

7 Geophysical logging, vertical borehole SE-02b

Downhole geophysical logging, carried out by the ICDP Operational Support Group, used a 600 m logging winch and

several sondes to measure fluid conductivity, temperature and pressure, magnetic susceptibility, electrical resistivity, fluid conductivity, natural gamma, and spontaneous potential to 180 m measured depth in borehole SE-02b (Fig. 7) (Weisenberger et al., 2019). To prevent collapse in the uppermost fractured tuff and to protect the logging sondes, the drill string remained in place to 39 m. Figure 7 shows a selection of these soundings and two derived parameters, the fluid salinity (NaCl) and the vertical pressure gradient (PGRAD). The measured fluid resistivity (MRES) of 0.1–0.14 Ω·m is typical for seawater (0.1–1 Ω·m), and variations closely follow the shape of the fluid temperature (TEMP) curve, as expected. The fluid salinity (NaCl) shows a near-constant value of 27 ppt NaCl below 90 m yet decreases towards the zone of tidal flux, indicating a transition towards less saline water in the uppermost part of the water column. SE-02b borehole fluids sampled in September 2017, 3 weeks after completion of drilling (Fig. 7), also show lower chloride concentrations above 90 m. The fluid samples from the SE-01 borehole, however, show a more pronounced decrease in chloride concentration from 55 to 90 m (Fig. 7). This suggests that the meteoric water–seawater zone (Ólafsson and Jakobsson, 2009) was not strongly disrupted by seawater circulating fluid during drilling. Rock resistivity (Rd) shows very low values (0.5–5 Ω·m), similar to the range of fluid resistivity values. The shape of the MRES curve is closely reflected in the shape of the Rd curve and yields a correlation coefficient of ≈ 0.8. This indicates highly permeable rock flushed with seawater (or a mixture of seawater and meteoric water). The relative increase in chloride, sulfate, and magnesium concentrations in fluid samples from the 1979 SE-01 borehole to the freshly drilled SE-02b borehole also indicates that the Rd and MRES values are influenced by residual seawater circulating fluid. The maximum temperature, 85.9 °C at 113 m, is almost 35 °C lower than the temperature measured in the SE-01 borehole at the same depth before the onset of drilling, 119–122 °C. This suggests that the observed SE-02b temperature decrease mainly reflects cooling from seawater circulating fluid during drilling. By contrast, pronounced local deviations between 143–150 m measured depth below the ground surface in several logs (TEMP, MRES, Rd), the derived salinity (NaCl), and the vertical pressure gradient (PGRAD) suggest an inflow zone where cooler water of higher salinity enters the borehole. These measurements correlate with deep porous layers identified in the 1979 drill core, which were inferred to channel the flow of cold seawater into the hydrothermal system (Jakobsson and Moore, 1982, 1986; Ólafsson and Jakobsson, 2009). The inflow of cooler water plays a role in recharging the system; it is heated as it percolates through the higher temperature rocks of the geothermal reservoir. Whole-rock compositional analyses of tuff samples from the 1979 SE-01 core show large decreases in CaO and K_2O and increases in MgO and Na_2O (Fig. 4), suggesting that the fluid flow pattern was established early in the life of the volcano. Increased chloride, sulfate, and magnesium in 2017 SE-01 fluid compositions (Fig. 8) in this zone indicate that the flow pattern has continued to the present time. Magnetic susceptibility (χ_{bulk}) in 2017 core reference samples increases in the zone of strongly hydrothermally altered tuff, 110–138 m; sharply decreases in the inflow zone at 148 m; increases slightly in the deeper zone of poorly consolidated tuff; and then decreases at 180 m measured depth. Dry density increases and water sorption decreases at 148 m measured depth (Fig. 3, Supplement Tables S1, S2).

8 Microbiological investigations

Fifty-six core samples for microbial detection and analysis were immediately fixed and frozen on-site. A 30 cm section was cut from the midsection of every third 3 m core run at the drill site and divided into three subsections: 10 cm for molecular analyses (MA), 8 cm for cultivation (Cu), and 2 cm for microscopic investigation (M) (Weisenberger et al., 2019). MA sections were kept in the plastic core liner, wrapped in plastic, and kept in liquid nitrogen (−196 °C) until delivery to long-term laboratory storage at −80 °C. Cu sections were immediately removed from the liner; placed in a sterile plastic bag, with oxygen removed; and stored at 4 °C. M sections were incubated in a solution of 1× phosphate buffer solution (PBS) and 2 % formaldehyde, washed twice with PBS 1X, transferred to a solution of PBS 1X and 96 % ethanol, and stored at −80 °C. To detect microbial contaminants introduced during drilling, circulating fluid was collected at each core sample depth and passed through a Sterivex filter to retain the microbial fraction. Samples were stored in liquid nitrogen at −196 °C on-site and then transferred to laboratory storage at −80 °C for future molecular analyses.

Preliminary investigations of the diversity, metabolism, and function of cultivated and non-cultivated microbes in SE-01 borehole fluids revealed the presence of thermophilic bacteria and archaea (Marteinsson et al., 2015). The 2017 core samples are now being enriched in diverse media for autotrophic methane, iron, and sulfur metabolisms and heterotrophic microorganisms at 22, 60, and 80 °C. Some enrichments show microbial growth. For example, eight different bacterial strains have been isolated and identified from a SE-02a sample at 15 m measured depth. At least one bacterial strain has been isolated at 80 °C from a SE-02b sample at 180 m. In addition to this cultivation-dependent approach, analyses using high-throughput amplicon sequencing, functional metagenomics, and metatranscriptomic analysis will be performed, and interactions between minerals and microorganisms will be studied with fluorescent in situ hybridization.

9 Magnetic, material, and geochemical characteristics of Surtsey basalt

Thirty-three reference samples were collected from the SE-02b and SE-03 cores, adjacent to the samples acquired for microbiological and fluid geochemical analyses, and distributed to science team members for collaborative, interdisciplinary investigations. Initial comparisons of the lapilli tuff from the time-lapse drill cores reveal that geochemical, mineralogical, and material changes have occurred from 1979 to 2017 (Figs. 2–4, Tables S1–S3). Dissolution and alteration of glass, plagioclase, and olivine since 1979 (Jakobsson and Moore, 1986) have produced additional smectitic clay mineral, principally nontronite, and authigenic zeolite and Al-tobermorite form complex surface textures. Dry density measured in 2017 shows slightly higher values overall compared with measurements by Oddsson (1982) (Fig. 3), possibly through the growth of mineral cements that fill vesicles and interstitial voids. Lapilli tuff density is higher overall in the sub-seafloor diatreme. Water absorption measured in 2017 (ASTM C97M-18) shows higher values, 8–20 wt %, than those obtained in 1979 measurements, in which samples were not oven-dried (Jakobsson and Moore, 1982). Even so, the pronounced increase at higher temperatures of the submarine hydrothermal zone, at 92–138 m measured depth below the ground surface, suggests progressive alteration of basaltic glass to expansive smectitic clay mineral. Whole-rock major element X-ray fluorescence analyses compare the compositions of archived 1979 core samples and the 2017 SE-02b reference samples. These confirm that geochemical changes have accompanied glass and mineral alteration processes (Fig. 4, Table S3). Decrease in CaO at 90–140 m results from dissolution of glass, as well as dissolution of labradorite crystals in this zone. As Na_2O increases, K_2O decreases. This may result from dissolution of glass and abundant precipitation of analcime in the submarine hydrothermal system, as well as alteration of early-formed phillipsite to analcime.

Measurements of the natural remanent magnetization (NRM) of the lapilli tuff reference samples vary from approximately 0.1 to 3.0 A m^{-1} (Fig. 3, Table S2). Remanence intensity increases with depth. It is typically higher in the hydrothermally altered submarine lapilli tuff than in the somewhat glassy, lapilli tuff above sea level and the inflow zone at 148 m measured depth. NRM is by far the highest in the basaltic intrusion at the base of the SE-03 borehole. Measurements of bulk magnetic susceptibility (χ_{bulk}) (Table S2) show a similar trend, also recorded in the SE-0b geophysical log (Fig. 7). Bulk magnetic susceptibility (values obtained using SI units) varies from approximately 6–11 $\times 10^{-4}$ in the still glassy lapilli tuff above sea level, to 7–16 $\times 10^{-4}$ in the more altered submarine lapilli tuff at the hydrothermal temperature maxima (65–138 m measured depth), to 7–10 $\times 10^{-4}$ in the less altered lapilli tuff at the base of the SE-02b borehole (148–180 m measured depth), and to 8–23 $\times 10^{-4}$ in the lapilli tuff of the deeper diatreme traversed by the SE-03 borehole (Fig. 3). The lowermost sample, a basaltic intrusion, has an exceptionally high bulk magnetic susceptibility, approximately 116 $\times 10^{-4}$. Frequency-dependent magnetic susceptibility (χ_{fd}) varies between 2 % and 6 % and indicates the presence of superparamagnetic grains, <20 nm for titanomagnetites and their partial oxidation products. Magnetite particles of this physical size carry no magnetic remanence but are typical of authigenic, diagenetic and biogenic alteration processes in marine lavas and sediments (e.g., Lovley et al., 1987; Jackson and Swanson-Hysell, 2012; Roberts, 2015). Variations in the abundance of superparamagnetic grains therefore may provide indications of fluid–microbial–basalt interactions.

10 Significance of time-lapse drilling on Surtsey

The 1979 and 2017 drilling projects at Surtsey volcano provide a record of global significance for studying the mechanics of submarine and emergent basaltic eruptions, the deep structure of young oceanic islands in shallow rift-zone environments, and the processes of tephra lithification that create the resistance of emerging islands to incessant marine erosion. The time-lapse drill cores precisely record the progression of hydrothermal alteration, the rapid evolution of magnetic properties, the diverse processes of glass dissolution and alteration, and the cycling of authigenic mineral cements and their influences on the material and physical properties of young basalt. Integrated investigations of the drill cores, hydrothermal fluid investigations, and incubation experiments in the Surtsey subsurface observatory are expected to provide foundational references for the initiation of microbial life in a pristine basaltic habitat, as well as the systematic, longitudinal characterization of water–microbial–basalt interactions in subaerial and submarine environments.

Data availability. Scientific data sets of the 2017 Surtsey Underwater volcanic System for Thermophiles, Alteration processes and INnovative concretes (SUSTAIN) drilling project at Surtsey volcano, Iceland, are available at GFZ Data Services, https://doi.org/10.5880/ICDP.5059.001.

Sample availability. Drill core samples are stored at the Icelandic Institute for Natural History (Náttúrufræðistofnun Íslands) Urriðaholtsstræti 6–8, 210, Garðabær, Iceland. Each IGSN number represents the sample set of the corresponding Surtsey borehole, for example, http://igsn.org/ICDP5059EHS2001. These are SE-1 (Hole ID:73552), CDP5059EHS2001; SE-2a (Hole ID:73553), ICDP5059EHT2001; SE-2b (Hole ID:73554), ICDP5059EHY2001; and SE-3 (Hole ID:73555), ICDP5059EHU2001.

Supplement. The supplement related to this article is available online at: https://doi.org/10.5194/sd-25-35-2019-supplement.

Author contributions. MDJ and MTG led the project. MDJ, MTG, SLJ, AS, VTM, WB, BZ, PC, JMR, JGM, JDLW, KJ, TBW, and JMcP formulated the project and acquired the funding. TBW, JMR, AS, BIK, VTM, AB, PB, SC, CFG, CG, ÁG, ÁTG, CH, KJ, SSJ, SLJ, AMK, BM, EM, JMcP, ESO, SP, SLO, SP, SPS, AT, JDLW, MTG, and MDJ performed on-site work and analyses. JK, MG, TBW, AMK, VTM, SSJ, BM, and MTG performed downhole logging. BM was the on-site drilling supervisor. AS, BIK, TBW, VTM, and AMK sampled borehole fluids. TBW, JMR, AB, PB, JGB, SC, MFF, CFG, CG, CH, KJ, AMK, SLJ, EM, JM, SLO, VP, SP, AT, JDLW, and MDJ logged the core. MDJ, PCL, and JMM measured rock physical properties. JMR, JGB, PGC, and MDJ performed solid rock geochemical and mineralogical analyses while AS, AMK, and BIK carried out fluid geochemical analyses. PB, VTM, AMK, PV, and SLJ performed microbiological analyses. KJ is the core curator. MDJ, MTG, TBW, JMR, AS, BIK, HIR, VTM, PV, PB, CFG, TH, SLJ, JGM, AT, and JDLW wrote the paper with contributions from all authors.

Competing interests. The authors declare that they have no conflict of interest.

Disclaimer. Any use of trade, firm, or product names is for descriptive purposes only and does not imply endorsement by the U.S. Government.

Acknowledgements. Funding for this project was provided by the International Continental Scientific Drilling Program (ICDP) through a grant to the SUSTAIN project (led by Marie D. Jackson); a grant of excellence from the Icelandic Research Fund, ICF-RANNÍS (the IceSUSTAIN consortium led by Magnús T. Gudmundsson); the Bergen Research Foundation and K.G. Jebsen Centre for Deep Sea Research at the University of Bergen, Norway (led by Steffen Leth Jørgensen); the German Research Foundation (DFG) (led by Wolfgang Bach and Bernd Zimanowski); and DiSTAR, Federico II, University of Naples, Federico II, Italy (led by Piergiulio Cappelletti). The University of Utah, USA (Marie D. Jackson), and the two Icelandic power companies Reykjavík Energy and Landsvirkjun contributed additional funds. In kind support by several Icelandic institutions and companies contributed greatly to the success of the project, as did the dedicated work of several volunteers. The logistical support provided by the Icelandic Coast Guard was instrumental in carrying out the drilling operation. Norðurflug Helicopters and the Vestmannaeyjar Rescue Group provided critical logistical support. Jeremy Fisher and Rowan McGuire contributed to this article. The DOSECC drilling team, Steve Cole, Justin Blouin, A. J. Vecchiarelli, Matthew Lyon, and Michael Vinson, did excellent work. Hjalti Franzson provided guidance, and Þorsteinn Jónsson, Bjarni Kristinsson, Gísli Sighvatsson, and Sveinbjörn Steinþórsson contributed to the logistical operation on Surtsey. Unpublished borehole temperature measurements were made during the annual Surtsey Research Society expedition in July 2018.

Review statement. This paper was edited by Thomas Wiersberg and reviewed by Karoly Nemeth and Martin Jutzeler.

References

Adkins, S.: Volcanic cores from Iceland's youngest island, Coring Magazine, 6, 38–39, 2018.

Alexandersson, T.: The sedimentary xenoliths from Surtsey: turbidites indicating shelf growth, Surtsey Res. Progr. Rept., 6, 101–116, 1972.

ASTM C97/C97M-18: Standard Test Methods for Absorption and Bulk Specific Gravity of Dimension Stone, ASTM International, West Conshohocken, PA, https://doi.org/10.1520/C0097_C0097M-18, 2018.

Baldursson, S. and Ingadóttir, Á.: Nomination of Surtsey for the UNESCO World Heritage List, Icelandic Institute of Natural History, Reykjavik, 2007.

Einarsson, P.: Plate boundaries, rifts and transforms in Iceland, Jökull, 58, 35–58, 2008.

Hafstað, Þ. H., Jónasson, Þ., and Hjaltadóttir, S.: Vestmannaeyjar. Borholur á Heimey og mælingar á þeim (in Icelandic), Vestmannaeyjar, Measurements in boreholes on Heimaey, Orkustofnun, Greinargerð ÞÞ-ÞJ-SHj-2002/13, 19 pp., 2002.

Jackson, M. and Swanson-Hysell, N. L.: Rock magnetism of remagnetized carbonate rocks: Another look, in: Remagnetization and Chemical Alteration of Sedimentary Rocks, edited by: Elmore, R. D., Muxworthy, A. R., Aldana, M. M., and Mena, M., Geological Society of London Special Publication, 371, 279–303, https://doi.org/10.1144/SP371.3, 2012.

Jackson, M. D., Gudmundsson, M. T., Bach, W., Cappelletti, P., Coleman, N. J., Ivarsson, M., Jónasson, K., Jørgensen, S. L., Marteinsson, V., McPhie, J., Moore, J. G., Nielson, D., Rhodes, J. M., Rispoli, C., Schiffman, P., Stefánsson, A., Türke, A., Vanorio, T., Weisenberger, T. B., White, J. D. L., Zierenberg, R., and Zimanowski, B.: Time-lapse characterization of hydrothermal seawater and microbial interactions with basaltic tephra at Surtsey Volcano, Sci. Dril., 20, 51–58, https://doi.org/10.5194/sd-20-51-2015, 2015.

Jakobsson, S. P.: Dredge hauls from Vestmannaeyjagrunn, Iceland, Surtsey Res. Progr. Rept., 9, 142–148, 1982.

Jakobsson, S. P.: Geological map of Surtsey, scale 1 : 5000, Icelandic Institute of Natural History and the Surtsey Research Society, Reykjavík, 2000.

Jakobsson, S. P. and Moore, J. G.: The Surtsey research drilling project of 1979, Surtsey Res. Progr. Rept., 9, 76–93, 1982.

Jakobsson, S. P. and Moore, J. G.: Hydrothermal minerals and alteration rates at Surtsey volcano, Iceland, Geol. Soc. Am. Bull., 97, 648–659, 1986.

Jakobsson, S. P., Gudmundsson, G., and Moore, J. G.: Geological monitoring of Surtsey, Iceland, 1967–1998, Surtsey Research, 11, 99–108, 2000.

Jakobsson, S. P., Thors, K., Vésteinsson, Á. T., and Ásbjörnsdóttir, L.: Some aspects of the seafloor morphology at Surtsey vol-

cano: the new multibeam bathymetric survey of 2007, Surtsey Research, 12, 9–20, 2009.

Kokelaar, B. P.: The mechanism of Surtseyan volcanism, J. Geological Society of London, 140, 939–944, 1983.

Lovley, D. R., Stolz, J. F., Nord Jr., L., and Phillips, E. J. P.: Anaerobic production of magnetite by a dissimulatory iron-reducing microorganism, Nature, 330, 252–254, 1987.

Magnússon, B., Magnússon, S. H., Ólafsson, E., and Sigurdsson, B. D.: Plant colonization, succession and ecosystem development on Surtsey with reference to neighbouring islands, Biogeosciences, 11, 5521–5537, https://doi.org/10.5194/bg-11-5521-2014, 2014.

Marteinsson, V., Klonowski, A., Reynisson, E., Vannier, P., Sigurdsson, B. D., and Ólafsson, M.: Microbial colonization in diverse surface soil types in Surtsey and diversity analysis of its subsurface microbiota, Biogeosciences, 12, 1191–1203, https://doi.org/10.5194/bg-12-1191-2015, 2015.

Moore, J. G.: Structure and eruptive mechanisms at Surtsey Volcano, Iceland, Geol. Magazine, 122, 649–661, 1985.

Oddsson, B.: Rock quality designation and drilling rate correlated with lithology and degree of alteration in volcanic rocks from the Surtsey 1979 drill hole, Surtsey Res. Prog. Rept., 9, 94–97, 1982.

Ólafsson, M. and Jakobsson, S. P.: Chemical composition of hydrothermal water and water-rock interactions on Surtsey volcanic island: A preliminary report, Surtsey Research, 12, 29–38, 2009.

Reynisson, R. F. and Jakobsson, S. P.: Xenoliths of exotic origin at Surtsey volcano, Iceland, Surtsey Research, 12, 21–27, 2009.

Rhodes, J. M. and Vollinger, M. J.: Composition of basaltic lavas sampled by phase-2 of the Hawaii Scientific Drilling Project: Geochemical stratigraphy and magma types, Geochem. Geophy. Geosy., 5, Q03G13, https://doi.org/10.1029/2002GC000434, 2004.

Roberts, A. P.: Magnetic mineral diagenesis, Earth Science Reviews, 151, 1–47, 2015.

Santelli, C. M., Orcutt, B. N., Banning, E., Bach, W., Moyer, C. L., Sogin, M. L., Staudigel, H., and Edwards, K. J.: Abundance and diversity of microbial life in ocean crust, Nature, 453, 653–656, 2008.

Schipper, C. I. and White, J. D. L.: Magma-slurry interaction in Surtseyan eruptions, Geology, 44, 195–198, 2016.

Schipper, C. I., Jakobsson, S. P., White, J. D. L., Palin, J. M., and Bush-Marcinowski, T.: The Surtsey magma series, Sci.-Rep.-UK, 5, 11498, https://doi.org/10.1038/srep11498, 2015.

Schipper C. I., Le Voyer, M., Moussallam, Y., White, J. D. L., Thordarson, T., Kimura, J.-I., and Chang, Q.: Degassing and magma mixing during the eruption of Surtsey Volcano (Iceland, 1963–1967): the signatures of a dynamic and discrete rift propagation event, Bull. Volcanol., 78, 1–19, 2016.

Staudigel, H.: Hydrothermal alteration processes in the oceanic crust. Treatise on geochemistry, edited by: Holland, H. D. and Turekian, K. K., 511–535, Amsterdam, Boston, Elsevier-Pergamon, 2004.

Thórarinsson, S.: Surtsey, The New Island in the North Atlantic, The Viking Press, New York, 1967.

Thórarinsson, S.: Sídustu thaettir Eyjaelda (English summary: The last phases of the Surtsey eruption), Náttúrufraedingurinn, 38, 113–135, 1969.

Thórarinsson, S., Einarsson, Th., Sigvaldason, G., and Elísson, G.: The submarine eruption off the Vestmann Islands 1963–64, Bull. Volcanol., 29, 435–455, 1964.

Thors, K. and Jakobsson, S. P.: Two seismic reflection profiles from the vicinity of Surtsey, Iceland, Surtsey Res. Progr. Rept. 9, 149–151, 1982.

Tómasson, J.: On the origin of sedimentary water beneath Vestmann Islands, Jökull, 17, 300–311, 1967.

Türke, A. T., Jackson, M. D., Bach, W., Kahl, W.-A., Gudmundsson, M. T., and Jørgensen, S. L.: Design of the Subsurface Observatory at Surtsey Volcano, Iceland, Sci. Dril., in press, 2019.

Weisenberger, T. B., Gudmundsson, M. T., Jackson, M. D., Gorny, C., Türke, A., Kleine, B. I., Marshall, B., Jørgensen, S. L., Marteinsson, V. Þ., Stefánsson, A., White, J. D. L., Barich, A., Bergsten, P., Bryce, J., Couper, S., Fahnestock, F., Franzson, H., Grimaldi, C., Groh, M., Guðmundsson, Á., , Gunnlaugsson Á. Þ., Hamlin, C., Högnadóttir, Þ., Jónasson, K., Jónsson, S. S., Klonowski, A., Kück, J., Magnússon, R. L., Massey, E., McPhie, J., Ólafsson, E. S., Onstad, S. L., Prause, S., Perez, V., Rhodes, J. M., and Snorrason, S. P.: Operational Report for the 2017 Surtsey Underwater volcanic System for Thermophiles, Alteration processes and INnovative Concretes (SUSTAIN) drilling project at Surtsey Volcano, Iceland, Geo Forschungs Zentrum (GFZ) German Research Centre for Geosciences, https://doi.org/10.2312/ICDP.5059.001, 2019.

White, J. D. L. and Ross, P.-S.: Maar-diatreme volcanoes: A review, J. Volc. Geotherm. Res., 201, 1–29, 2011.

Witke, A.: Iceland drilling project aims to unearth how islands form, Nature, 547, 387–388, 2017.

Sci. Dril., 25, 47–56, 2019
https://doi.org/10.5194/sd-25-47-2019

Scientific Drilling
Open Access

Stratigraphy and sedimentology of the Orakei maar lake sediment sequence (Auckland Volcanic Field, New Zealand)

Leonie Peti and Paul C. Augustinus

School of Environment, The University of Auckland, Private Bag 920129, Auckland 1142, New Zealand

Correspondence: Leonie Peti (lpet986@aucklanduni.ac.nz)

Received: 28 February 2019 – Revised: 4 April 2019 – Accepted: 10 April 2019 – Published: 12 June 2019

Abstract. Global paleo-climate reconstructions are largely based on observations from the Northern Hemisphere despite increasing recognition of the importance of the Southern Hemisphere mid-latitudes for understanding the drivers of the global climate system. Unfortunately, the required complete and high-resolution terrestrial records from the Southern Hemisphere mid-latitudes are few. However, the maar lakes in the Auckland Volcanic Field (AVF), New Zealand, are crucial in this regard as they form outstanding depositional basins due to their small surface-to-depth ratio, restricted catchment, and absence of ice cover since their formation, hence ensuring continuous sedimentation with anoxic bottom water. Significantly, the estimated age of the AVF of ca. 250 ka may allow development of a continuous sediment record spanning the last two glacial cycles. The Orakei maar lake sediment sequence examined in this study spans the Last Glacial Cycle (ca. 126 to ca. 9.5 ka cal BP) from the phreatomagmatic eruption to the crater rim breach due to post-glacial sea-level rise. Two overlapping cores of >100 m sediment were retrieved and combined to develop a complete composite stratigraphy that is presently undergoing a wide range of multi-proxy analyses.

1 Introduction

Lake sediments are important archives for Quaternary paleo-environmental and paleo-climatic reconstruction, particularly when sedimentation has been continuous and sedimentation rates high, as they offer a variety of high-resolution proxy records of environmental change. In the context of the location of New Zealand in the Southern Hemisphere mid-latitudes, lakes act as important recorders of past climate in the south-western Pacific (Alloway et al., 2007). Furthermore, Auckland is situated at an ecological and climatic boundary between the subtropical north and the south of New Zealand influenced by subpolar climatic and oceanographic systems (Augustinus, 2007). Consequently, the up to 250 ka duration and high-resolution laminated sediment cores retrieved from maar lakes in the Auckland Volcanic Field (AVF) constitute ideal recorders of past regional climatic variability over the last two glacial cycles.

Due to their low diameter-to-depth ratio and limited catchment area (dominated by the lake itself), allochthonous sedimentation is a minor component of the infill, so that maar lake sediment is largely a direct archive of regional climatic signals (e.g. Augustinus et al., 2011; Brauer et al., 1999; Horrocks et al., 2005; Sandiford et al., 2003; Zolitschka et al., 2013). AVF maar lakes also preserve complete archives of eruptions of the local basaltic volcanoes as well as rhyolitic and andesitic volcanic systems situated in the Taupo Volcanic Zone (TVZ) and Egmont Volcano (Fig. 1) to the south of Auckland (Hopkins et al., 2015; Molloy et al., 2009; Shane, 2005; Shane and Hoverd, 2002). This is of importance as the City of Auckland, with >1.5 million inhabitants, is situated on a potentially active volcanic field for which eruption frequencies cannot be derived from the historical record (Edbrooke et al., 2003; Molloy et al., 2009; Newnham et al., 1999). Many basaltic tephra layers have been recorded in the AVF maar sediment cores, but age estimates rely on sedimentation rate extrapolation to and correlation with the source volcanoes, which mostly have not been dated unambiguously (Hopkins et al., 2015, 2017; Leonard et al., 2017; Lindsay et al., 2011; Molloy et al., 2009). Here, we focus

on the Orakei maar paleo-lake, which contains a finely laminated sediment sequence with high sedimentation rates (average $\sim 0.7\,\mathrm{mm\,yr^{-1}}$) possibly spanning the Eemian (MIS 5e) to the earliest Holocene. After an initial coring campaign in 2007, which established the potential of the Orakei maar record (Hopkins et al., 2015; Molloy et al., 2009), two overlapping cores were recovered in 2016 that reached the primary volcanic ejecta at the base of the crater at ca. 105 m depth below the sediment–water interface. Emphasis in the present study lies in establishing a detailed composite stratigraphy by aligning the overlapping sediment cores collected.

Many sediment records rely on one master record stitched together from two or more cores from a sedimentary sequence, although it is often not explained how these master records are derived. Nakagawa et al. (2012) summarised an incomplete early sediment sequence retrieved from Lake Suigetsu (Japan) resulting in potentially erroneous interpretations. Furthermore, they reported details of aligned sediment core sections from the Lake Suigetsu (Japan) sequence drilled in 2006, which largely relied on visual identification of marker layers (i.e. tephra and flood layers), as well as intervals of lower confidence in the alignment of the sediment cores without abundant visual markers. A recent approach using core-scanning X-ray fluorescence (XRF) by Mischke et al. (2017) aligned two cores using visually distinct features in the down-core elemental variation, but also noted the need to delete a number of "second order markers" to avoid conflicting and likely incorrect stratigraphic ordering.

Here we (1) provide details of the approach used for robust construction of a composite stratigraphy from two (or more) overlapping cores based on visual markers, and, if the latter are absent, guided by μ-XRF-based geochemical variability; and (2) introduce and describe the Orakei maar paleo-lake in a lithostratigraphic framework. In so doing we highlight the outstanding potential of the sequence for paleo-climatic reconstructions from an under-studied region of crucial importance to understanding the behaviour of the global climate system over the Last Glacial Cycle.

2 Regional setting

Auckland is located in the northern part of the North Island of New Zealand (Fig. 1a). The coring site, Orakei Basin, is a tidal lagoon with artificially controlled inflow and outflow to maintain water levels for water sports and allow regular flushing of pollutants. Subsequent to the highly explosive maar-forming phreatomagmatic eruption, a lake filled the crater until ca. 9.5 ka cal BP, when post-glacial sea-level rise breached the crater rim and connected the lake to the sea, allowing mass influx of tidal mud (Hayward et al., 2008). The modern surroundings of Orakei Basin are characterised by residential buildings to its south and the crater rim collapse identifiable from active landslides (Fig. 1d). Erosion and collapse of the steep crater walls and successive crater widening have led to repeated pulses of recycled eruptive material (juvenile clast and accidental ejecta/country rock) into the basin (Németh et al., 2012). Figure 1d shows the location of the two cores retrieved in 2016. No GPS position was recorded for the core retrieved in 2007, but the position was noted as near the centre of the basin. No shallow seismic survey of the sediment strata below the sediment–water interface has been undertaken. Hence, lateral extent and distribution of strata remain speculative.

3 Methods

3.1 Coring

Initial coring of Orakei Basin was undertaken from a floating barge in 2007 using a rotating barrel system, with a single core that penetrated to 81 m depth below the water–sediment interface. A further set of two overlapping cores with 50 cm vertical offset between them was collected in 2016 from a barge using wireline drilling and core collection in 1 m long sections. The lateral offset between the OB16A and OB16B core was 8 m.

3.2 Core description and visual facies identification

Split-core surfaces were described in detail for visually distinct changes in composition, qualitative grain size (clay, silt, very fine to coarse sand), colour (Munsell Color, 1975), thickness and shape of laminations, signs of bioturbation (burrows), (coring-induced and natural) disturbance of laminations and sedimentary features, presence of macrofossils (pieces of wood/bark and small twigs), and tephra layers. Each facies unit contains sediment of similar colour, composition, and laminae structure (or absence of laminations). Subunits differentiate between intervals of smaller differences, i.e. a change in lamination thickness or a slight colour change with overall similar sediment type and appearance. Most facies units have sharp contacts and are hence easily identified.

3.3 μ-XRF core scanning and magnetic susceptibility

The Orakei sediment cores were scanned using an Itrax μ-XRF core scanner (Cox Analytical Systems (Gothenburg, Sweden) at the School of Environment, University of Auckland, New Zealand. μ-XRF core scanning records down-core elemental variation in the range Al to U (on the Mo X-ray tube) rapidly, non-destructively, and with very little sample preparation (Croudace et al., 2006; Croudace and Rothwell, 2015). Here, μ-XRF data were acquired for all cores with the Mo X-ray tube (at 30 kv, 55 mA) at 1 mm spatial resolution and 10 s/step exposure time. High-resolution optical images (at 47 µm) and radiographic images (at 60 kV, 50 mA and 1 mm resolution) were recorded during the same scanning process. Magnetic susceptibility was acquired automati-

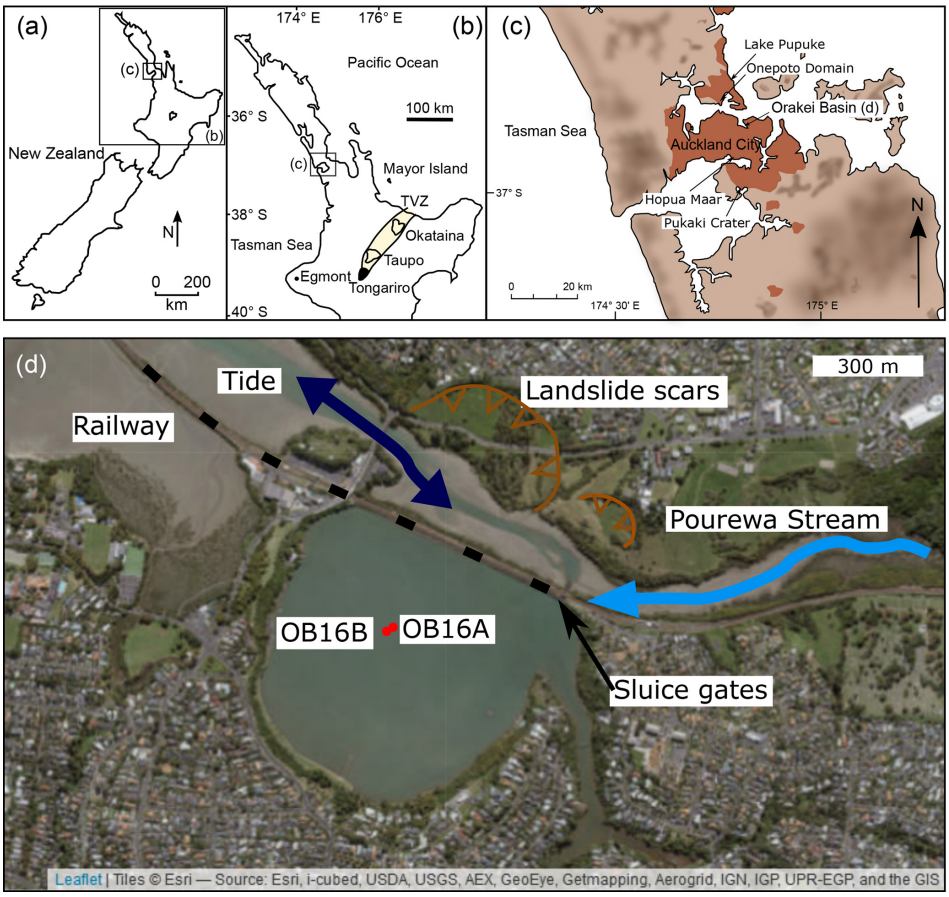

Figure 1. Map of the Orakei maar study area. **(a)** New Zealand with insets **(b)** and **(c)** marked. **(b)** New Zealand's North Island with Auckland (inset **c**) and the major volcanic source centres marked. **(c)** Auckland area showing the position of Orakei Basin. Red shading in populated areas; dark shading shows increased elevation. **(d)** Satellite image (ESRI world imagery) show the coring locations with red dots and other important features of the surroundings of the maar.

cally by the same Itrax core scanner at 5 mm resolution for all cores with a Bartington Magnetic Susceptibility MS2e surface scanning sensor.

3.4 Establishing the composite stratigraphy

The two cores retrieved in 2016 were drilled with at least 50 cm vertical offset to allow for overlaps between both cores around core breaks. The alignment of these overlapping sections is straightforward by visual means in the finely laminated sediment sections of the core. However, it is more difficult to establish a composite stratigraphy in the coarser sediment where clear marker layers are often absent. Consequently, magnetic susceptibility and μ-XRF data were used to aid the correlation of the overlapping cores as described below.

Visually prominent marker layers allowed most of the correlation using tephra layers (Table S2 in the Supplement), thick mass movement deposits, and major sharp facies contacts (i.e. onset of laminations, strong changes in grain size or colour) as outlined in Figs. 2 and 3. Finely laminated sediment was aligned on a sub-centimetre scale visually as highlighted by the high-resolution images in Fig. 2 (left). Coarse sediment showing no clear features along which to align the cores is shown in Fig. 2 (right). To obtain a complete composite stratigraphy, these intervals are correlated with reduced certainty (marked yellow in Fig. 3). These intervals constitute ca. 15 % of the entire sediment sequence and are confined by sharp upper and lower contacts. K and Fe (normalised to incoherent scatter (inc)) have been identified as showing the highest potential for cross-core correlation and have been used to identify chemical changes where visual markers are absent. The feasibility of this approach is underlined by the alignment of the finely laminated sediment where XRF-based correlation is in agreement with visual correlation as shown in Fig. 2 (left). Prominent minima or maxima in the geochemical XRF curve (i.e. K/inc) occur at sediment horizons different from sediment below and/or above, such as event layers or facies changes. It is reasonable to assume that these horizons are recorded in all sedi-

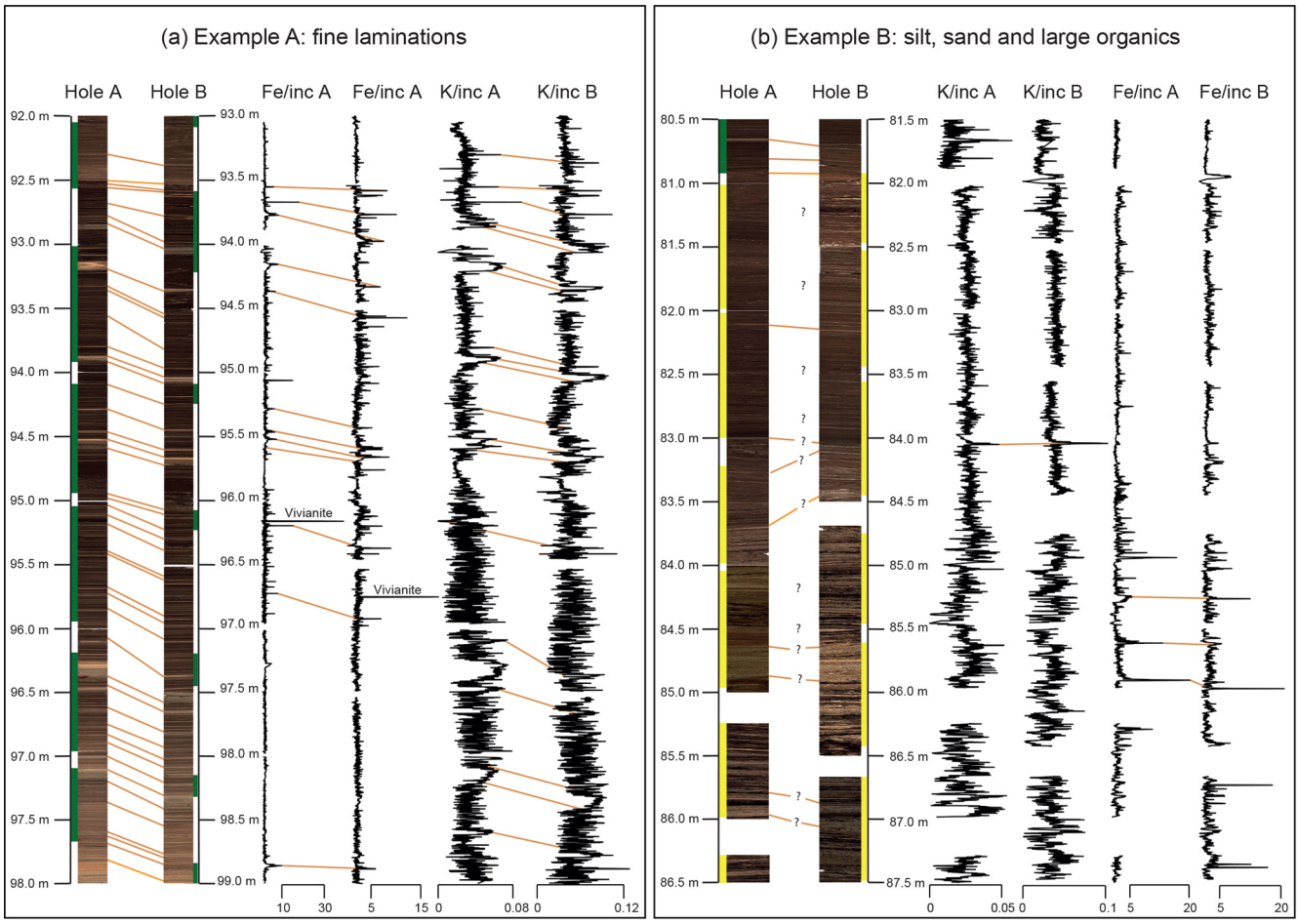

Figure 2. Examples of core photos from the Orakei maar paleo-lake record and their correlation. **(a)** Laminated facies easily correlated using visual marker layers. Down-core μ-XRF variation can be used for correlation, but does not offer additional markers. Green bands along the depth axis indicate the record of higher quality, which is adopted for the composite μ-XRF and MS record. **(b)** Facies comprised of silt, sand, and large subfossil wood fragments which are very difficult to correlate unambiguously. Visual correlation may be incorrect in large sections, but cannot be improved easily with μ-XRF variation either. Hence, yellow bands alongside the depth axis indicate unsure correlation, which is carried forward in the master record.

ment cores of the same depositional basin, which underlines their potential as marker layers. In this way, the down-core elemental variability has been used as an additional aid to establishing an overlapping composite stratigraphy. Where no other constraint on correlation could be established, it was guided by the common offset of the A-core usually showing distinct features $\sim$ 1 m higher than the B-core (note the offset depth scales in Fig. 2 for visualisation purposes). Horizons of instantaneous deposition such as tephra layers and mass movement deposits were removed on the event-corrected depth scale (ECD).

4 Results and discussion

4.1 Lithostratigraphic units

Figure 3 summarises the 16 major lithostratigraphic units (numbers) with 31 subunits (letters). Their differentiation is driven by visual changes in colour, grain size, dominant structure, and lamination thickness. Facies descriptions of the units are provided in Table S1 in the Supplement and are shown in Fig. 3, with example core photos in Fig. 4.

4.2 Preliminary age model

The dated rhyolitic tephra marker layers and one radiocarbon date near the top of the sequence from the 2007 core published in Hayward et al. (2008) (NZA28865: 9512 $\pm$ 19 cal ka BP, calibrated with SHCal13; Hogg et al., 2013) allow for the construction of a preliminary, simplified age

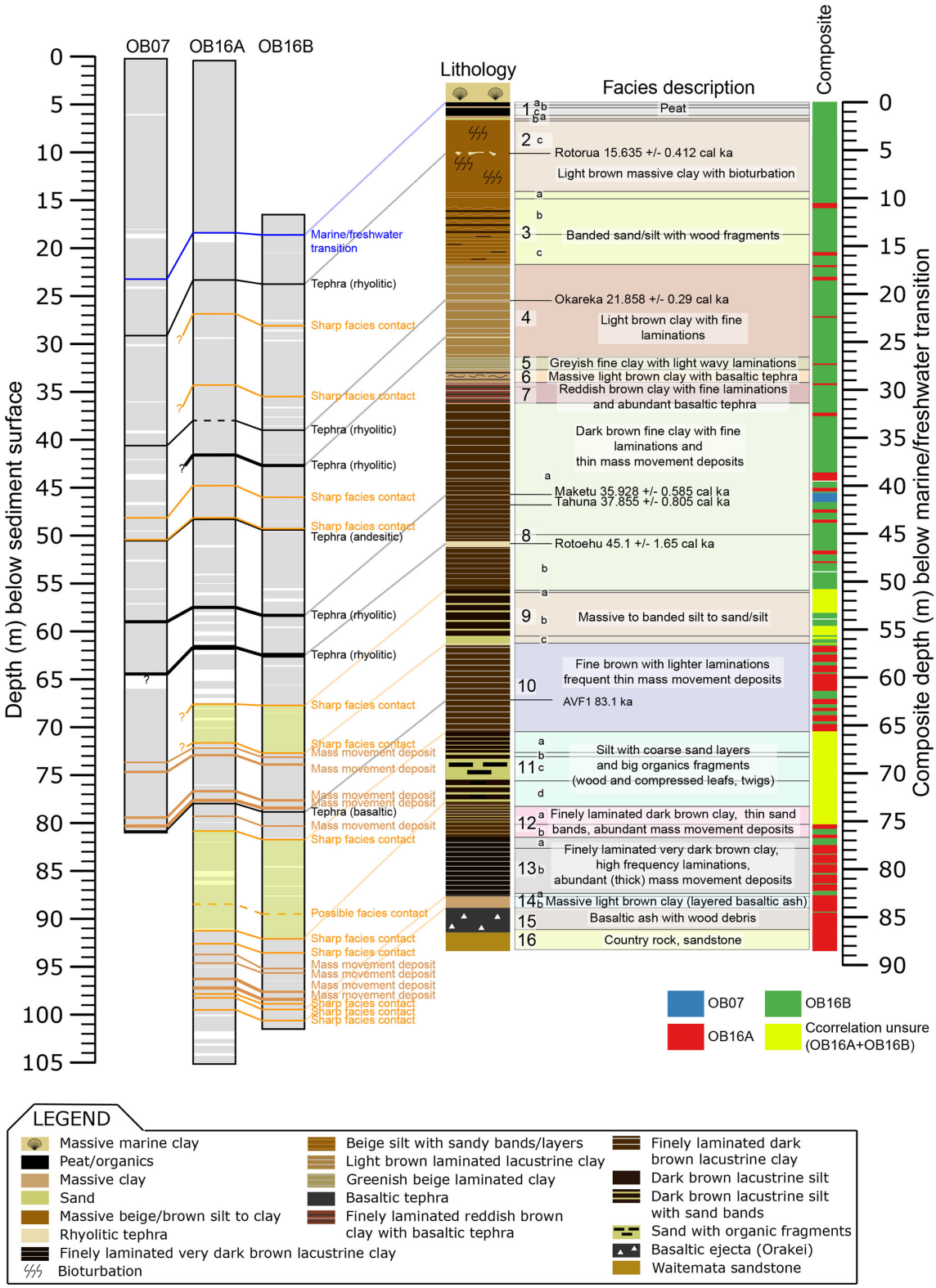

Figure 3. Orakei maar paleo-lake composite stratigraphy, lithological description, and rhyolitic marker tephra layers with ages (tephra layers from Peti et al., 2019).

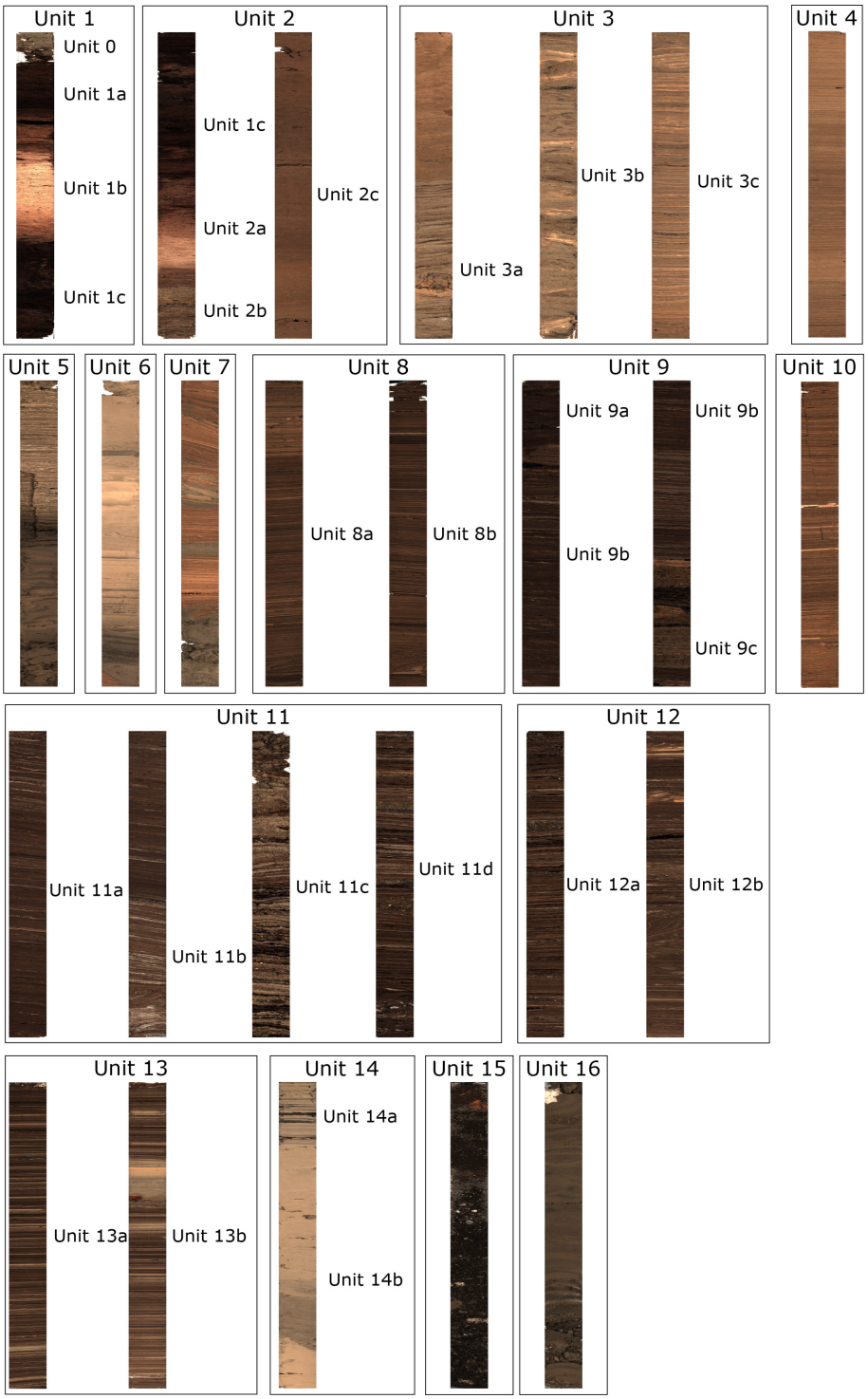

Figure 4. Example core photographs of the 16 facies units and subunits. Each core photo graphed is ∼ 1 m long.

model (Fig. 5). The finely laminated sediment between the Tahuna and Rotoehu tephra is largely representative for most of the Orakei sediment sequence below 40 m (ECD). The thick sand bands of facies units 9 and 11 have been removed on the ECD, explaining the difference of 4.83 m between Figs. 3 and 5. The sediment between those bands is mostly laminated silt, and we assume a similar sedimentation rate both above and below for this preliminary age estimate for the core base (Fig. 5). Extrapolation of the sedimentation rate between the Tahuna and Rotoehu tephras (2300 yr m^{-1})

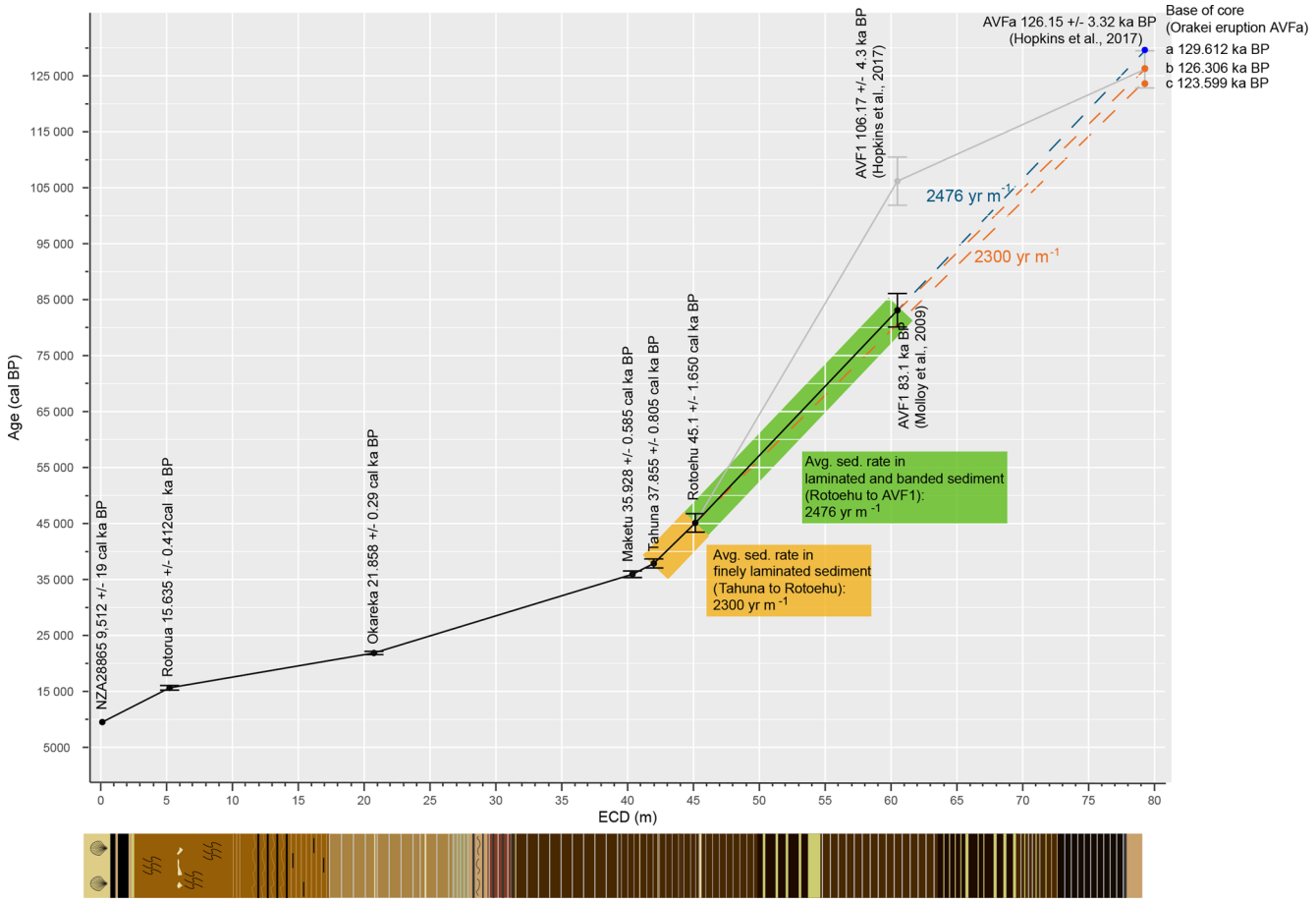

Figure 5. Preliminary age model established from rhyolitic tephra marker layers (Table S2) and extrapolation of an assumed continuous sedimentation rate to the core base compared with inferred ages in Hopkins et al. (2017).

to the base of the sequence (hence, eruption age of Orakei crater) produces an age of ca. 123.6 ka BP (Fig. 5, age c). Using the same approach, the age for basaltic tephra layer AVF1 is estimated to be ca. 80.4 ka BP, only slightly younger than the 83.1 ka BP estimated by Molloy et al. (2009) and well within typical errors of tephra ages pre-21 ka BP of ±1–2 ka (Molloy et al., 2009). Hopkins et al. (2017; Fig. 5) inferred an older age for AVF1 of 106.17 ± 4.3 ka BP together with a basal age of 126.15 ± 3.32 ka BP. Although the age estimate of the base of the sequence (i.e. the Orakei eruption, correlated with the AVFa horizon in Hopkins et al., 2017) agrees very well with our estimates, the AVF1 age appears > 20 kyr older compared to the estimate from the Orakei sediment accumulation rates (Fig. 5). This age–depth relationship would result in a low sedimentation rate between Rotoehu and AVF1 and a marked increase between AVF1 and the sequence base. Although it is possible that very thin mass movement deposits have not been recognised which could cause this higher sedimentation rate, the same would be true for facies units 8 and 10 above the AVF1 layer (Fig. 3). More rapid infilling of the crater could be associated with facies units 9 and 11 despite removal of the event layers. On the other hand, a slower observed sedimentation rate could also be caused by periods of non-deposition during significantly lower lake levels. Sharp facies contacts may indicate erosion and non-deposition. However, we consider this to represent only short time durations since the clay and silt intervals between the sand bands in facies units 9 and 11 show laminations indicating continuous sedimentation under deep-lake conditions (Fig. 3). Consequently, the inferred near-constant sedimentation rate model is preferred here. This model suggests that the Orakei eruption occurred just after Termination II (ca. 130 ka BP; Lisiecki and Raymo, 2005) early in the onset of the Last Interglacial (MIS 5e). Therefore, we infer that the Orakei sediment sequence spans most of the Last Glacial Cycle. However, these are necessarily crude estimates based on linear interpolation and extrapolation, and they are being refined (see Sect. 5).

5 Possible outcomes of the Orakei maar sediment sequence

A high-resolution multi-method chronology is currently being established for the Orakei sediment sequence based on radiocarbon dating, tephrochronology, post-IR IRSL (luminescence) dating, relative paleo-intensity variation of the Earth's magnetic field, and ^{10}Be cosmogenic nuclide flux into the lake. Coeval with this work, pollen and chironomid analyses are underway to enable detailed reconstruction of changes in the paleo-vegetation and climatic conditions. Itrax μ-XRF core scanning data alongside traditional measurements of loss-on-ignition, carbon and nitrogen content, as well as stable oxygen and carbon isotopes, will be combined to reconstruct the climatic development of the area over the Last Glacial Cycle. Micro-facies studies on resin-impregnated sediment slabs and large-scale thin sections will allow identification of abrupt climate shifts and events as well as identification of changes in seasonality recorded in the Orakei composite sediment sequence.

The Orakei maar paleo-lake sequence is expected to do the following.

1. Constrain the frequency and magnitude of eruptions of the Auckland Volcanic Field through provision of better age estimates for past basaltic eruptions.

2. Constrain the nature, drivers, magnitude, and timing of climatic changes in this part of the south-western Pacific. In addition, accurate and precise dating of the age markers and correlation with cosmogenic nuclide production variation (^{10}Be) may enable identification of climate leads and lags between the Northern and Southern Hemisphere mid-latitudes, including European maar lake and polar ice core records.

3. Understand the role of the westerly winds in climate change on a millennial to sub-decadal timescale in the south-western Pacific over the Last Glacial Cycle, with thick laminae likely reflecting a response to strong south-westerly winds with increased precipitation over the region depositing wind-blown dust and, hence, controlling biological productivity in the lake.

6 Conclusions

Even the most detailed observations and most sophisticated coring techniques cannot produce a perfect sediment core composite stratigraphy. In the case of finely laminated sediment and no to little coring disturbance, it is relatively straightforward to align overlapping cores along prominent sedimentary features, such as mass movement deposits, unique alternations of laminations, sharp facies contacts, or tephra layers. In the case of coarse sand and macroscopic organic detritus (e.g. facies units 9 and 11), core alignments prove to be more challenging. Despite the close proximity of the two coring positions in Orakei maar (Fig. 1, 10 m distance), the uneven distribution of mass movement deposits/slumps at the lake bottom results in small differences of the sediment stratigraphy that reduce confidence in the development of the composite stratigraphy over these intervals. While it is important to be aware of this source of uncertainty, the affected interval will reduce in relative thickness when the record is viewed against a timescale as opposed to a depth scale (metres below the marine water–freshwater transition).

Overall, the Orakei maar paleo-lake record constitutes an exceptional, continuous, long, high-resolution sedimentary record that captures environmental and climatic changes in the northern North Island of New Zealand over the Last Glacial Cycle. The history of the lake commenced with the maar-forming phreatomagmatic eruption, through various stages of changing deep lacustrine conditions, minor mass movement events associated with erosion/collapse of the crater rim, and deposition of distal rhyolitic and locally derived basaltic tephra layers. The deep lake phase was terminated by fluvial sediment influx at ca. 20.3 cal ka BP (onset of facies unit 3) and peat accumulation to infill the basin before an episodic breach of the crater rim associated with rising post-glacial sea level in the early Holocene drove rapid marine sediment influx to create the modern tidal basin. Correlation of the Orakei maar lake sediment sequence with those developed from Pupuke and Onepoto maars (Fig. 1) will enable development of an AVF master stratigraphy and robust reconstruction of environmental and climatic conditions spanning the last two glacial cycles for the first time from subtropical northern New Zealand.

Data availability. Preliminary data presented in this progress report are not publicly available as they are still being evaluated and expanded. Upon completion, all data will be made available when scientific papers and reports are published.

Supplement. The supplement related to this article is available online at: https://doi.org/10.5194/sd-25-47-2019-supplement.

Author contributions. PCA leads the AVF maar project, secured funding, and is involved in all aspects of the work. LP conducted the core descriptions, Itrax μ-XRF core scans, and development of the composite stratigraphy. LP wrote the original version of this report with refinements from PCA.

Competing interests. The authors declare that they have no conflict of interest.

Acknowledgements. The drilling investigation team included Paul Augustinus, Jan Lindsay, Phil Shane, Elaine Smid (University of Auckland), Jenni Hopkins and Graham Leonard (GNS Science), Valerie van den Bos (Victoria University of Wellington), Tim Shanahan and Natalia Piatrunia (University of Texas at Austin), and Frank Sirocko (University of Mainz). The project was funded by DeVORA (funded by New Zealand's Earthquake Commission and the Auckland Council), and a grant from the Royal Society of New Zealand Marsden Fund (UOA1415 to Paul C. Augustinus). Leonie Peti thanks Patricia Gadd (ANSTO, Australia) and Per Engström (Cox Analytical, Sweden) for outstanding help with Itrax data. We thank Bernd Zolitschka and David Lowe for thoughtful comments and improvements on the manuscript and Ulrich Harms for efficient editorial handling.

Review statement. This paper was edited by Ulrich Harms and reviewed by David Lowe and Bernd Zolitschka.

References

Alloway, B. V., Lowe, D. J., Barrell, D. J. A., Newnham, R. M., Almond, P. C., Augustinus, P. C., Bertler, N. A. N., Carter, L., Litchfield, N. J., McGlone, M. S., Shulmeister, J., Vandergoes, M. J., Williams, P. W., and NZ-INTIMATE members: Towards a Climate Event Stratigraphy for New Zealand over the past 30 000 years (NZ-INTIMATE project), J. Quaternary Sci., 22, 9–35, https://doi.org/10.1002/Jqs.1079, 2007.

Augustinus, P.: NZ-Maars: Extracting high resolution paleoclimate records from maar crater lakes, Auckland, New Zealand, PAGES News, 15, 18–20, 2007.

Augustinus, P., D'Costa, D., Deng, Y., Hagg, J., and Shane, P.: A multi-proxy record of changing environments from ca. 30 000 to 9000 cal. a BP: Onepoto maar palaeolake, Auckland, New Zealand, J. Quaternary Sci., 26, 389–401, https://doi.org/10.1002/jqs.1463, 2011.

Brauer, A., Endres, C., and Negendank, J. F. W.: Lateglacial calendar year chronology based on annually laminated sediments from Lake Meerfelder Maar, Germany, Quaternary Int., 61, 17–25, https://doi.org/10.1016/S1040-6182(99)00014-2, 1999.

Croudace, I. W. and Rothwell, R. G. (Eds.): Micro-XRF Studies of Sediment Cores: Applications of a non-destructive tool for the environmental sciences, Springer, DPER Series 17, Dordrecht, 656 pp., 2015.

Croudace, I. W., Rindby, A., and Rothwell, R. G.: ITRAX: description and evaluation of a new multi-function X-ray core scanner, Geol. Soc. Lond. Spec. Publ., 267, 51–63, https://doi.org/10.1144/GSL.SP.2006.267.01.04, 2006.

Edbrooke, S. W., Mazengarb, C., and Stephenson, W.: Geology and geological hazards of the Auckland urban area, New Zealand, Quaternary Int., 103, 3–21, https://doi.org/10.1016/S1040-6182(02)00129-5, 2003.

Hayward, B. W., Morley, M. S., Sabaa, A. T., Grenfell, H. R., Daymond-King, R., Molloy, C., Shane, P. A., and Augustinus, P. A.: Fossil Record of the Post-Glacial Marine Breaching of Auckland's Volcanic Maar Craters, Rec. Auckl. Museum, 45, 79–99, 2008.

Hogg, A., Hua, Q., Blackwell, P. G., Niu, M., Buck, C. E., Guilderson, T. P., Heaton, T. J., Palmer, J. G., Reimer, P. J., Reimer, R. W., Turney, C. S. M., and Zimmerman, S. R. H.: SHCal13 Southern Hemisphere Calibration, 0–50,000 Years cal BP, Radiocarbon, 55, 1889–1903, https://doi.org/10.2458/azu_js_rc.55.16783, 2013.

Hopkins, J. L., Millet, M. A., Timm, C., Wilson, C. J. N., Leonard, G. S., Palin, J. M., and Neil, H.: Tools and techniques for developing tephra stratigraphies in lake cores: A case study from the basaltic Auckland Volcanic Field, New Zealand, Quaternary Sci. Rev., 123, 58–75, https://doi.org/10.1016/j.quascirev.2015.06.014, 2015.

Hopkins, J. L., Wilson, C. J. N., Millet, M. A., Leonard, G. S., Timm, C., McGee, L. E., Smith, I. E. M., and Smith, E. G. C.: Multi-criteria correlation of tephra deposits to source centres applied in the Auckland Volcanic Field, New Zealand, B. Volcanol., 79, 55, https://doi.org/10.1007/s00445-017-1131-y, 2017.

Horrocks, M., Augustinus, P., Deng, Y., Shane, P., and Andersson, S.: Holocene vegetation, environment, and tephra recorded from Lake Pupuke, Auckland, New Zealand, New Zeal. J. Geol. Geop., 48, 85–94, https://doi.org/10.1080/00288306.2005.9515100, 2005.

Leonard, G. S., Calvert, A. T., Hopkins, J. L., Wilson, C. J. N., Smid, E. R., Lindsay, J. M., and Champion, D. E.: High-precision $^{40}Ar/^{39}Ar$ dating of Quaternary basalts from Auckland Volcanic Field, New Zealand, with implications for eruption rates and paleomagnetic correlations, J. Volcanol. Geoth. Res., 343, 60–74, https://doi.org/10.1016/j.jvolgeores.2017.05.033, 2017.

Lindsay, J., Leonard, G., Smid, E., and Hayward, B.: Age of the Auckland Volcanic Field: a review of existing data, New Zeal. J. Geol. Geop., 54, 379–401, https://doi.org/10.1080/00288306.2011.595805, 2011.

Lisiecki, L. E. and Raymo, M. E.: A Pliocene-Pleistocene stack of 57 globally distributed benthic $\delta^{18}O$ records, Paleoceanography, 20, 1–17, https://doi.org/10.1029/2004PA001071, 2005.

Mischke, S., Lai, Z., Aichner, B., Heinecke, L., Mahmoudov, Z., Kuessner, M., and Herzschuh, U.: Quaternary Geochronology Radiocarbon and optically stimulated luminescence dating of sediments from Lake Karakul, Tajikistan, Quat. Geochronol., 41, 51–61, https://doi.org/10.1016/j.quageo.2017.05.008, 2017.

Molloy, C., Shane, P., and Augustinus, P.: Eruption recurrence rates in a basaltic volcanic field based on tephralayers in maar sediments: Implications for hazards in the Auckland volcanic field, Bull. Geol. Soc. Am., 121, 1666–1677, https://doi.org/10.1130/B26447.1, 2009.

Munsell Color: Munsell soil color charts, Munsell Color, Baltimore, Md., 1975.

Nakagawa, T., Gotanda, K., Haraguchi, T., Danhara, T., Yonenobu, H., Brauer, A., Yokoyama, Y., Tada, R., Takemura, K., Staff, R. A., Payne, R., Bronk Ramsey, C., Bryant, C., Brock, F., Schlolaut, G., Marshall, M., Tarasov, P., and Lamb, H.: SG06, a fully continuous and varved sediment core from Lake Suigetsu, Japan: Stratigraphy and potential for improving the radiocarbon calibration model and understanding of late Quaternary climate changes, Quaternary Sci. Rev., 36, 164–176, https://doi.org/10.1016/j.quascirev.2010.12.013, 2012.

Németh, K., Cronin, S. J., Smith, I. E. M., and Agustin Flores, J.: Amplified hazard of small-volume monogenetic eruptions due to environmental controls, Orakei Basin, Auckland

Volcanic Field, New Zealand, B. Volcanol., 74, 2121–2137, https://doi.org/10.1007/s00445-012-0653-6, 2012.

Newnham, R. M., Lowe, D. J., and Alloway, B. V.: Volcanic hazards in Auckland, New Zealand: a preliminary assessment of the threat posed by central North Island silicic volcanism based on the Quaternary tephrostratigraphical record, Volcanoes Quat., 161, 27–45, https://doi.org/10.1144/GSL.SP.1999.161.01.04, 1999.

Peti, L., et al.: Reliability and repeatability of bulk μ-XRF measurements of rhyolitic tephra for their rapid and non-destructive identification, J. Quaternary Sci., in review, 2019.

Sandiford, A., Newnham, R., Alloway, B., and Ogden, J.: A 28 000–7600 cal yr BP pollen record of vegetation and climate change from Pukaki Crater, northern New Zealand, Palaeogeogr. Palaeocl., 201, 235–247, https://doi.org/10.1016/S0031-0182(03)00611-4, 2003.

Shane, P.: Towards a comprehensive distal andesitic tephrostratigraphic framework for New Zealand based on eruptions from Egmont volcano, J. Quaternary Sci., 20, 45–57, https://doi.org/10.1002/jqs.897, 2005.

Shane, P. and Hoverd, J.: Distal record of multi-sourced tephra in Onepoto Basin, Auckland, New Zealand: Implications for volcanic chronology, frequency and hazards, B. Volcanol., 64, 441–454, https://doi.org/10.1007/s00445-002-0217-2, 2002.

Zolitschka, B., Anselmetti, F., Ariztegui, D., Corbella, H., Francus, P., Lücke, A., Maidana, N. I., Ohlendorf, C., Schäbitz, F., and Wastegård, S.: Environment and climate of the last 51,000 years – new insights from the Potrok Aike maar lake Sediment Archive Drilling prOject (PASADO), Quaternary Sci. Rev., 71, 1–12, https://doi.org/10.1016/j.quascirev.2012.11.024, 2013.

Sci. Dril., 25, 57–62, 2019
https://doi.org/10.5194/sd-25-57-2019

Scientific Drilling
Open Access

Design of the subsurface observatory at Surtsey volcano, Iceland

Andreas Türke[1], Marie D. Jackson[2], Wolfgang Bach[1], Wolf-Achim Kahl[1], Brian Grzybowski[3], Beau Marshall[4], Magnús T. Gudmundsson[5], and Steffen Leth Jørgensen[6]

[1]Department of Geosciences and MARUM, University of Bremen, Bremen 28357, Germany
[2]Department of Geology and Geophysics, University of Utah, Salt Lake City, Utah 84102, USA
[3]L3 Technologies Inc., Communications and Networked Systems, Salt Lake City, Utah 84116, USA
[4]DOSECC Exploration Services, Salt Lake City, Utah 84101, USA
[5]Nordvulk, Institute of Earth Sciences, University of Iceland, Reykjavík, Iceland
[6]K.G. Jebsen Centre for Deep Sea Research, Department of Earth Science, University of Bergen, Bergen, Norway

Correspondence: Steffen Leth Jørgensen (steffen.jorgensen@bio.uib.no)

Received: 26 November 2018 – Revised: 29 April 2019 – Accepted: 3 May 2019 – Published: 12 June 2019

Abstract. Surtsey, the youngest of the islands of Vestmannaeyjar, is an oceanic volcano created by explosive basaltic eruptions during 1963–1967 off the southern coast of Iceland. The subsurface deposits of the volcano were first sampled by a cored borehole in 1979. In summer 2017, three cored boreholes were drilled through the active hydrothermal system of the volcano by the International Continental Scientific Drilling Program (ICDP) SUSTAIN Expedition 5059. These cores are expected to provide the first glimpse of microbial life in very young and native basaltic tuff of the oceanic crust. To reduce the contamination of the subsurface environment, seawater circulating fluid was filtered and passed through two UV-sterilizing treatments. One of the boreholes has been equipped with a subsurface observatory dedicated in situ experiments for monitoring water–rock interactions and microbial processes in sterile, artificial basaltic glass and in olivine granules. With temperatures ranging from 25 to 125 °C, the subsurface observatory provides a precise geothermal window into an active hydrothermal system and thus represents an exceptional natural laboratory for studying fluid–rock–microbe interactions at different temperature regimes and facilitates experimental validation of active submarine microbial processes at the limit of functional life, about 121 °C. Comparisons with the 1979 and 2019 drill cores will provide time-lapse observations of hydrothermal processes over a 50-year timescale. Here, we present the technical design of the observatory and the incubation chamber experiments deployed from September 2017 to summer 2019.

1 Introduction

Surtsey volcano forms the southernmost expression of Vestmannaeyjar, an oceanic archipelago created by basaltic eruptions in the offshore extension of the eastern Icelandic rift zone (Jakobsson et al., 2009). Explosive eruptions, followed by effusive lava flows from 1963–1967, constructed the island from a seafloor depth of about 130 m (Thors and Jakobsson, 1982; Fig. 1a). A cored borehole achieved in 1979 traversed hydrothermally altered basaltic tephra, tuff and intrusions to 181 m below the surface (m b.s.) but did not reach the pre-eruption seafloor (Jakobsson and Moore, 1982, 1986). Borehole temperatures varied from 25 to 141 °C in 1980. Investigations of 16S rRNA gene amplicons from fluids sampled in 2009 from the 1979 borehole (SE-01) identified microbial communities dominated by Archaea, primarily thermotolerant Methanobacteria at 172 m b.s. (54 °C) and by thermophilic Archaeoglobus-related sequences at 145 m b.s. (80 °C; Marteinsson et al., 2015). In summer 2017, the International Continental Scientific Drilling Program (ICDP) 5059 expedition, the Surtsey Underwater volcanic System for Thermophiles, Alteration processes and INnovative Con-

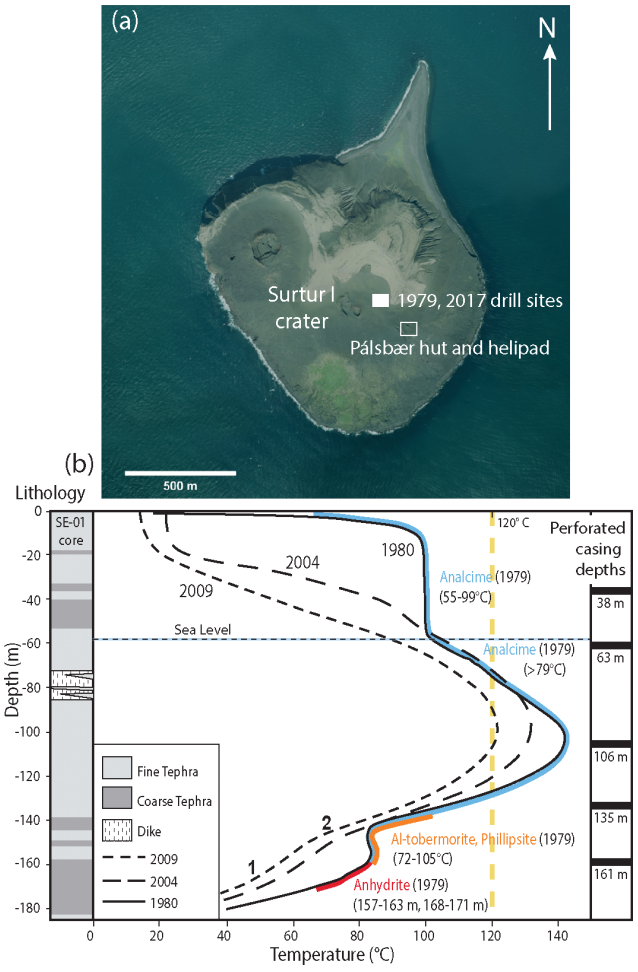

Figure 1. Setting of the Surtsey subsurface observatory in the 5059-1-C (SE-02b) cored borehole (latitude 63°18.09739′ N, longitude 20°35.99020′ W). **(a)** Aerial photograph of Surtsey, 26 July 2016 (courtesy of Loftmyndir ehf.); **(b)** temperature profile of the 1979 SE-01 cored borehole (after Jakobsson and Moore, 1986; Jackson et al., 2015) showing the 2009 site 1 and site 2 microbial communities (Marteinsson et al., 2015) and depths of the perforated casing segments. The yellow dashed line indicates the upper limit for functional microbial life, at about 121 °C.

cretes (SUSTAIN), recovered nearly 700 m of drill core from the basaltic deposits (Jackson et al., 2015, 2019).

While microbial life has been detected in native subsurface oceanic basalts (e.g. Lysnes et al., 2004; Lever et al., 2013; Jørgensen and Zhao, 2016), little is known about the factors that control habitability and the actual extent of the deep crustal biosphere, in terms of cellular mass and spatial distribution (Baquiran et al., 2016). Even less is known about microbial functions and their potential significance in this environment. Energy sources thought to sustain this biosphere could be provided through both chemical and physical processes occurring when volcanic rocks, which make up the majority of the hydrologically active oceanic crust, interact with seawater (Bach, 2016). Most observations of the deep biosphere hosted in basalt stem from subsurface observatories deployed at submarine drill holes (e.g. Orcutt et al., 2011; Edwards et al., 2012; Baquiran et al., 2016). While these observations have provided fundamental new knowledge, they focus on oceanic basalts several million years in age, and their accessibility is limited by costly oceanic expeditions, in situ technologies and long travel times.

The Surtsey subsurface observatory, by contrast, provides relatively straightforward access to an exceptionally young and pristine environment that records the initiation of subsurface microbial life in basaltic tephra in a broad range of temperatures, 25–125 °C, measured in the parallel 1979 (SE-01) borehole in 2017 (Fig. 1b), and varying hydrothermal fluid compositions (Jackson et al., 2019). The island is a protected UNESCO World Heritage Site that contains a unique scientific record of colonization of new land by plants, animals and marine organisms through long-term studies of primary biological succession (Baldursson and Ingadóttir, 2007). The time-lapse drill cores obtained in 1979 and 2017 and their associated fluids provide a first glimpse of subsurface marine microbial life in oceanic basalt. The steep temperature gradients in the young hydrothermal system – including a section that in 1979 exceeded the known temperature limit of life, 121 °C (Fig. 1b; Takai et al., 2008) – offer a unique opportunity to assess temperature dependency of microbial activity in the deep biosphere hosted by oceanic basalt.

2 Surtsey subsurface observatory design

The 5059-1-C (SE-02b) borehole began with rotary drilling for a steel HWT conductor casing with an outer diameter (OD) of 11.43 cm (4 1/2 in.) that extends to a casing shoe depth of 9.54 m.b.s. (Fig. 2a). The core was then drilled with a HQ3 bit (63.5 mm core diameter) to 191.64 m vertical depth from 18 to 26 August 2017 using seawater as the circulating fluid. To reduce contamination from live microbes, the seawater was passed through a 30 µm cartridge filter to remove fine debris and a WEDECO AQUA 4ALT UV light sterilization system at a flow rate $\leq 1.58\,\mathrm{L\,s^{-1}}$ before storage in 1000 L reservoir tanks. During pumping to the drill head the treated seawater was passed through a second UV light sterilization system (Weisenberger et al., 2019). Although great efforts were made to avoid contamination during drilling, a few applications of Florigel attapulgite mud were employed to secure borehole stability. After retrieval of the original HQ casing (88.9 mm OD), downhole logging of the borehole was undertaken by the ICDP Operational Support Group (Jackson et al., 2019; Weisenberger et al., 2019). The T-6061 anodized extruded aluminium NQ (69 mm OD) tubes that form the casing of the observatory were then were lowered to a landing depth of 181.25 m and hung in the borehole (Fig. 3c). A custom shoe was designed with a conical

Table 1. List of depth intervals for each incubation experiment, and the corresponding temperatures measured in the 1979 borehole (SE-01) in 2017 before the initiation of drilling.

Incubation experiment	Perforated casing interval (m b.s.)	Temperature (°C)
no. 1	37.01–38.63	41
no. 2	62.74–63.96	96
no. 3	106.11–107.33	124
no. 4	135.03–136.25	101
no. 5	160.48–161.70	61

shape to prevent infill of residual tephra and drilling debris during installation (Fig. 2d).

The 50 threaded NQ aluminium pipes that comprise the casing have an OD of 69 mm (2 3/4 in.), a 6.35 mm (0.25 in.) wall thickness and a 57 mm (2 1/4 in.) inner diameter. These occur in three lengths, 3.45, 3.60 and 3.75 m, due to sourcing constraints encountered by the provider (Arconic Energy Systems, 7211 Spring Cypress Road, Spring, Texas 77379, USA). Five of the tubes are perforated (Figs. 2e, 4a). They have a pattern of five 6.35 mm diameter (1/4 in.) holes, spaced equally in 72° angular increments, on 29 equally spaced cross sections that extend over 1.21 m (4 ft) centred in the mid-section of each pipe (Fig. 4a). The perforated sections are placed at 37.01–38.63, 62.74–63.96, 106.11–107.33, 135.03–136.25, and 160.48–161.70 m.b.s. at the sites of the incubation experiments (Fig. 1b; Table 1).

The casing is designed to hang freely within the open walls of the SE-02b borehole. It is assembled with a proprietary thread design developed by Arconic Energy Systems, tailored to meet the requirements for the casing size and application loads. The threaded flush joints were wrapped with Teflon™ tape and wrenched together by hand. The Teflon™ tape concentrates a small amount of organic polytetrafluoroethylene (PTFE) compound at the joint. Paste lubricants were not used, since they could have been smeared along casing surfaces, potentially contaminating the observatory.

At the top of the borehole, the aluminium casing hanger attaches to the uppermost section of aluminium pipe (Fig. 2b). The hanger has a shoulder that is larger in diameter than the internal landing shoulder on the steel wellhead. An elastomer O-ring centres the aluminium casing hanger in the bore of the steel wellhead. A Teflon™ shim is installed between the aluminium casing hanger and the steel landing shoulder to prevent corrosion of the aluminium. Polyvinyl chloride (PVC) centralizer tubes are installed between the aluminium casing and the HWT conductor casing to several metres depth also to minimize corrosion (Fig. 2b, c). A custom wellhead flange and hinged cover holds the Vectran™ rope with the five incubation experiments, which are suspended in the centre of the perforated aluminium casing segments (Fig. 2c). The flange cover is installed 0.21 m above the reference ground level. The hinged cover prevents ingress of environmental contaminants, such as rainwater, and is secured with hex cap screws (Fig. 2c). The wellhead can easily be opened to retrieve the incubators during subsequent observatory experiments or data acquisition retrieval operations.

3 Incubation experiments

The Vectran™ rope is currently equipped with 40 perforated incubation polyether ether ketone chambers or PEEKins (Fig. 3) designed to investigate chemical, mineral and microbial alteration over an expected 2-year period, from September 2017 to summer 2019. Each PEEKin has an outer diameter of 18 mm and an inner diameter of 14 mm. The perforations encourage the flow of in situ fluids and microbes into the chambers. Each PEEKin is attached with PEEK cable ties to an 8 mm diameter Vectran™ rope hung from the borehole wellhead. The PEEKins are deployed as packages of eight (4×2) to ensure replicates at each of the five perforated segment depths (38, 64, 108, 137 and 162 m.b.s.). A HOBO temperature logger monitors in situ temperature every 30 min at each depth. Artificial and sterile tephra, melted and quenched from Surtsey lava flows and separate packages of olivine crystals with compositions similar to those of Surtsey basalt (Fo 90, 90 % forsterite, Mg_2SiO_4; 10 % fayalite, Fe_2SiO_4; Jakobsson and Moore, 1986), are used as substrates in the current PEEKin chambers. The samples and data will be collected from the observatory in summer 2019.

Recharge of the hydrothermal system at Surtsey is thought to occur through the inflow of cool seawater in porous, poorly consolidated tuff within the deeper zones of the submarine deposits; heating occurs as the water percolates upwards through the higher temperature rocks of the geothermal reservoir (Jakobsson and Moore, 1982, 1986; Ólafsson and Jakobsson, 2009). Pronounced deviations in several geophysical logs at 143–150 m.b.s. in the SE-02b borehole confirm this inflow zone, where cooler water of higher salinity enters the borehole (Jackson et al., 2019). Vertical convection could initiate within the subsurface observatory but, based on the small casing diameter and temperature gradients, the flow rate would not strongly influence the alteration of the granules over the 2-year incubation periods.

Analytical investigations will evaluate rates of glass and mineral alteration, identify pioneering microorganisms, community dynamics and stability, and, potentially, provide pristine textural biosignatures of microbe–mineral interactions. The samples will be further analysed in terms of microbial genomics, including (1) community profiling by high throughput sequencing of prokaryotic 16S ribosomal gene amplicons libraries, (2) shotgun sequencing of genomic DNA, and (3) quantification of key functional genes, such as 16S rRNA, *mcrA* and *dsrB*. Atomic force microscopy combined with vertical scanning interferometry (AFM–VSI) as well as synchrotron X-ray microdiffraction studies will be

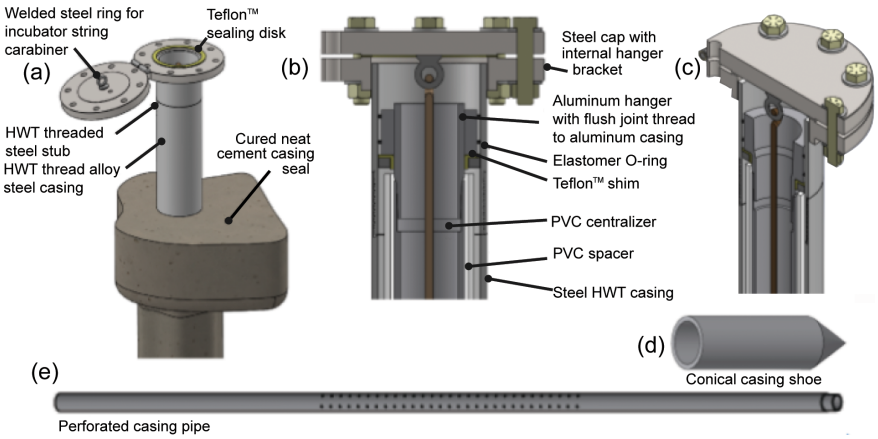

Figure 2. Borehole components of the Surtsey subsurface observatory. **(a)** HWT (11.43 cm outer diameter) steel casing surrounds the aluminium casing to 9.54 m.b.s.; **(b, c)** components of the wellhead. **(d)** Conical NQ (69 mm OD) aluminium casing shoe, 25.4 cm (10 in.) in length. **(e)** Perforated NQ aluminium casing pipe, 3.66 m (12 ft) in length.

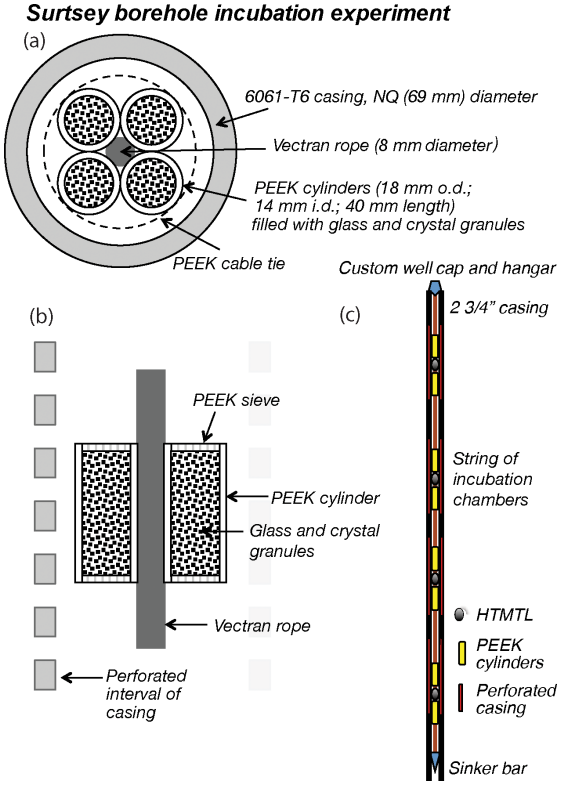

Figure 3. Design of the PEEK incubation chambers (PEEKins) and subsurface observatory in ICDP borehole 5059-1-C (SE-02b). **(a)** Schematic top view of the PEEKin as it is deployed in the borehole; **(b)** schematic side view of the PEEKin at intervals where the casing is perforated. **(c)** Sketch of the downhole observatory, which comprises an NQ anodized aluminium casing with five perforated sections, an inner Vectran™ rope hung from the wellhead with a sinker bar attached at its lower end and five incubation experiments placed at the perforated sections (Table 1).

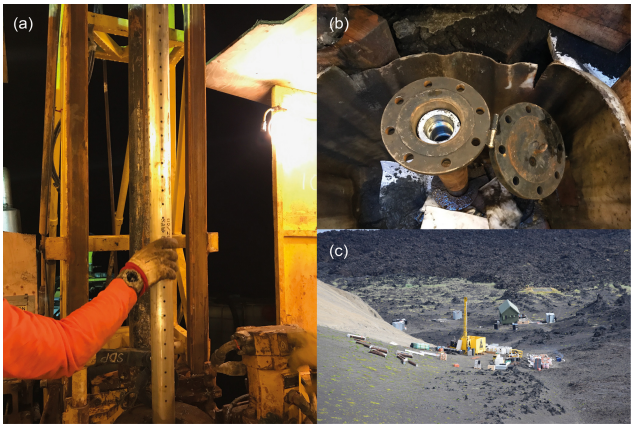

Figure 4. Photographs of drilling operations illustrating components of the borehole observatory. **(a)** Perforated casing interval as it is lowered into the borehole; **(b)** the open wellhead of the observatory. **(c)** Drill site and operations on Surtsey volcano. Photo credits: **(a)** Andreas Türke, **(b)** Stephen Cole and **(c)** Beau Marshall.

performed on the glass and olivine samples retrieved from the observatory.

4 Outlook and perspectives

The Surtsey subsurface observatory and its current experiments provide an unprecedented opportunity to study very young submarine basalt without the need for expensive and risky deep ocean operations. The current iteration of experiments and instruments deployed in the observatory will be retrieved in summer 2019. The observatory will be open to a broad scientific community from summer 2019 onwards, with priority granted to the SUSTAIN team members during the 4 years following the current experiment. The long-term management of the Surtsey subsurface observatory occurs

through the commitment of the Surtsey Research Society. The borehole observatory is planned to remain operational and open for research for many decades. Information on access to the observatory and application procedures for future research projects is listed on the webpage of the Surtsey Research Society (http://www.surtsey.is).

Data availability. The article is a technical description of the Surtsey Subsurface Observatory. Initial data are expected in autumn 2019, so there is no data repository at present. Information on access to the observatory and application procedures for future research projects is listed on the webpage of the Surtsey Research Society (http://www.surtsey.is).

Author contributions. MDJ and MTG led the drilling project. BM was the drilling operation supervisor. AT, WB, W-AK, and SLJ designed the components of the incubation chambers. BG, MDJ, BM, and SLJ designed the components of the borehole casing. AT and MDJ wrote the article and created the figures with the assistance of SLJ, BG, WB, W-AK, and MTG.

Competing interests. The authors declare that they have no conflict of interest.

Disclaimer. Any use of trade, firm, or product names is for descriptive purposes only.

Acknowledgements. We thank all members of the SUSTAIN onsite and science teams and the Surtsey Research Society for their contributions to the drilling project. Bernd Zimanowski, at the University of Würzburg, produced the sterile basaltic glass for the current in situ experiments. The SUSTAIN project was funded by the International Continental Scientific Drilling Program (ICDP; led by Marie D. Jackson), the Icelandic Science Fund, ICF-RANNÍS (the IceSUSTAIN consortium led by Magnús T. Guðmundsson), the Bergen Research Foundation and K. G. Jebsen Centre for Deep Sea Research at the University of Bergen, Norway (led by Steffen Leth Jørgensen), the German Research Foundation (DFG; led by Wolfgang Bach and Bernd Zimanowski), and DiSTAR, University of Naples, Federico II, Italy (led by Piergiulio Cappelletti). The University of Utah, USA (Marie D. Jackson) and the two Icelandic power companies, Reykjavík Energy and Landsvirkjun, contributed additional funds. Anonymous reviewers made valuable improvements to the report.

Review statement. This paper was edited by Ulrich Harms and reviewed by two anonymous referees.

References

Bach, W.: Some compositional and kinetic controls on the bioenergetic landscapes in oceanic basement, Front. Microbiol., 7, 107, https://doi.org/10.3389/fmicb.2016.00107, 2016.

Baldursson, S. and Ingadóttir, Á.: Nomination of Surtsey for the UNESCO World Heritage List, Icelandic Institute of Natural History, Reykjavik, 2007.

Baquiran, J. P. M., Ramírez, G. A., Haddad, A. G., Toner, B. M., Hulme, S., Wheat, C. G., Edwards, K. J., and Orcutt, B. N.: Temperature and redox effect on mineral colonization in Juan deFuca Ridge Flank subsurface crustal fluids, Front. Microbiol., 7, 396, https://doi.org/10.3389/fmicb.2016.00396, 2016.

Edwards, K. J., Wheat, C. G., Orcutt, B., Hulme, S., Becker, K., Jannasch, H., Haddad, A., Pettigrew, T., and Bach, W.: Design and deployment of borehole observatories and experiments during IODP Expedition 336, Mid-Atlantic Ridge flank at North Pond. Integrated Ocean Drilling Program. Proceedings, Expedition Reports, 336, 109–109, 2012.

Jackson, M. D., Gudmundsson, M. T., Bach, W., Cappelletti, P., Coleman, N. J., Ivarsson, M., Jónasson, K., Jørgensen, S. L., Marteinsson, V., McPhie, J., Moore, J. G., Nielson, D., Rhodes, J. M., Rispoli, C., Schiffman, P., Stefánsson, A., Türke, A., Vanorio, T., Weisenberger, T. B., White, J. D. L., Zierenberg, R., and Zimanowski, B.: Time-lapse characterization of hydrothermal seawater and microbial interactions with basaltic tephra at Surtsey Volcano, Sci. Dril., 20, 51–58, https://doi.org/10.5194/sd-20-51-2015, 2015.

Jackson, M. D., Gudmundsson, M. T., Weisenberger, T. B., Rhodes, J. M., Stefánsson, A., Kleine, B. I., Lippert, P. C., Marquardt, J. M., Reynolds, H. I., Kück, J., Marteinsson, V. T., Vannier, P., Bach, W., Barich, A., Bergsten, P., Bryce, J. G., Cappelletti, P., Couper, S., Fahnestock, M. F., Gorny, C. F., Grimaldi, C., Groh, M., Gudmundsson, Á, Gunnlaugsson, Á. T., Hamlin, C., Högnadóttir, Th., Jónasson, K., Jónsson, S. S., Jørgensen, S. L., Klonowski, A. M., Marshall, B., Massey, E., McPhie, J., Moore, J. G., Ólafsson, E. S., Onstag, S. L., Perez, V., Prause, S., Snorrason, S. P., Türke, A., White, J. D. L., and Zimanowski, B.: SUSTAIN drilling at Surtsey volcano, Iceland, tracks hydrothermal and microbiological interactions in basalt 50 years after eruption: Sci. Drilling, in press, 2019.

Jakobsson, S. P. and Moore, J. G.: The Surtsey research drilling project of 1979, Surtsey Research, 9, 76–93, 1982.

Jakobsson, S. P. and Moore, J. G.: Hydrothermal minerals and alteration rates at Surtsey volcano, Iceland, Geol. Soc. Am. Bul., 97, 648–659, 1986.

Jakobsson, S. P., Thors, K., Vésteinsson, Á. T., and Ásbjörnsdóttir, L.: Some aspects of the seafloor morphology at Surtsey volcano: The new multibeam bathymetric survey of 2007, Surtsey Research, 12, 9–20, 2009.

Jørgensen, S. L. and Zhao, R.: Microbial inventory of deeply buried oceanic crust from a young ridge flank, Front. Microbiol., 7, 820, https://doi.org/10.3389/fmicb.2016.00396, 2016.

Lever, M. A., Rouxel, O., Alt, J. C., Shimizu, N., Ono, S., Coggon, R. M., Shanks W. C., Lepham, L., Elvert, M., Prieto-Mollar, X., Hinrichs, K. U., Inagaki, F., and Teske, A.: Evidence for microbial carbon and sulfur cycling in deeply buried ridge flank basalt, Science, 339, 1305–1308, 2013.

Lysnes, K., Thorseth, I. H., Steinsbu, B. O., Øvreås, L., Torsvik, T., and Pedersen, R. B.: Microbial community diversity in seafloor basalt from the Arctic spreading ridges, FEMS Microbiol. Ecol., 50, 213–230, 2004.

Marteinsson, V., Klonowski, A., Reynisson, E., Vannier, P., Sigurdsson, B. D., and Ólafsson, M.: Microbial colonization in diverse surface soil types in Surtsey and diversity analysis of its subsurface microbiota, Biogeosciences, 12, 1191–1203, https://doi.org/10.5194/bg-12-1191-2015, 2015.

Ólafsson, M. and Jakobsson, S. P.: Chemical composition of hydrothermal water and water-rock interactions on Surtsey volcanic island: A preliminary report, Surtsey Research, 12, 29–38, 2009.

Orcutt, B. N., Bach, W., Becker, K., Fisher, A. T., Hentscher, M., Toner, B. M., Wheat, G., and Edwards, K. J.: Colonization of subsurface microbial observatories deployed in young ocean crust, The ISME journal, 5, 692, https://doi.org/10.1038/ismej.2010.157, 2011.

Takai, K., Nakamura, K., Toki, T., Tsunogai, U., Miyazaki, M., Miyazaki, J., Hirayama, H., Nakagawa, S., Nunoura, T., and Horikoshi, K.: Cell proliferation at 122° C and isotopically heavy CH_4 production by a hyperthermophilic methanogen under high-pressure cultivation, National Academy of Sciences Proceedings, 105, 10949–10954, 2008.

Thors, K. and Jakobsson, S. P.: Two seismic reflection profiles from the vicinity of Surtsey, Iceland, Surtsey Res. Progr. Rep., 9, 149–151, 1982.

Weisenberger, T. B., Gudmundsson, M. T., Jackson, M. D., Gorny, C. F., Türke, A., Kleine, B. I., Marshall, B., Jørgensen, S. L., Marteinsson, V. T., Stefánsson, A., White, J. D. L., Barich, A., Bergsten, P., Bryce, J. G., Couper, S., Fahnestock, M. F., Franzson, H., Grimaldi, C., Groh, M., Guðmundsson, Á., Gunnlaugsson, Á. T., Hamlin, C., Högnadóttir, Th., Jónasson, K., Jónsson, S., S., Klonowski, A., Kück, J., Magnússon, R. L., Massey, E., McPhie, J., Ólafsson, E. S., Onstad, S. L., Prause, S., Perez, V., Rhodes, J. M., and Snorrason, S. P.: Operational Report for the 2017 Surtsey Underwater volcanic System for Thermophiles, Alteration processes and INnovative Concretes (SUSTAIN) drilling project at Surtsey Volcano, Iceland, Geo Forschungs Zentrum report, 2019.

Sci. Dril., 25, 63–70, 2019
https://doi.org/10.5194/sd-25-63-2019

Scientific Drilling
Open Access

ICDP workshop on scientific drilling of Nam Co on the Tibetan Plateau: 1 million years of paleoenvironmental history, geomicrobiology, tectonics and paleomagnetism derived from sediments of a high-altitude lake

Torsten Haberzettl[1], Gerhard Daut[2], Nora Schulze[3], Volkhard Spiess[3], Junbo Wang[4], Liping Zhu[4], and the 2018 Nam Co workshop party[*]

[1]University of Greifswald, Institute of Geography and Geology, Physical Geography, Friedrich-Ludwig-Jahn-Str. 16, 17489 Greifswald, Germany
[2]Friedrich-Schiller-University Jena, Institute of Geography, Physical Geography, Löbdergraben 32, 07743 Jena, Germany
[3]Department of Geosciences, Marine Technology and Environmental Research, University of Bremen, Bremen, Germany
[4]Institute of Tibetan Plateau Research, Chinese Academy of Sciences, No. 16 Lincui Road, Chaoyang District, Beijing 100101, China
[*]A full list of authors and their affiliations appears at the end of the paper.

Correspondence: Torsten Haberzettl (torsten.haberzettl@uni-greifswald.de)

Received: 10 September 2018 – Revised: 21 November 2018 – Accepted: 22 November 2018 – Published: 12 June 2019

Abstract. The Tibetan Plateau is of peculiar societal relevance as it provides freshwater from the so-called "Water Tower of Asia" to a large portion of the Asian population. However, future climate change will affect the hydrological cycle in this area. To define parameters for future climate change scenarios it is necessary to improve the knowledge about thresholds, timing, pace and intensity of past climatic changes and associated environmental impacts. Sedimentary archives reaching far back in time and spanning several glacial–interglacial cycles such as Nam Co provide the unique possibility to extract such information. In order to explore the scientific opportunities that an ICDP drilling effort at Nam Co would provide, 40 scientists from 13 countries representing various scientific disciplines met in Beijing from 22 to 24 May 2018. Besides paleoclimatic investigations, opportunities for paleomagnetic, deep biosphere, tectonic and paleobiological studies were discussed. After having explored the technical and logistical challenges and the scientific opportunities all participants agreed on the great value and need to drill this extraordinary archive, which has a sediment thickness of more than 1 km, likely covering more than 1 Ma.

1 Introduction

With a mean elevation of > 4000 m above sea level, the Tibetan Plateau is often considered as the "Third Pole", as it is the third largest storage of ice on earth (Qiu, 2008). Its isolated setting at high altitudes resulted from its long tectonic evolution and made it home to unique ecosystems with a large number of endemic species, particularly in aquatic systems (von Oheimb et al., 2011). The Tibetan Plateau is also of peculiar social relevance as it is the source of several major rivers, providing freshwater from the so-called "Water Tower of Asia" to a large portion of the Asian population (Lau et al., 2010) and sediment for associated mega deltas with areas larger than 10 000 km^2, being home to millions of people (Cruz et al., 2007). Future climate change, as shown in the 5th IPCC assessment report (Masson-Delmotte et al., 2013), will impact the hydrological cycle in this area and consequently the ecology and economy. To define parameters

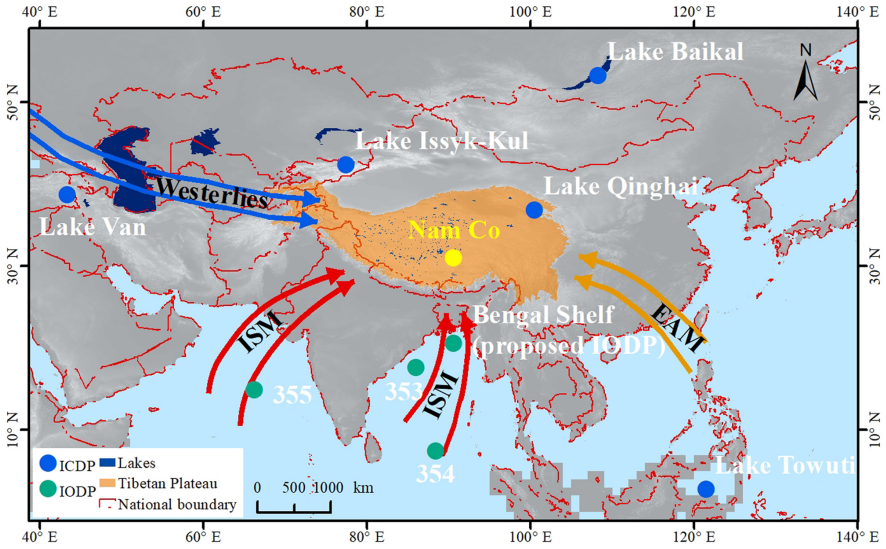

Figure 1. Strategic location of Nam Co (yellow dot) on the Tibetan Plateau (orange area) with respect to further ICDP and IODP sites (blue and green dots). Numbers represent IODP expeditions, ISM: Indian Summer Monsoon, EAM: East Asian Monsoon. Source map: Shuttle Radar Topography Mission digital elevation model (SRTM DEM) from the US Geological Survey (https://lta.cr.usgs.gov/citation, last access: 12 November 2018).

for future climate change scenarios and their consequences for ecosystems and society, it is necessary to improve our knowledge about the thresholds, timing, pace and intensity of past climatic changes and associated environmental impacts, not just on short (modern to Last Glacial Maximum) but also on long geologic timescales and with high resolution.

High-resolution archives, such as lacustrine sediments, are abundant on the Tibetan Plateau but the depositional histories are rather short and often discontinuous, because an arid climate led to repeated desiccation. On the northern TP, Lake Qinghai is an archive where one of the longest paleoclimatic records (32 cal ka BP) from the Tibetan Plateau was produced (An et al., 2012). On the western plateau, Bangong Co (co = lake) bears a Holocene paleoclimatic record (Fontes et al., 1996) and in the south, at Puma Yumco, paleoclimatic variations of the past 19 cal kyr BP were investigated (Nishimura et al., 2014). However, none of these investigations exceeds the Last Glacial. Thus, large and deep lacustrine systems with sizeable catchment areas, integrating regional climatic signals, represent the only suitable continuous paleoclimate archives. Previous studies have shown that Nam Co is one of those lakes (Kasper et al., 2015).

During the past 10 years, transect studies focusing on paleoclimate on the Tibetan Plateau, including Nam Co, have been carried out (Ahlborn et al., 2017; Alivernini et al., 2018; Dietze et al., 2014). In addition, physical and chemical limnological seasonal processes as well as climate parameters at Nam Co have been monitored. Further information on environmental dynamics in the Nam Co catchment is available for glacier dynamics (Bolch et al., 2010), hydrology (Krause et al., 2010), regional geology (Wu et al., 2011), geomorphology (Keil et al., 2010) and meteorology (Ma et al., 2008). This makes the Nam Co area one of the best-surveyed areas on the Tibetan Plateau.

Because of the location of Nam Co on the central Tibetan Plateau at the intersection of westerly and monsoonal air masses (Fig. 1) and its continuous sedimentation history, it represents an ideal drilling target to disentangle long-term changes in climate. A record from Nam Co will enable the following: the relation of climate signals in Tibet to interregional and/or global atmospheric circulation patterns using, for example, sediment cores recovered in IODP; the study of paired ocean and continent archives in appropriate locations with adequate resolution; the investigation of upstream and downstream processes (Thurow et al., 2009) and fill a gap in two ICDP/IODP continental scale transects (Fig. 1, N–S: Lake Baikal, Lake Qinghai, Bay of Bengal; W–E: Lake Van, Lake Issyk-Kul, Lake Towuti). These transects (especially the N–S) will contribute to the Baikal to Bengal transect, which focuses on the internal dynamics of the monsoonal system. This follows previous discussions on utilizing combined ICDP and IODP drilling projects for maximizing the scientific progress in paleoclimate research (Thurow et al., 2009).

2 Site description

Nam Co has a flat central basin with a water depth > 95 m and a smaller and shallower basin of only about 60 m water depth in the NE (Fig. 2) (Wang et al., 2009). The lake covers

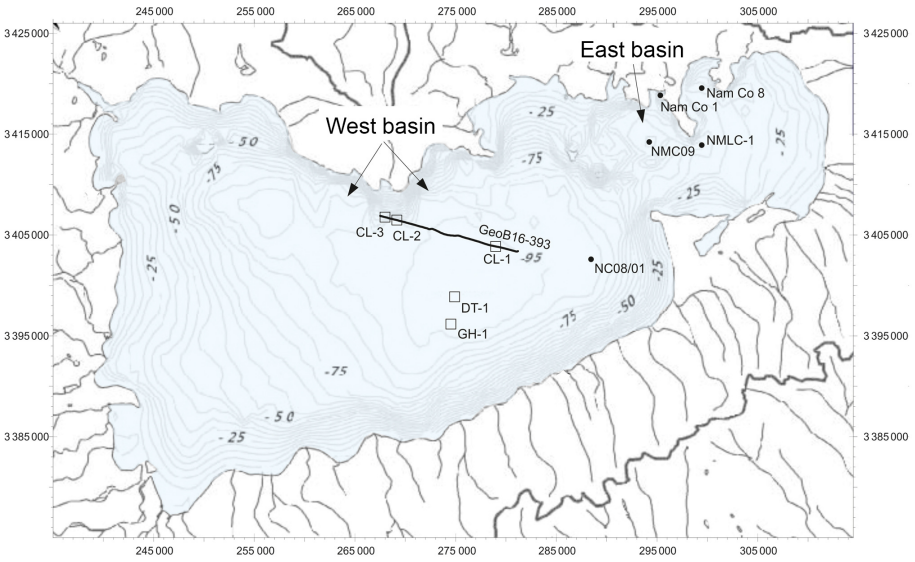

Figure 2. Bathymetry of Nam Co (Wang et al., 2009). Potential drill sites for three piston cores (CL-1, CL-2, CL-3) along profile GeoB16-393 (Fig. 4), a deep core (DT-1) and a glacial history core (GH-1) are indicated. Also indicated are previously investigated sediment cores NMLC1 (Zhu et al., 2008), Nam Co 8 (Mügler et al., 2010), NC08/01 (Kasper et al., 2015) and NMC09 (Li et al., 2017).

an area of 2015.4 km^2 (Zhu et al., 2010) and has a catchment area of 10 680 km^2 (Zhou et al., 2013). The drainage area hosts more than 60 streams, most of them draining the glaciated Nyainqêntanglha mountain range (> 7000 m a.s.l.) in the S and SW of the lake (Xie et al., 2009). Annual precipitation is around 420 mm, with more than 90 % from intensive monsoonal rainfall from June to September. Dry conditions with low precipitation prevail from October to May (Zhang et al., 2011). As Nam Co is situated in a closed basin, the water balance is primarily controlled by precipitation, evaporation, permafrost glacier meltwater, and groundwater. Annual lake-level fluctuations in the range of 2 m are clearly related to monsoonal precipitation during summer and evaporation during the rest of the year. Nowadays Nam Co is a dimictic, oligotrophic, slightly alkaline (8.04–9.85, averaging 9.21, Wang et al., 2009) and saline lake (1.851 mS cm^{-1}, Wang et al., 2009) with a waterbody that shows a stable thermal stratification during summer (June to early November) and complete oxygenation throughout the year even during ice coverage (February to mid-May). Allochthonous input by high-density underflows dominates modern sedimentation. The surface distribution patterns of many allochthonous input indicators show that sediment focusing effects occur in the deepest parts of both subbasins.

Nam Co is surrounded by Cretaceous sedimentary rocks as well as Jurassic sediments to the east, and Permian and Carboniferous rocks to the south. Magmatic rocks are found in the northeast of the lake and, together with mainly metamorphic rocks, also form the main part of the glaciated Nyainqêntanglha mountain range in the south (Fig. 3).

Although the main active faults of the Yadong–Gulu rift system lie outside the Nam Co basin (Armijo et al., 1986; Harrison et al., 1995; Styron et al., 2010), minor faulting may occur across the basin. These faults may be either north–south-trending normal faults or northwest–southeast-trending strike-slip faults or a combination of both. Geology and tectonics (Fig. 3) as well as evidence from own seismic data (Fig. 4) indicate deformation in the Quaternary in the Nam Co basin.

3 Previous investigations

High-resolution (centennial to decadal) multiproxy studies on four sediment cores from different water depths and locations (Fig. 2, NMLC1, Zhu et al., 2008; Nam Co 8, Mügler et al., 2010; NC08/01, Kasper et al., 2015; NMC09, Li et al., 2017) within Nam Co underline the high potential of Nam Co sediments as an environmental archive. Studies integrate results from inorganic geochemistry; sedimentology; mineralogy (Doberschütz et al., 2014); organic geochemistry, including compound-specific (*n*-alkanes) stable isotopes (Günther et al., 2011); micropaleontological (ostracod and diatom ecology) analyses, including ostracod-based transfer functions (salinity, water depth) and stable isotopes, as well as trace elements from their shells (Yang et al., 2014); paleomagnetic and environmental magnetic investigations (Haberzettl et al., 2015; Kasper et al., 2012; Su et al., 2013); and modern and fossil pollen composition (Zhu et al., 2015).

The longest of the hitherto recovered sediment cores, NC08/01 (10.4 m) from the deepest part of the lake, includes many discoveries made in shorter sediment cores in earlier studies and is therefore used as a reference core. This core covers the past 24 cal kyr BP (Kasper et al., 2015), but high

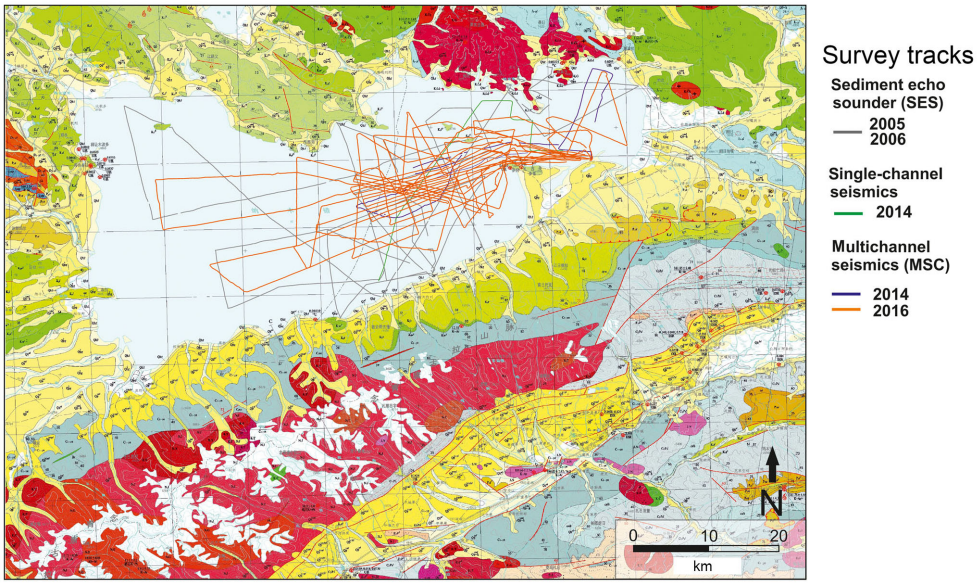

Figure 3. Geological map of the Nam Co area (green: Cretaceous; blue: Jurassic; gray: Permian and Carboniferous; red: magmatic and metamorphic; yellow: Quaternary; white: modern glaciers of the Nyainqêntanglha mountain range) (Wu et al., 2011, modified) and cruise tracks of 2005/2006 echosounder (gray), 2014 single channel (green), and 2014/2016 multichannel seismic surveys (purple and orange).

stand lacustrine deposits up to 139.2 m above today's lake level of Nam Co, dated back to 115.9 ± 12.1 ka, prove the existence of the lake for a much longer period, potentially as part of an ancient megalake on the Tibetan Plateau (Zhu et al., 2004). In addition, molecular clock analyses of recent endemic gastropods (*Radix* spp.) occurring in the Nam Co area indicate that their regional diversification started > 1 Ma ago. This suggests a continuous existence of water bodies in the Nam Co area at least since the middle Pleistocene (von Oheimb et al., 2011).

In 2005 and 2006, about 420 km of seismic profiles (Fig. 3) was acquired with a parametric sediment echo sounder (Innomar SES 96 light), providing a signal penetration to 30–35 m sediment depth. After a preliminary deep seismic survey (signal penetration to ~ 800 m) in 2014 (~ 160 km) an extensive pre-site survey funded by the Deutsche Forschungsgemeinschaft (DFG, German Research Foundation) took place in June–July 2016 to refine the opportunities for a deep drilling ICDP project (Fig. 3). A further goal of this multichannel seismic survey (MCS) was the investigation of the tectonic framework and sedimentary environment to develop stratigraphic and evolutionary scenarios for Nam Co. For this purpose, a micro GI Gun (2×0.1 L chamber volume) combined with a multichannel streamer (Teledyne, 32 channels, 64 m active length) was utilized. In total, 91 deep penetration seismic profiles were recorded, allowing good coverage of the basin (860 km).

4 Seismic results

Seismic profiles reveal at least several hundred meters of sediment infill with varying thicknesses. In the eastern part of the lake a penetration depth of only 250 ms TWT (two-way travel time) (~ 200 m) was reached, whereas the western part allowed a penetration of > 1 s TWT (~ 800 m). Fault patterns in the sediment fill of Nam Co likely represent the predominant regional deformation in the Quaternary. Fig. 4 displays a seismic profile along the NW–SE axis of the lake (GeoB16-393), comprising well-layered sedimentary sequences down to 960 ms TWT, with densely spaced steep faults, indicating a predominant strike-slip tectonic regime. E–W-trending positive and negative flower structures (Fig. 4) indicate local subsidence and the creation of accommodation space. The interplay of tectonics and sedimentation has apparently maintained a closed basin in the late Quaternary. We suppose that during extensional phases subsidence has significantly influenced sediment accumulation within the basin. Combining the new seismic data and drilling results will provide depositional boundary conditions, e.g. timing of tectonic activity and subsidence rates.

A preliminary seismic stratigraphy was derived using overall reflection strength to distinguish high and low lake-level settings as well as transitional periods. Also, in MCS data (Fig. 4), low-amplitude seismic facies can be assigned to lake-level high stands and deposition of mostly fine-grained sediments, comparable to the modern situation. A uniform thickness of this uppermost unit is indicative of a widespread deposition of mostly suspended material. During periods of lower lake levels, higher amplitude reflectors indicate coarser

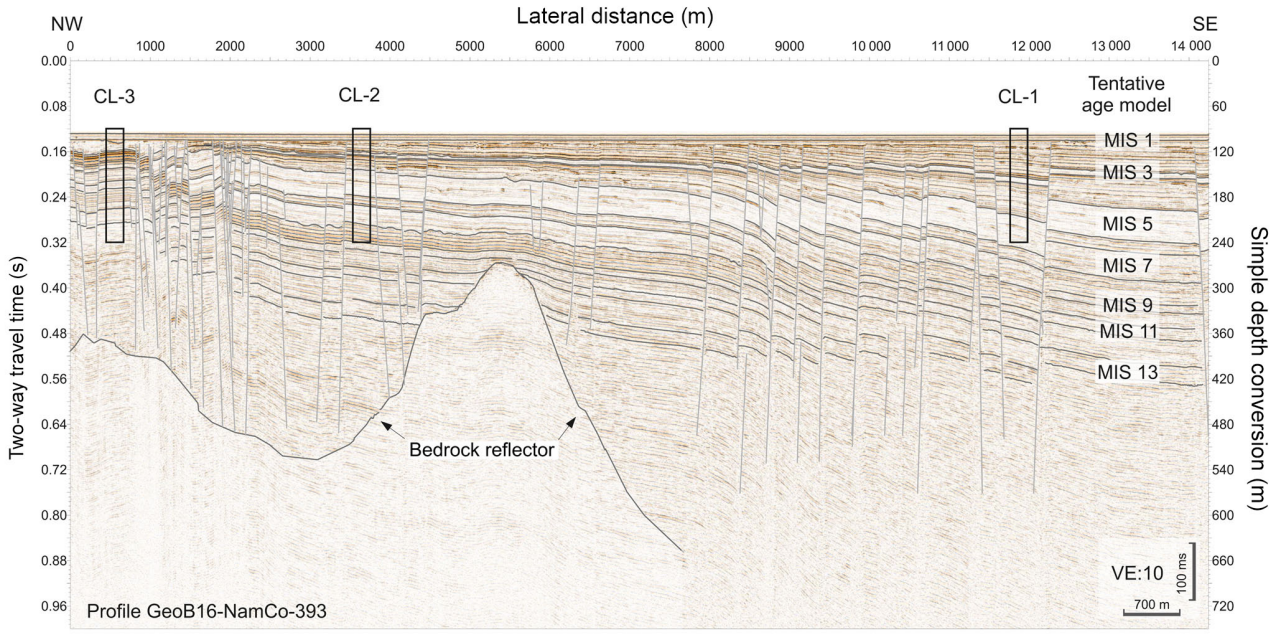

Figure 4. Multichannel seismic profile GeoB16-393 showing several hundred meters of sediment infill. Sediment thickness is increasing towards the center of the lake in the SE due to the additional subsidence of ca. 300 m. Simple depth conversion with 1500 m s^{-1}. A tentative age model is given with marine isotope stages (MISs). Potential piston coring locations (CL-1, CL-2, CL-3) at which sediment cores can well be parallelized to form a composite sediment sequence using strong reflectors in the seismic images are indicated by black boxes.

material. This and minor incisions in shallower parts of the lake as well as irregular topography hint to erosion in a shallow lake. In Fig. 4 extrapolation of the sedimentation rates and the acoustic behavior observed in the reference core confirm that at least 13 MIS stages are imaged (Fig. 4), with older sedimentary sections present.

5 Workshop

With these data in mind 40 scientists from 13 countries, representing various fields, met in Beijing from 22 to 24 May 2018 to discuss the further scientific opportunities that an ICDP drilling effort would provide. In addition, drilling strategies as well as logistical requirements of a deep drilling at Nam Co were discussed. Contributions of the participants included the following topics:

- the tectonic setting of Nam Co;
- the global relevance of a long climate record from Nam Co;
- paleoclimatological work which had been and will be carried out at Nam Co;
- seismic stratigraphy of Nam Co;
- archives for comparison;
- lake drilling project management, drilling operations, and fundamental core analyses;
- geochronology;
- bioindicators and deep biosphere;
- downhole logging;
- paleomagnetism;
- provenance analyses.

In addition, an excursion to Nam Co was planned for late 2018 to consider possible lake access points and base camps for future drilling and science teams as well as other logistic challenges.

Several discussion groups were organized to focus on the themes noted above and were charged with writing short reports to identify the major questions and develop hypotheses that will be addressed by studying Nam Co sediments through an ICDP deep drilling project. These groups included (1) sedimentology, (2) pollen, (3) bioindicators, (4) chronology and (5) tectonics. Scientific hypotheses were subsequently reviewed by all workshop participants and revisited by the breakout groups on the last day of the workshop. This reiterating process led to scientific hypotheses which can be tested by scientific drilling, such as the following for example:

- The timing and magnitude of Indian monsoon variability is controlled by eccentricity- and/or precession-driven insolation during the last million years.

- The land–ocean temperature gradient is greatest in transitions from terminations to interglacials, increasing precipitation (decreasing evaporation/inflow).
- Hemispheric climate controls species diversity, functional diversity and evolution of high-altitude ecosystems during the last 1 Ma.
- Aquatic and terrestrial biomes respond independently to environmental forcing over multiple glacial to interglacial cycles.
- High-altitude ecosystems are resilient from interglacial to interglacial which results in similar community structures and functions.
- The activity and diversity of the subsurface biosphere in high-altitude lake basins is dependent on their relationship to climate-driven carbon cycling and nutrient availability.
- The permanent lake system of Nam Co provided a refugium during glacials and, due to its unique location and size, was instrumental in the survival and recolonization of high-altitude species endemic to the Tibetan Plateau.
- The denudation rate of the Nyainqêntanglha mountain range controls sediment accumulation in the closed Nam Co basin.
- Deformation in the basin is consistent in space and time with regional tectonics.

These hypotheses will be used and revisited for the preparation of an ICDP full proposal. Participants saw dating as the most important prerequisite to be able to test the abovementioned hypotheses. It was concluded that 200 radiocarbon ages in combination with 200–400 OSL ages will provide a sound chronology for the younger part of the sequence, allowing the "calibration" of the paleomagnetic signal which should be used to date the older part. The use of U-Th dating as another dating technique was seen as questionable as more recent sediments showed a high detrital Th component. Therefore, the use of U-Th as an additional dating technique will have to be tested for older sediments. Amino acid dating might also be used for dating if suitable material can be extracted from the sediment sequence.

The last part of the workshop was dedicated to drilling strategies, on-site work and budgeting as well as outreach opportunities. Since Nam Co is characterized by ongoing tectonism, new accommodation space is constantly created in different parts of the lake. As this is a "quasi" continuous process, younger sediments are found at the top of the sequences in the southern part and older sediments at the top of the sequences in the northern part, with intermediate sequences in between (Fig. 4). Considering this architecture, one promising drilling strategy which was discussed by the participants was to build a composite record using three to four overlapping cores in rather high resolution and of good quality, recovered from different sites (Fig. 4). Using, for example, three to four 100–150 m long piston cores (e.g. CL-1 to 3 in Fig. 4) in a N–S transect a continuous, high-core-quality composite sequence going back to MIS 13 (according to the seismic interpretation) will be obtained. These sites should be covered by triple cores. The construction of a continuous log will be improved by downhole logging data. Also possible depth shifts will be corrected using these data. This composite record will be complemented by a $\sim$ 700–800 m long core (DT-1 in Fig. 2) going back to $\sim$ 1 Ma which most likely can only be cored as a single hole due to time constraints. Modern process studies show that different subbasins of Nam Co show different signals. For example, oxygen isotopes reveal an offset of 2 ‰ between basins. Thus, the long core will be used to calibrate signal changes in proxies detected in the high-quality "short" piston cores. Finally, two $\sim$ 100 m parallel cores forming the composite sequence GH-1 will be recovered from the very southern shore (Fig. 2) in order to investigate the role of glacial activity and its impact on the lake. The ICDP's Deep Lake Drilling System was generally seen as a reasonable tool for drilling Nam Co as it has been successfully applied to other challenging environmental systems (e.g. the Dead Sea in Israel).

Since Nam Co is located at an altitude of 4730 m a.s.l. there was intense discussion of how much man power will be needed to guarantee a smooth drilling operation. Everybody agreed that on-site work should at least include measurements of magnetic susceptibility and density to calculate porosity, which is important for OSL dating, using a Multi-Sensor Core Logger (MSCL). A mobile nuclear magnetic resonance (NMR) device will enable water content and thus porosity to be even more precisely determined. This will be complemented by pore water extraction and a clean lab for microbiological investigations. If manpower permits microscopes could also potentially be set up on-site.

6 Conclusions

All participants agreed that Nam Co sediments hold an extraordinary potential to answer questions of global social relevance, including past, modern and future climate change, biological development, tectonic evolution, and understanding of paleomagnetic variations and water resources which are coupled to the hydrological cycle. The workshop allowed the refinement of the scientific questions and discussion of the logistical issues of a scientific drilling of Nam Co in the framework of ICDP. Moreover, it allowed the transfer of knowledge between the different participants, increasing international visibility and promoting multidisciplinarity.

Data availability. No data sets were used in this article.

Team list. Guillaume St-Onge (University of Quebec, Rimouski, Canada), Fahu Chen (Institute of Tibetan Plateau Research, CAS, Beijing, China), Xingqi Liu (Beijing Normal University, Beijing, China), Xinmiao Lyu (Institute of Tibetan Plateau Research, CAS, Beijing, China), Jianting Ju (Institute of Tibetan Plateau Research, CAS, Beijing, China), Qingfeng Ma (Institute of Tibetan Plateau Research, CAS, Beijing, China), Zhonghai Wu (Chinese Academy of Geological Sciences, Beijing, China), Bernd Wünnemann (East China Normal University, Shanghai, China), Dada Yan (East China Normal University, Shanghai, China), Shuangwen Yi (Nanjing University, Nanjing, China), Hanzhi Zhang (Nanjing University, Nanjing, China), Yan Zhao (Institute of Geographic Sciences and Natural Resources Research, CAS, Beijing, China), Hongbo Zhao (China Geological Survey (Beijing Institute of Exploration Engineering), Bejing, China), Jan-Pieter Buylaert (Aarhus University, Aarhus, Denmark), Andrew Murray (Aarhus University, Aarhus, Denmark), Jerome van der Woerd (University of Strasbourg, Strasbourg, France), Peter Frenzel (Friedrich-Schiller-University, Jena, Germany), Gerd Gleixner (MPI Jena, Germany), Uli Harms (Scientific Drilling Operational Support Group ICDP, Potsdam, Germany), Klaus Reicherter (RWTH Aachen University, Aachen, Germany), Antje Schwalb (Technische Universität Braunschweig, Braunschweig, Germany), Arne Ulfers (Leibniz Institute for Applied Geophysics (LIAG), Hanover, Germany), Gábor Újvári (Research Centre for Astronomy and Earth sciences, Hungarian Academy of Sciences, Budapest, Hungary), Nivedita Mehrotra (Birbal Sahni Institute of Palaeosciences, Lucknow, India), Nicolas Waldmann (University of Haifa, Haifa, Israel), Andrea Lami (Italian National Research Council, Rome, Italy), Daniel Ariztegui (University of Geneva, Geneva, Switzerland), Natasha Barbolini (University of Amsterdam, Amsterdam, the Netherlands), Philippa Ascough (Scottish Universities Environmental Research Centre, East Kilbride, UK), Leon Clarke (Manchester Metropolitan University, Manchester, UK), Andrew Henderson (Newcastle University, Newcastle upon Tyne, UK), Richard Staff (Scottish Universities Environmental Research Centre, East Kilbride, UK), Anders Noren (LacCore Facility, University of Minnesota, Minneapolis, USA), Trisha Spanbauer (University of Texas at Austin, Austin, USA), Joseph Stoner (Oregon State University, Corvallis, USA).

Author contributions. All authors jointly organized the workshop. TH drafted the paper and NS drafted Figs. 2 to 4. All coauthors jointly contributed to the content of the final version of the paper. Listed workshop participants enthusiastically discussed the scientific objectives of a scientific drilling at Nam Co, contributed to the compilation of the hypotheses listed above and commented on the paper.

Competing interests. The authors declare that they have no conflict of interest.

Acknowledgements. We would like to acknowledge funding from ICDP and the Institute of Tibetan Plateau Research to carry out the workshop in Beijing. We would also like to thank Thomas Kasper and Ruimin Yang for drafting Fig. 1.

Edited by: Ulrich Harms
Reviewed by: two anonymous referees

References

Ahlborn, M., Haberzettl, T., Wang, J., Henkel, K., Kasper, T., Daut, G., Zhu, L., and Mäusbacher, R.: Synchronous pattern of moisture availability on the southern Tibetan Plateau since 17.5 cal. ka BP-the Tangra Yumco lake sediment record, Boreas, 46, 229–241, 2017.

Alivernini, M., Akita, L. G., Ahlborn, M., Börner, N., Haberzettl, T., Kasper, T., Plessen, B., Peng, P., Schwalb, A., Wang, J., and Frenzel, P.: Ostracod-based reconstruction of Late Quaternary lake level changes within the Tangra Yumco lake system (southern Tibetan Plateau), J. Quaternary Sci., 33, 713–720, 2018.

An, Z., Colman, S. M., Zhou, W., Li, X., Brown, E. T., Jull, A. J. T., Cai, Y., Huang, Y., Lu, X., Chang, H., Song, Y., Sun, Y., Xu, H., Liu, W., Jin, Z., Liu, X., Cheng, P., Liu, Y., Ai, L., Li, X., Liu, X., Yan, L., Shi, Z., Wang, X., Wu, F., Qiang, X., Dong, J., Lu, F., and Xu, X.: Interplay between the Westerlies and Asian monsoon recorded in Lake Qinghai sediments since 32 ka, Nat. Sci. Rep., 2, 1–6, 2012.

Armijo, R., Tapponnier, P., Mercier, J., and Han, T. L.: Quaternary extension in southern Tibet: Field observations and tectonic implications, J. Geophys. Res.-Sol. Ea., 91, 13803–13872, 1986.

Bolch, T., Yao, T., Kang, S., Buchroithner, M. F., Scherer, D., Maussion, F., Huintjes, E., and Schneider, C.: A glacier inventory for the western Nyainqentanglha Range and the Nam Co Basin, Tibet, and glacier changes 1976–2009, The Cryosphere, 4, 419–433, https://doi.org/10.5194/tc-4-419-2010, 2010.

Cruz, R. V., Harasawa, H., Lal, M., Wu, S., Anokhin, Y., Punsalmaa, B., Honda, Y., Jafari, M., Li, C., and Huu Ninh, N.: Asia – Climate Change 2007: Impacts, Adaptation and Vulnerability, Contribution of Working Group II to the Fourth Assessment Report of the Intergovernmental Panel on Climate Change, Cambridge, 469–506, 2007.

Dietze, E., Maussion, F., Ahlborn, M., Diekmann, B., Hartmann, K., Henkel, K., Kasper, T., Lockot, G., Opitz, S., and Haberzettl, T.: Sediment transport processes across the Tibetan Plateau inferred from robust grain-size end members in lake sediments, Clim. Past, 10, 91–106, https://doi.org/10.5194/cp-10-91-2014, 2014.

Doberschütz, S., Frenzel, P., Haberzettl, T., Kasper, T., Wang, J., Zhu, L., Daut, G., Schwalb, A., and Mäusbacher, R.: Monsoonal forcing of Holocene paleoenvironmental change on the central Tibetan Plateau inferred using a sediment record from Lake Nam Co (Xizang, China), J. Paleolimnol., 51, 253–266, 2014.

Fontes, J.-C., Gasse, F., and Gibert, E.: Holocene environmental changes in Lake Bangong basin (Western Tibet), Part 1: Chronology and stable isotopes of carbonates of a Holocene lacustrine core, Palaeogeogr. Palaeocl., 120, 25–47, 1996.

Günther, F., Mügler, I., Mäusbacher, R., Daut, G., Leopold, K., Gerstmann, U. C., Xu, B., Yao, T., and Gleixner, G.: Response of δD values of sedimentary n-alkanes to variations in source water isotope signals and climate proxies at lake Nam Co, Tibetan Plateau, Quatern. Int., 236, 82–90, 2011.

Haberzettl, T., Henkel, K., Kasper, T., Ahlborn, M., Su, Y., Wang, J., Appel, E., St-Onge, G., Stoner, J., Daut, G., Zhu, L., and Mäusbacher, R.: Independently dated paleomagnetic secular variation

records from the Tibetan Plateau, Earth Planet. Sc. Lett., 416, 98–108, 2015.

Harrison, T. M., Copeland, P., Kidd, W., and Lovera, O. M.: Activation of the Nyainqentanghla shear zone: Implications for uplift of the southern Tibetan Plateau, Tectonics, 14, 658–676, 1995.

Kasper, T., Haberzettl, T., Doberschütz, S., Daut, G., Wang, J., Zhu, L., Nowaczyk, N., and Mäusbacher, R.: Indian Ocean Summer Monsoon (IOSM)-dynamics within the past 4 ka recorded in the sediments of Lake Nam Co, central Tibetan Plateau (China), Quaternary Sci. Rev., 39, 73–85, 2012.

Kasper, T., Haberzettl, T., Wang, J., Daut, G., Zhu, L., and Mäusbacher, R.: Hydrological variations on the Central Tibetan Plateau since the LGM and their teleconnection to inter-regional and hemispheric climate variations, J. Quaternary Sci., 30, 70–78, 2015.

Keil, A., Berking, J., Mügler, I., Schütt, B., Schwalb, A., and Steeb, P.: Hydrological and geomorphological basin and catchment characteristics of Lake Nam Co, South-Central Tibet, Quatern. Int., 218, 118–130, 2010.

Krause, P., Biskop, S., Helmschrot, J., Flügel, W. A., Kang, S., and Gao, T.: Hydrological system analysis and modelling of the Nam Co basin in Tibet, Adv. Geosci., 27, 29–36, 2010.

Lau, W. K. M., Kim, M. K., Kim, K. M., and Lee, W. S.: Enhanced surface warming and accelerated snow melt in the Himalayas and Tibetan Plateau induced by absorbing aerosols, Environ. Res. Lett., 5, 025204, https://doi.org/10.1088/1748-9326/5/2/025204, 2010.

Li, C., Yan, F., Kang, S., Chen, P., Han, X., Hu, Z., Zhang, G., Hong, Y., Gao, S., Qu, B., Zhu, Z., Li, J., Chen, B., and Sillanpää, M.: Re-evaluating black carbon in the Himalayas and the Tibetan Plateau: concentrations and deposition, Atmos. Chem. Phys., 17, 11899–11912, https://doi.org/10.5194/acp-17-11899-2017, 2017.

Ma, Y., Kang, S., Zhu, L., Xu, B., Tian, L., and Yao, T.: ROOF OF THE WORLD: Tibetan Observation and Research Platform, B. Am. Meteorol. Soc., 89, 1487–1492, 2008.

Masson-Delmotte, V., Schulz, M., Abe-Ouchi, A., Beer, J., Ganopolski, A., Rouco, J. F. G., Jansen, E., Lambeck, K., Luterbacher, J., Naish, T., Osborn, T., Otto-Bliesner, B., Quinn, T., Ramesh, R., Rojas, M., Shao, X., and Timmermann, A.: Information from Paleoclimate Archives, Cambridge, New York, 2013.

Mügler, I., Gleixner, G., Günther, F., Mäusbacher, R., Daut, G., Schütt, B., Berking, J., Schwalb, A., Schwark, L., Xu, B., Yao, T., Zhu, L., and Yi, C.: A multi-proxy approach to reconstruct hydrological changes and Holocene climate development of Nam Co, Central Tibet, J. Paleolimnol., 43, 625–648, 2010.

Nishimura, M., Matsunaka, T., Morita, Y., Watanabe, T., Nakamura, T., Zhu, L., Nara, F. W., Imai, A., Izutsu, Y., and Hasuike, K.: Paleoclimatic changes on the southern Tibetan Plateau over the past 19,000 years recorded in Lake Pumoyum Co, and their implications for the southwest monsoon evolution, Palaeogeogr. Palaeocl., 396, 75–92, 2014.

Qiu, J.: China: The third pole, Nature, 454, 393–396, 2008.

Styron, R., Taylor, M., and Okoronkwo, K.: Database of active structures from the Indo-Asian collision, Eos T. Am. Geophys. Un., 91, 181–182, 2010.

Su, Y., Gao, X., Liu, Q., Hu, P., Duan, Z., Jiang, Z., Wang, J., Zhu, L., Doberschütz, S., Mäusbacher, R., Daut, G., and Haberzettl, T.: Mechanism of variations in environmental magnetic proxies of lake sediments from Nam Co, Tibet during the Holocene, Chin. Sci. Bull., 58, 1568–1578, 2013.

Thurow, J., Peterson, L. C., Harms, U., Hodell, D. A., Cheshire, H., Brumsack, H.-J., Irino, T., Schulz, M., Masson-Delmotte, V., and Tada, R.: Acquiring High to Ultra-High Resolution Geological Records of Past Climate Change by Scientific Drilling, Sci. Dril., 8, 46–56, https://doi.org/10.2204/iodp.sd.8.08.2009, 2009.

von Oheimb, P. V., Albrecht, C., Riedel, F., Du, L. N., Yang, J. X., Aldridge, D. C., Bossneck, U., Zhang, H. C., and Wilke, T.: Freshwater Biogeography and Limnological Evolution of the Tibetan Plateau – Insights from a Plateau-Wide Distributed Gastropod Taxon (Radix spp.), Plos One, 6, e26307, https://doi.org/10.1371/journal.pone.0026307, 2011.

Wang, J., Zhu, L., Daut, G., Ju, J., Lin, X., Wang, Y., and Zhen, X.: Investigation of bathymetry and water quality of Lake Nam Co, the largest lake on the central Tibetan Plateau, China, Limnology, 10, 149–158, 2009.

Wu, Z. H., Meng, X. G., and Hu, D. G.: Regional Geological Survey Report of China (Damxong), China University of Geosciences Press, Wuhan, China, 346 pp., 2011.

Xie, M., Zhu, L., Peng, P., Wang, J., Wang, Y., and Schwalb, A.: Ostracod assemblages and their environmental significance from the lake core of the Nam Co on the Tibetan Plateau 8.4 ka BP, J. Geogr. Sci., 19, 387–402, 2009.

Yang, Q., Jochum, K. P., Stoll, B., Weis, U., Börner, N., Schwalb, A., Frenzel, P., Scholz, D., Doberschütz, S., Haberzettl, T., Gleixner, G., Mäusbacher, R., Zhu, L., and Andreae, M. O.: Trace element variability in single ostracod valves as a proxy for hydrochemical change in Nam Co, central Tibet, during the Holocene, Palaeogeogr. Palaeocl., 399, 225–235, 2014.

Zhang, Y. J., Kang, S. C., and You, Q. L.: Climate in Nam Co Basin, in: Modern Environmental Processes and Changes in the Nam Co Basin Tibetan Plateau, edited by: Kang, S. C., China Meteorological Press, 15–35, 2011.

Zhou, S., Kang, S., Chen, F., and Joswiak, D. R.: Water balance observations reveal significant subsurface water seepage from Lake Nam Co, south-central Tibetan Plateau, J. Hydrol., 491, 89–99, 2013.

Zhu, D. G., Meng, X. G., Zhao, X. T., Shao, Z. G., Xu, Z. F., Yang, C. B., Ma, Z. B., Wu, Z. G., Wu, Z. H., and Wang, J. P.: Evolution of an Ancient Large Lake in the Southeast of the Northern Tibetan Plateau, Acta Geol. Sin.-Engl., 78, 982–992, 2004.

Zhu, L., Wu, Y., Wang, J., Lin, X., Ju, J., Xie, M., Li, M., Mäusbacher, R., Schwalb, A., and Daut, G.: Environmental changes since 8.4 ka reflected in the lacustrine core sediments from Nam Co, central Tibetan Plateau, China, The Holocene, 18, 831–839, 2008.

Zhu, L., Peng, P., Xie, M., Wang, J., Frenzel, P., Wrozyna, C., and Schwalb, A.: Ostracod-based environmental reconstruction over the last 8,400 years of Nam Co Lake on the Tibetan plateau, Hydrobiologia, 648, 157–174, 2010.

Zhu, L., Lü, X., Wang, J., Peng, P., Kasper, T., Daut, G., Haberzettl, T., Frenzel, P., Li, Q., Yang, R., Schwalb, A., and Mäusbacher, R.: Climate change on the Tibetan Plateau in response to shifting atmospheric circulation since the LGM, Sci. Rep., 5, 13318, https://doi.org/10.1038/srep13318, 2015.

IODP begins planning for its next phase

Scientific ocean drilling celebrated its 50th anniversary in 2018 with numerous conference sessions, symposia and, earlier this year, a special ocean-drilling-themed issue of the journal Oceanography (https://tos.org/oceanography/issue/volume-32-issue-01). But even as these commemorative events around the globe were celebrating ocean drilling's history and achievements, various IODP entities were laying the groundwork for the programme's next phase.

The current decadal scientific ocean drilling science plan (http://www.iodp.org/about-iodp/iodp-science-plan-2013-2023) runs through 2023, only four years away, and the various IODP funding agencies are in agreement that planning for the successor to IODP, including an updated science plan, must begin now if the transition to a new programme is to proceed smoothly. In addition, although the US National Science Board passed a resolution in February 2019 approving continued funding for the riserless US drilling vessel JOIDES Resolution through 2024, the US IODP community hopes at the end of this period to replace the aging JR with a modern, next-generation vessel that will provide advanced capabilities, including increased laboratory space, active heave compensation, faster pipe tripping, a greener footprint, and other scientific and environmental efficiencies. A new science plan will be necessary to justify this investment and to secure funding for the other IODP platform providers.

Four workshops were held in April and May of 2019 to begin the planning process, with a fifth (IODP-China) planned for over the summer. All of the workshops focused on developing conceptual structures for an updated science plan. While member priorities and outcomes varied somewhat from nation to nation, there was a remarkably strong consensus across IODP member nations and consortia that a less "vertical" and more "cross-cutting" science plan structure is desirable in the next programme phase.

Japan was first to convene a workshop, "Scientific Ocean Drilling Beyond 2023", held on 2–3 April at the Yokohama Institute for Earth Sciences. In addition to focusing on the development of a new science plan, the workshop also explored possible links to the International Continental Drilling Program (ICDP), general interdisciplinary fusion, and how the riser-equipped Japanese vessel Chikyu can maximize the scientific return for Japan and its IODP partners as the programme moves into the future.

The Japanese workshop was followed the next weekend by Europe's "PROCEED – Expanding Frontiers of Scientific Ocean Drilling", held 6–7 April at the Austrian Academy of Sciences in Vienna, immediately prior to the annual European Geosciences Union meeting. PROCEED featured breakout sessions that mixed scientists with different thematic expertise, with the goal of examining the scientific, technological and programmatic goals for the European Consortium for Ocean Research Drilling (ECORD) beyond 2023, particularly in the context of ECORD's mission-specific platform strategy.

The Australian and New Zealand IODP Consortium (ANZIC) held its "Ocean Planet Workshop" on 14–16 April at The Australian National University in Canberra, Australia. The organizers welcomed white papers from its community members on targets for ocean drilling in the next phase, and the workshop's first day was devoted to early-career and mid-career researchers. Primary goals of the workshop were the identification of gaps in the current IODP science plan and "improved engineering, technological, drilling, logging and observing capabilities".

Finally, on 6–7 May, the US convened a workshop in Denver entitled, "NEXT: Scientific Ocean Drilling Beyond 2023", with the objectives of updating existing scientific challenges, as well as identifying new challenges, for ocean drilling, and prioritizing the technologies needed to address them in the next phase. The workshop featured a presentation by the JOIDES Resolution Science Operator on a proposed design of a successor vessel to the JR and produced a straw-man science plan structure that included eight strategic objectives and emphasized connections and threads rather than themes.

Each of the four workshops was open to international attendees, which promoted collaboration and momentum across the international community. A likely next step will be a summer meeting among the coordinators of the workshops in order to consolidate the various workshop outcomes into a single blueprint that will serve as the structure for the next IODP science plan. This will be presented at the IODP Forum meeting in Osaka, Japan, in September. Either at or just after the forum meeting, a writing team will be assembled to begin development of the plan, with the goal of producing a completed product by the summer of 2020.

Schedules

IODP – expedition schedule http://www.iodp.org/expeditions/

USIO operations	Platform	Dates	Port of origin
1 Exp 383: Dynamics of Pacific Antarctic Circumpolar Current	JOIDES Resolution	May 20–July 20, 2019	Punta Arenas
2 Exp 385T: Panama Basin Crustal Architecture (504B) and Restoring Hole 896A	JOIDES Resolution	Aug 18–Sep 16, 2019	Antofagasta
3 Exp 385: Guaymas Basin Tectonics and Biosphere	JOIDES Resolution	Sep 16–Nov 16, 2019	San Diego
4 Exp 378: South Pacific Paleogene Climate	JOIDES Resolution	Jan 3–Mar 4, 2020	Fiji

ICDP – Project schedule http://www.icdp-online.org/projects/

ICDP project	Drilling dates	Location
1 Eger Rift	Nov 2018–Oct 2019	West Bohemia, Czech Republic
2 DOVE	May 2019–Feb 2020	Alps
3 GRIND	June 2019–Feb 2020	Namibia, Brazil, China
4 STAR	July 2019	Northern Apennines, Italy
5 JET	Oct 2019–Dec 2019	Cheshire Basin, UK
6 Trans-Amazon	Nov 2019–June 2020	Brazil (multiple locations)

Locations

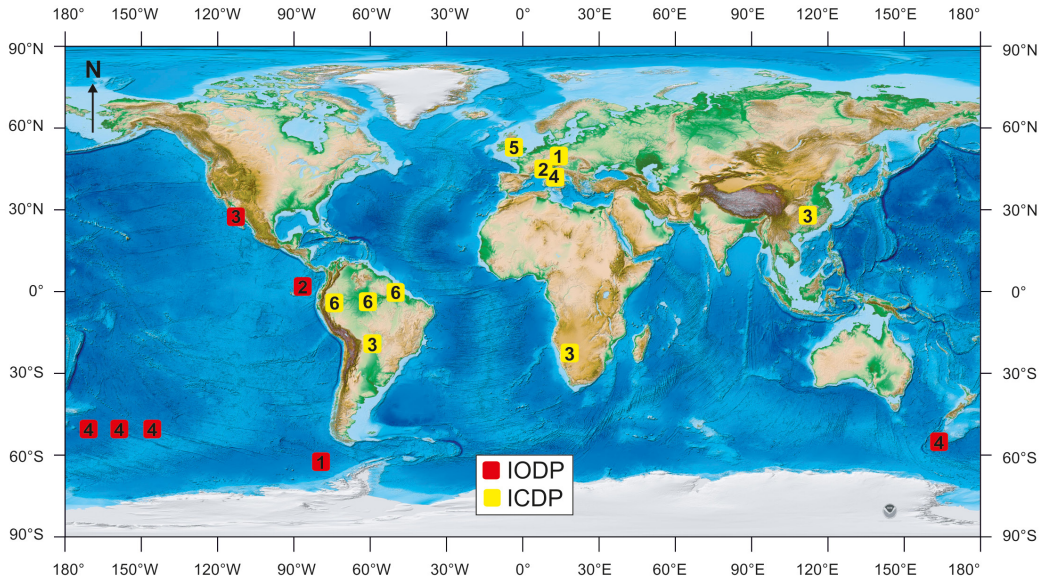

Topographic/bathymetric maps courtesy of NOAA (Amante, C. and B.W. Eakins, 2009. ETOPO1 1 Arc-Minute Global Relief Model: Procedures, Data Sources and Analysis. NOAA Technical Memorandum NESDIS NGDC-24. National Geophysical Data Center, NOAA. doi:10.7289/V5C8276M).